CURRENT TRANSPORT MODELING OF CARBON NANOTUBE FIELD EFFECT TRANSISTORS FOR ANALYSIS AND DESIGN OF INTEGRATED CIRCUITS

A Dissertation

Submitted to the Graduate Faculty of the
Louisiana State University and
Agricultural and Mechanical College
in partial fulfillment of the
requirements for the degree of
Doctor of Philosophy

in

The Department of Electrical and Computer Engineering

by

Jose Mauricio Marulanda Prado
B.S.E.E., Louisiana State University, Baton Rouge, U.S.A. 2001
M.S.E.E., Louisiana State University, Baton Rouge, U.S.A. 2002

August 2008

To my parents Armando Marulanda Blanco and Ana Lucia Prado de Marulanda

and

To my sisters Lyna Maria and Ana Maritza

Without their patience, understanding support and most of all love,

the completion of this dissertation would not have been possible.

ACKOWLEDGMENTS

My thanks and special appreciation to my advisor and mentor Dr. Ashok Srivastava. I am very thankful for his guidance, patience and understanding throughout my dissertation research. I would have not completed this research without his suggestions, discussions and constant encouragement.

I would like to thank Committee members Dr. Pratul Ajmera, Dr. Martin Feldman, Dr. Georgios Veronis and Dr. Michael Cherry for being a part of my committee.

I am thankful to Dr. Ashwani K. Sharma of US Air Force Research Laboratory, Kirtland Air Force Base, New Mexico, for his support and encouragement for the research carried out in this project. I am also thankful to Dr. Rajendra K. Nahar of Central Electronics Engineering Research Institute, Pilani (India) for his feedback and helpful suggestions.

Above all, I am deeply grateful to my fellow co-workers, Siva Yellampalli, Yao Xu and Yang Li and to my close friends, Thomas Lagarde, Alejandra Diaz, Claudia Tamacas and Geber Urbina for their friendship and support.

TABLE OF CONTENTS

LIST OF TABLES

LIST OF FIGURES

ABSTRACT

The purpose of this study was to develop a complete current transport model for carbon nanotube field effect transistors (CNT-FETs) applicable in the analysis and design of integrated circuits. The model was derived by investigating the electronic structure of carbon nanotubes and using basic laws of electrostatics describing a field effect transistor.

We first derived analytical expressions for the carrier concentration in carbon nanotubes for different chiral vectors (n,m) by studying and characterizing their electronic structure. Results showed a strong relation to the diameter and wrapping angle of carbon nanotubes.

The charge distribution in a CNT-FET is characterized from the charge neutrality and potential balance conditions. Mathematical techniques are used to derive analytically approximated equations describing the carbon nanotube potential in terms of the terminal voltages. These equations are validated by comparing them with the respective numerical solutions; furthermore, the expressions for the carbon nanotube potential are used to derive current transport equations for normal and subthreshold operations. Threshold and saturation voltages expressions are each derived in the process and the I-V characteristics for CNT-FETs are calculated using different combinations of chiral vectors. Results showed a strong dependence of the I-V characteristics on the wrapping angle and diameter of carbon nanotubes, as expected from the carrier concentration modeling. Results were also compared with available experimental data showing close agreement within the limitations and approximations used in the analysis.

In addition, the current model equations were used to generate the voltage transfer characteristics for basic logic circuits based on complementary CNT-FETs. The voltage transfer characteristics exhibit characteristics similar to the voltage transfer characteristics of

standard CMOS logic devices, with a sharp transition near the logic threshold voltage depending on the input conditions. A small-signal radio frequency (rf) model was also developed and it is shown to have cut-off frequencies in the upper GHz range with a strong dependence on the chiral vector and corresponding transconductance (g_m).

Finally, due to the rapid growth of carbon nanotubes as bio- and chemical sensing devices, we have also presented, using our current model equations, possible methods to interpret and analyze CNT-FETs when utilized as biosensors.

CHAPTER 1

INTRODUCTION

1.1 Introduction to Carbon Nanotubes

In 1960, Bacon of Union Carbide [1] reported observing straight hollow tubes of carbon that appeared as graphene layers of carbon. In 1970s, Oberlin et al., [2] observed these tubes again by a catalysis-enhanced chemical vapor deposition (CVD) process. In 1985, random events led to the discovery of a new molecule made entirely of carbon, sixty carbons arranged in a soccer ball shape [3]. In fact, what had been discovered was an infinite number of molecules: the fullerenes, C_{60}, C_{70}, C_{84}, etc., every molecule with the characteristic of being a pure carbon cage. These molecules were mostly seen in a spherical shape. However, it was until 1991 that Iijima [4] of NEC observed a tubular shape in the form of coaxial tubes of graphitic sheets, ranging from two shells to approximately 50. Later, this structure was called multi-walled carbon nanotube (MWNT). Two years later, Bethune et al., [5] and Iijima and Ichihashi [6] managed to observe the same tubular structure, but with only a single atomic layer of graphene, which became known as a single-walled carbon nanotube (SWNT).

Semiconductor Research Corporation (SRC) in its International Technology Roadmap of Semiconductors (ITRS 2003) report has refereed to several non-classical devices, which could be the candidates of future technology as the end of Moore's law approaches (~2020). Carbon nanotubes (CNTs) are being explored extensively as the structure material for making future CMOS devices and circuits [7-9]. One of the interesting features of a carbon nanotube is that it can be metallic or semiconducting with a bandgap depending on its diameter [10]. Since CNTs are planar graphene sheets wrapped into tubes, electrical characteristics vary with the tube diameter and the wrapping angle of graphene [11]. Carbon nanotubes are classified in two

categories, multi-walled carbon nanotubes (MWNTs) and single-walled carbon nanotubes (SWNTs). Single-walled nanotubes are one-dimensional graphene sheets rolled into a tubular structure of nanometer size with properties very similar to graphene [12]. These SWNTs are one dimensional metals or semimetals with properties determined by their chiral vector [13]. Multi-walled nanotubes on the other hand, exhibit the same properties as SWNTs, however while SWNTs consist of one shell, MWNTs comprise multi-shells of graphene sheets rolled into a tubular structure [14].

1.2 Synthesis of Carbon Nanotubes

Following the rapid advancement of carbon nanotubes and applications, different techniques to produce carbon nanotubes have been developed. Carbon nanotubes can be fabricated using the following techniques: arc discharge, laser ablation, high-pressure carbon monoxide (HiPCO), and chemical vapor deposition (CVD) methods. Among these techniques, CVD method has shown the best performance towards CNT-FET applications.

1.2.1 Arc Discharge

This was the first available method to fabricate carbon nanotubes. An electric arc discharge is an electrical breakdown of a gas producing a plasma discharge, very similar to a spark, which is the flow of current through a nonconductive medium such as the air or an insulator. In a conventional carbon arc discharge fabrication, a plasma discharge is generated in a small gap between two graphite electrodes. In this method, carbon nanotubes are produced at the core in the cathode deposit [15].

1.2.2 Laser Ablation

A standard laser ablation process involves a block of graphite mixed with a catalytic metal, such as Co, Pt, Ni, Cu, etc. The composite block is formed by mixing graphite with the catalytic metal in a tube furnace heated to about 1473 K [16]. The graphite block is then

targeted with a laser and argon (Ar) gas is pumped in the direction of the laser. As the laser ablates the target, carbon nanotubes are formed and are carried by the gas flow onto a cool copper collector.

1.2.3 High Pressure Carbon Monoxide (HiPCO)

The HiPCO is a technique that produces single-walled carbon nanotubes in a continuous gas flow phase. This process uses CO as the source of carbon and $Fe(CO)_5$ as the catalyst precursor. The carbon monoxide flows into a heated reactor where it gets mixed with a small amount of $Fe(CO)_5$ yielding single-walled carbon nanotubes. The size and diameter can be roughly controlled by regulating the pressure of the CO [17].

1.2.4 Chemical Vapor Deposition

A typical CVD process involves a substrate, which is exposed to one or more volatile precursors, which then react and decompose on the substrate surface producing the desired deposit. Byproducts are removed by a gas flow through the reaction chamber. Carbon nanotubes are produced generally by the reaction of a gas containing carbon such as ethylene, acetylene, ethanol, etc. with a metal catalyst (cobalt, nickel, iron, etc.) at temperatures above 700 °C [18].

1.2.5 Flame Synthesis

Recent work has shown that flame synthesis is an inexpensive large scale method to produce single-walled carbon nanotubes [19,20]. In a flame synthesis process, the combustion of hydrocarbon fuel is responsible to produce enough heat to establish the required temperature environment for the process and to form small aerosol metal catalyst islands. Single-walled carbon nanotubes are grown in these catalyst islands in the same way as in the arc discharge and laser ablation processes [21,22].

1.3 Structure of Carbon Nanotubes

There are four types of natural occurring carbon: diamond, graphite, ceraphite, and fullerenes. Fullerenes are molecules formed entirely of carbon and take the shape of a hollow sphere, ellipsoid, or a tube. Fullerenes, which take the shape of a tube are called buckytubes or nanotubes.

Carbon nanotubes exhibit promising mechanical and electrical properties. They can be pictured as a result of folding graphene layers into a tubular structure as seen in Fig. 1.1(a). These cylinders form a carbon nanotube and they can be single-walled or multi-walled depending on the number of shells that form the tubular structure [14]. Single-walled nanotubes (SWNTs) are composed of one shell of carbon atoms. Multi-walled nanotubes (MWNTs) have multiple nested shells of carbon. In addition, single-walled carbon nanotubes tend to adhere strongly to each other forming ropes or bundles of nanotubes as shown in Fig. 1.1(b) exhibiting physical properties of both metallic and semiconducting materials.

SWNTs have risen as the most likely candidates for miniaturizing electronics beyond current technology. They exhibit phenomenal electrical and mechanical properties. The most fundamental application of SWNTs is in field effect transistors (FETs). N-type carbon nanotube field effect transistors and p-type carbon nanotube field effect transistors have been made [23], showing a behavior similar to current MOSFETs. The work presented in the dissertation will focus on carbon nanotube field effect transistors (CNT-FETs) made using single-walled carbon nanotubes (SWNTs).

1.4 Properties of Single-Walled Carbon Nanotubes

Single-walled carbon nanotubes are best characterized by its chirality or chiral vector. The chirality is an adapted concept uniquely of each type of nanotube that determines its properties and diameter [13]. The chirality is represented with a pair of indices (n,m) called the

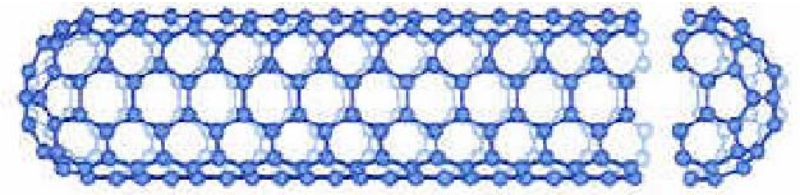

(a)

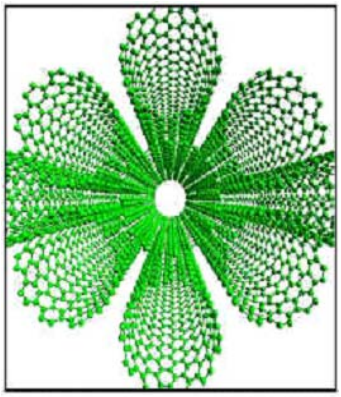

(b)

Figure 1.1: (a) Single-walled carbon nanotube and (b) bundle of single-walled carbon nanotubes.

chiral vector. The chiral vector is a line that traces the CNT around its circumference from one carbon atom, called the reference point (point O) back to itself (point C) in Fig. 1.2. [24,25]. The circumference described by the line $\overrightarrow{OC}$ in Fig. 1.2 is best represented with the following mathematical expression,

$$C_h = na_1 + ma_2 \ , \tag{1.1}$$

where a_1 and a_2 are the unit vectors for the graphene hexagonal structure, and (n,m) are integers that represents the number of hexagons away from the reference point (O) to point (C), in the a_1 and a_2 directions, respectively (Fig. 1.2). The schematic representation of a SWNT in two dimensions is shown in Fig. 1.2. Each hexagon in Fig. 1.2 represents a single unit cell [25].

A CNT can thus be described by the notation (n,m), referring to the chiral vector. In Fig. 1.2 two wrapping angles have been defined, θ and ϕ. The angle θ, known as the chiral angle, is defined as the angle between the zigzag axis and the chiral vector; the angle ϕ, on the other hand, is defined between the armchair axis and the chiral vector. Using the n, m indices and the chiral angle carbon nanotubes can be classified in three groups: armchair nanotubes for $n = m$, with a chiral angle $\theta = 30^o$, zigzag nanotubes for $n = 0$ or $m = 0$, with $\theta = 0^o$ and chiral nanotubes for any other combination with $0^o < \theta < 30^o$.

Furthermore, the n, m integers also determine whether a CNT is metallic or semiconducting, when $n - m = 3l$ (l being an integer), the nanotube is metallic, and when $n - m \neq 3l$, the nanotube is semiconducting with an energy gap depending on its diameter as follows [13],

$$E_{gap} = 2V_{pp\pi}a_{c-c}/d, \tag{1.2}$$

where $V_{pp\pi}$ is the carbon-carbon (C-C) tight binding overlap energy, $a_{c\text{-}c}$ is the nearest neighbor distance between C-C bonds (0.144 nm) and d is the diameter of the carbon nanotube.

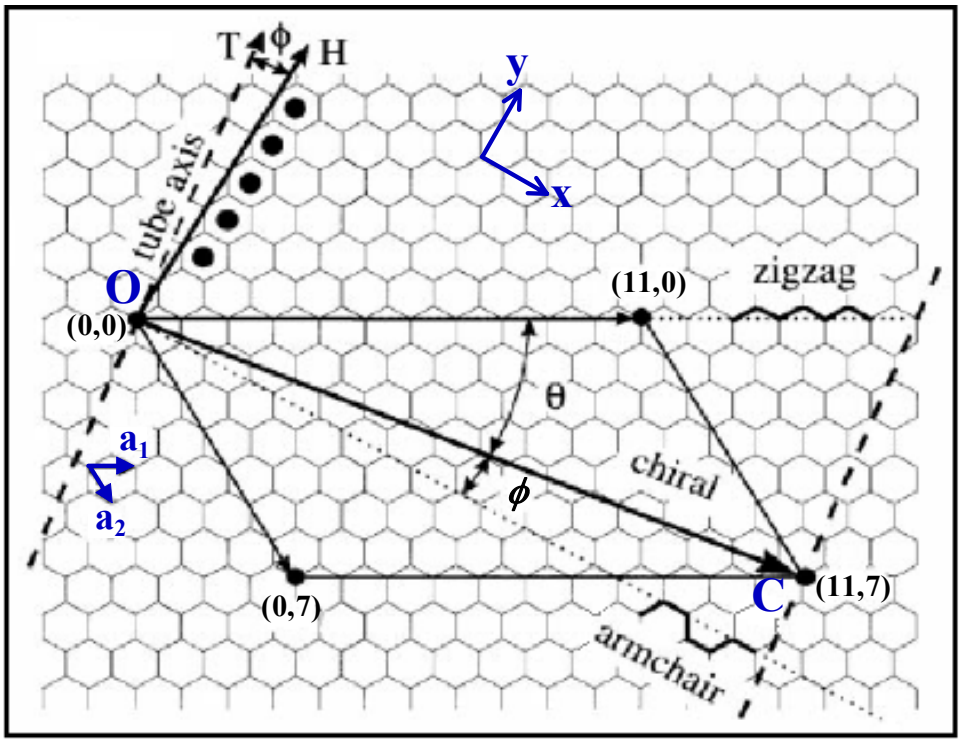

Figure 1.2: Schematic representation of a chiral vector in the crystal lattice of a carbon nanotube (figure reprinted from [25] with the respective copyright permissions of the authors).

1.5 Electronic Band Structure

In order to examine the electronic structure of carbon nanotubes, it is necessary to define the structural configuration. Carbon nanotube structures are defined by the indices (n,m) inscribed in the chiral vector. The chiral vector is a vector along the perimeter of the carbon nanotube, from which the lattice cell structure can be generated as explained earlier.

1.5.1 Crystal Lattice

The primitive cell of a carbon nanotube can be described from the unit vectors [11,26]:

$$R_1 = \frac{a}{2}\left(\sqrt{3}\hat{x} + \hat{y}\right) \quad \text{and} \quad R_2 = \frac{a}{2}\left(\sqrt{3}\hat{x} - \hat{y}\right), \tag{1.3}$$

where R_1 and R_2 are the unit cell vectors, a is the lattice constant with a value of $\sqrt{3}\, a_{cc}$ and a_{cc} is the nearest distance between two carbon atoms.

Figure 1.3 shows a plot of the crystal lattice structure for a carbon nanotube with a chiral vector (4,3) generated from the chiral vector and the unit vectors from Eqs. (1.2) and (1.3), respectively.

1.5.2 Reciprocal Lattice

The reciprocal lattice vectors, b_1 and b_2 are of the form [11,26]:

$$b_1 = \frac{2\pi}{a}\left(\frac{1}{\sqrt{3}}\hat{x} + \hat{y}\right), \quad \text{and} \quad b_1 = \frac{2\pi}{a}\left(\frac{1}{\sqrt{3}}\hat{x} - \hat{y}\right). \tag{1.4}$$

Figure 1.4 shows a plot of the reciprocal lattice structure for a carbon nanotube with a chiral vector (4,3) generated from the reciprocal vectors of Eq. (1.4).

1.5.3 Energy Dispersion Relation

The energy dispersion relation for carbon nanotubes can be calculated from the electronic structure of graphene. The energy dispersion of graphene is given by [24,27,28]

$$E_{2D}(K) = \pm V_{pp\pi}\left\{3 + 2Cos(K.R_1) + 2Cos(K.R_2) + 2Cos\left[K(R_1 - R_2)\right]\right\}^{1/2}, \tag{1.5}$$

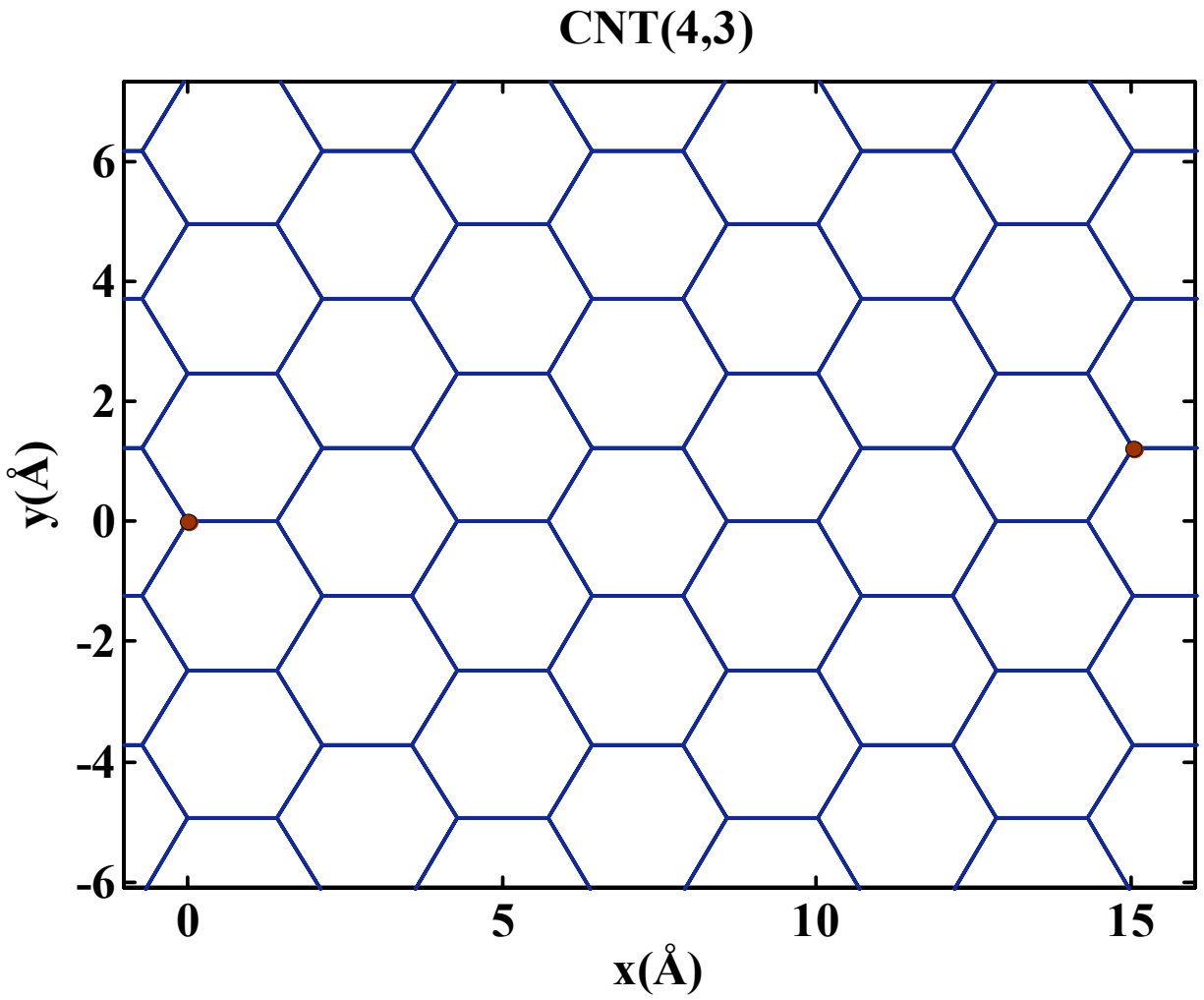

Figure 1.3: Schematic representation of the crystal lattice of a carbon nanotube with chiral vector (4,3).

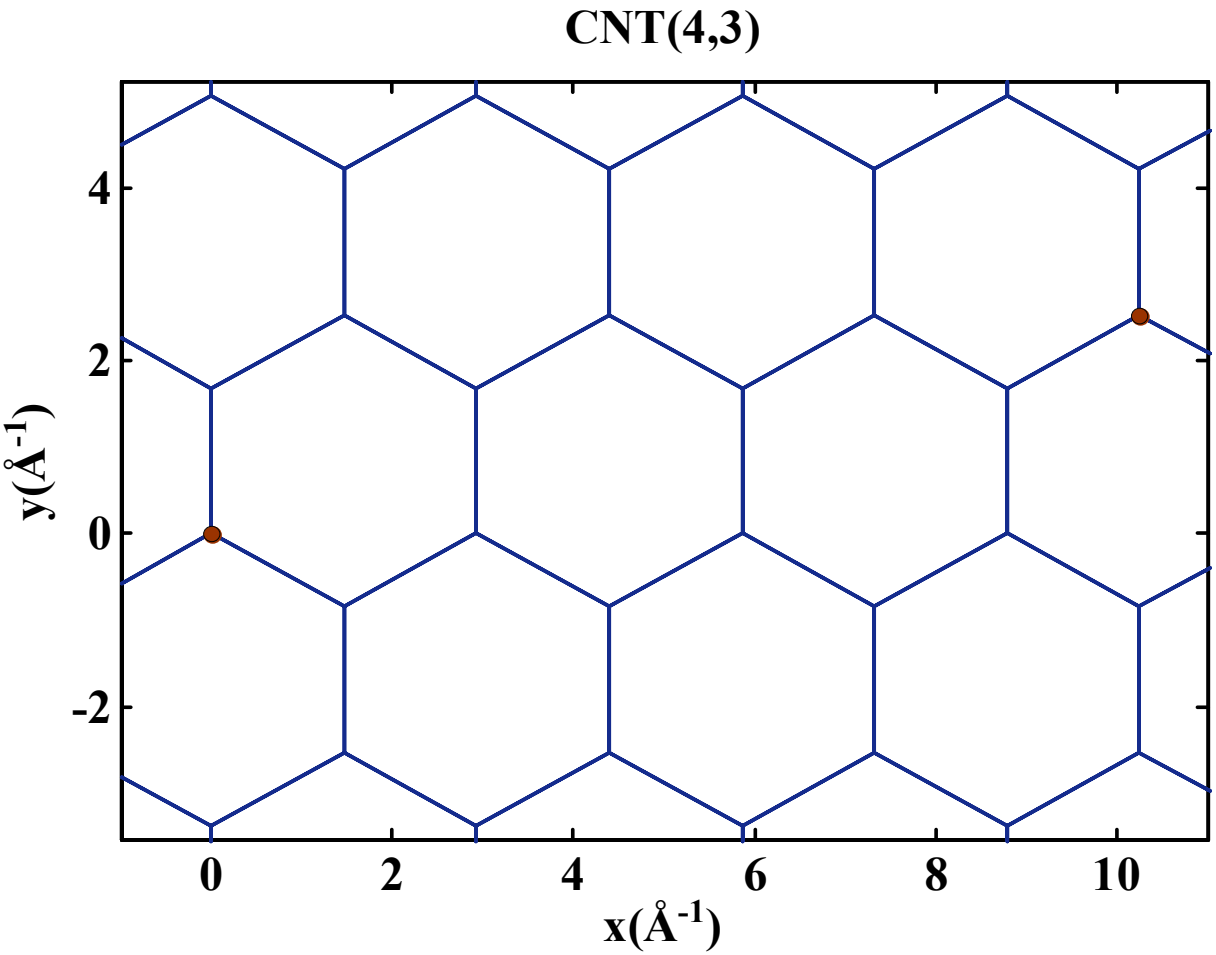

Figure 1.4: Schematic representation of the reciprocal lattice of a carbon nanotube with chiral vector (4,3).

where $V_{pp\pi}$ is the nearest neighbor transfer integral and K is the wave vector.

One-dimensional (1D) energy band can be adopted from Eq. (1.5) for single-walled carbon nanotubes (SWNTs) as follows [26]:

$$E_{1D}(k) = \pm V_{pp\pi}\left[1 + 4Cos\left(\frac{\sqrt{3}K_x}{2}a\right)Cos\left(\frac{K_y}{2}a\right) + 4Cos^2\left(\frac{K_y}{2}a\right)\right]^{1/2}, \tag{1.6}$$

where the wave vectors K_x and K_y are found using the relation,

$$\left(K_x, K_y\right) = \left(k\frac{K_2}{|K_2|} + qK1\right) \tag{1.7}$$

for $\left(-\frac{\pi}{|T|} < k < \frac{\pi}{|T|},\ and\ \ q = 1,...,N\right)$,

where k is the wave vector along the nanotube axis, $|T|$ is the magnitude of the translational vector and N is the number of hexagons within a unit cell. $|T|$ and N are given by [11],

$$|T| = \frac{\sqrt{3}\pi d_t}{d_R} \quad \text{and} \quad N = \frac{2\left(n^2 + nm + m^2\right)}{d_R}, \tag{1.8}$$

where d_R is the greatest common divisor of $(2n+m)$ and $(2m+n)$. In addition, K_1 and K_2 denote the allowed reciprocal wave vectors along the tube and circumference axis are given by [11,26]

$$K_1 = \frac{(2n+m)b_1 + (2m+n)b_2}{Nd_R} \quad \text{and} \quad K_2 = \frac{mb_1 - nb_2}{N}. \tag{1.9}$$

Equation (1.7) can be utilized to plot the allowed wave vectors in k-space as shown in Fig. 1.5. Each hexagon constitutes the size of the reciprocal lattice and each line represents an allowed K vector. Using the allowed K vectors, we can plot the energy band diagram in k-space from Eq. (1.6) as shown in Fig. 1.6.

1.6 Density of States

The k-vectors in momentum (k) space depend on vectors K_1 and K_2 as shown in Fig. 1.5.

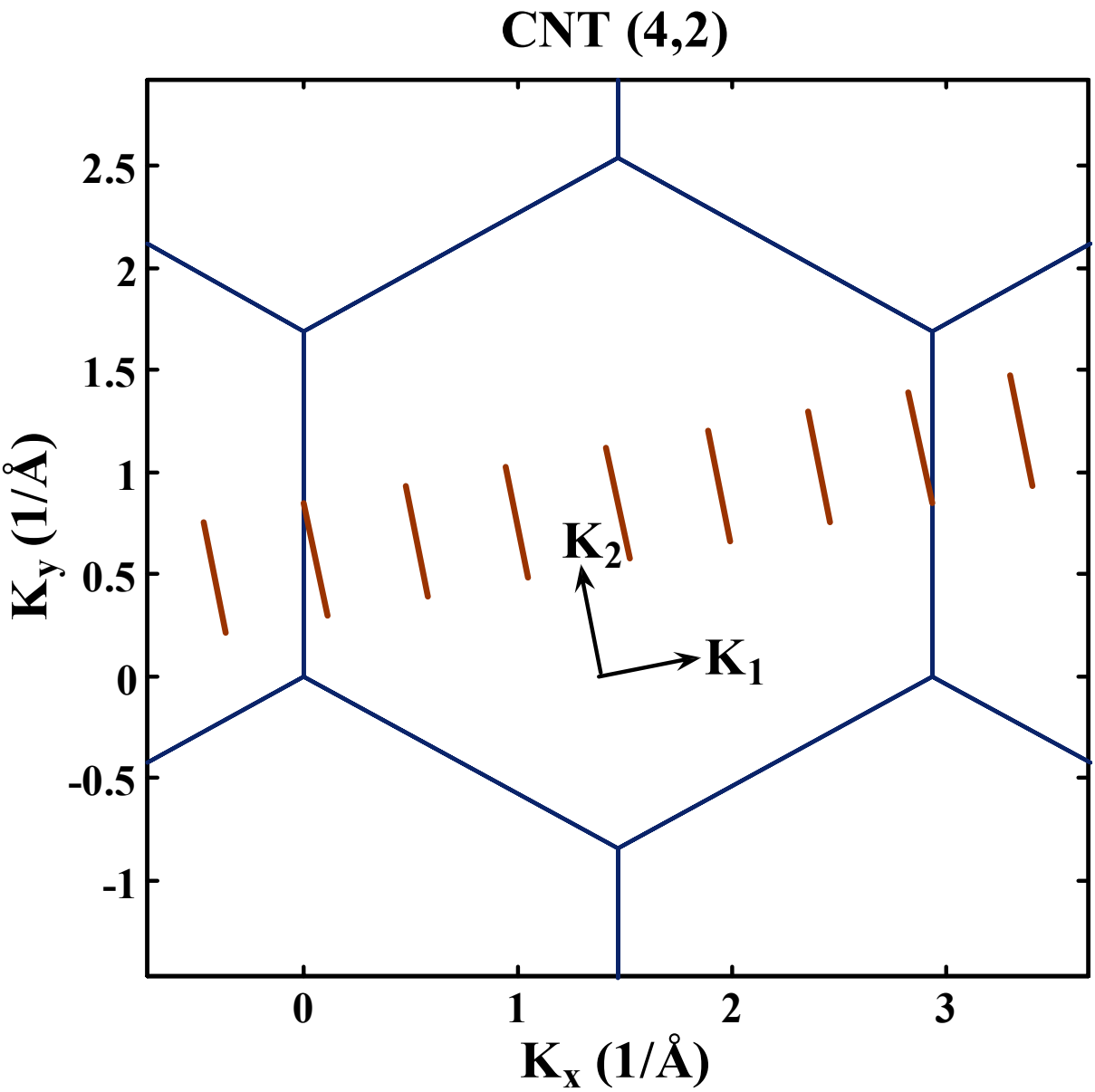

Figure 1.5: Plot of the allowed wave vectors in k-space for a CNT with chiral vector (4,2).

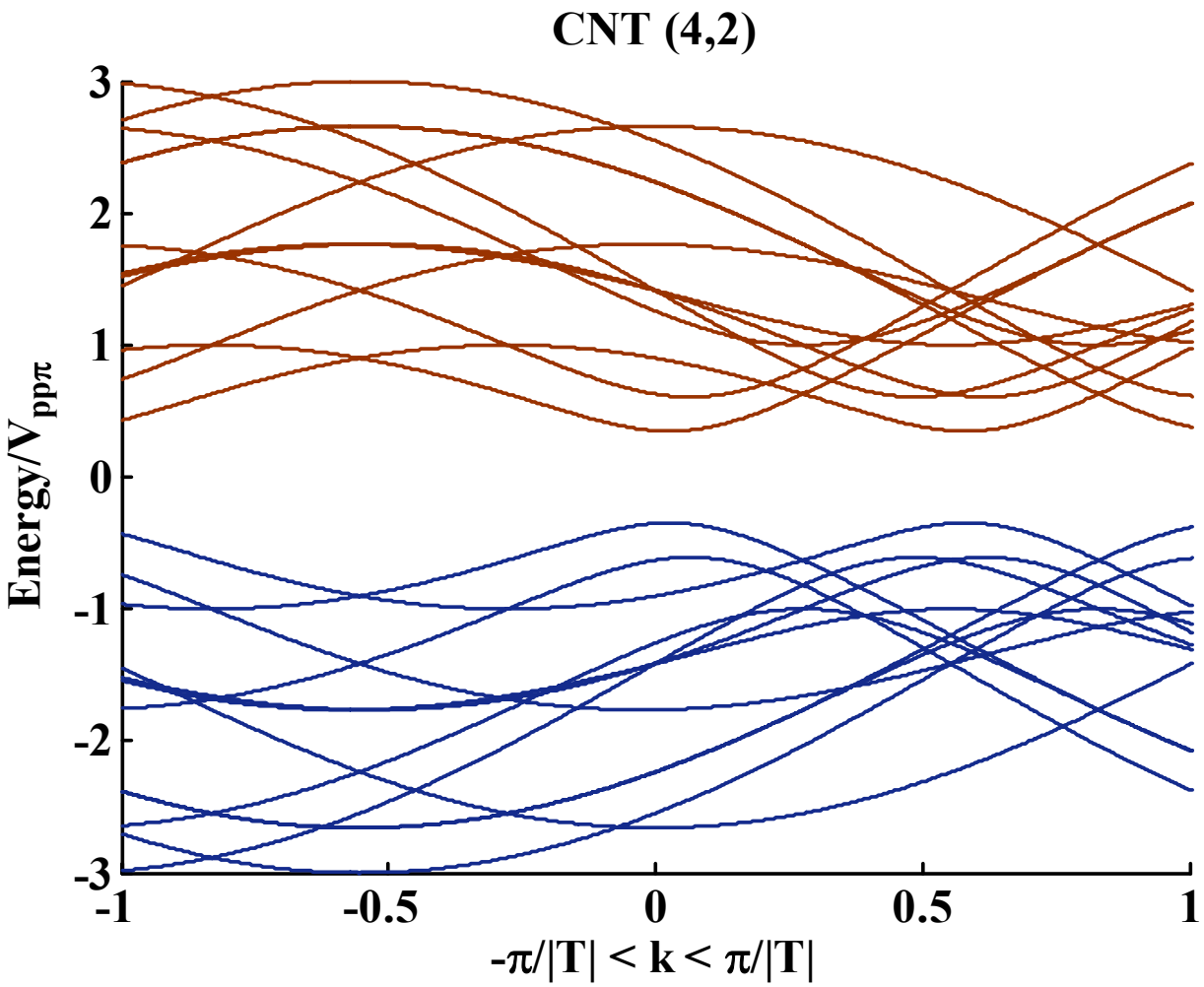

Figure 1.6: Plot of the energy band diagram in k-space for a CNT with chiral vector (4,2).

It is possible to represent the area in momentum space for a single state as, $A_p^{1-state} = \hbar^2 \left|K_1\right\|K_2\left|/2\right.$, and a differential area as, $dA_p = \hbar^2 \left|K_1\right| dk$, where *dk* is in the direction of K_2 and $\hbar$ is Planck's constant divided by 2π. As a result, the density of states per unit energy can be defined as follows [29-31]:

$$D(E)dE = 2\frac{dA}{A_p^{1-state}} = \frac{4}{\hbar^2 \left|K_1\right\|K_2\left|\right.} \hbar^2 \left|K_1\right| \frac{dk}{dE} dE = \frac{2\left|T\right|}{\pi} \left(\frac{dE}{dk}\right)^{-1} dE . \tag{1.10}$$

Equations (1.6) and (1.10) can be used to plot the density of states for any (n,m) carbon nanotube. Figure 1.7 shows a plot for a CNT (4,3). Each peak in Fig. 1.7 is called a Van Hove Singularity (VHS) and its respective energy represents a conduction energy-band minimum value. The total number of Van Hove Singularities is the number of bands a CNT has.

The density of states calculation shown in Fig. 1.7 requires usage of mathematical solving techniques due to the complexity and relationship of the variables. However, using an approximate energy dispersion relation calculated in [29,32,33] an equation for the 1D density of states of carbon nanotubes per unit length can be found as,

$$D(E)dE = \sum_i^{AllBands} \frac{4}{\pi V_{pp\pi} a\sqrt{3}} \frac{E}{\sqrt{E^2 - E_{c\min_i}^2}} dE , \tag{1.11}$$

where Ec_{min_i} is the energy conduction minimum for the given band. This minimum energy value is found using Fig. 1.7. Therefore, the density of states can be recalculated using Eq. (1.11); the approximate plot of the density of states is shown in Fig. 1.8. It is to be mentioned here that the density of states in Fig. 1.7 corresponds to a unit cell of a carbon nanotube.

1.7 Carbon Nanotube Field Effect Transistors (CNT-FETs)

Field effect transistors are devices where the current flow depends on the influence of an applied electric field. Devices such as the MOSFET achieve full conduction under the influence

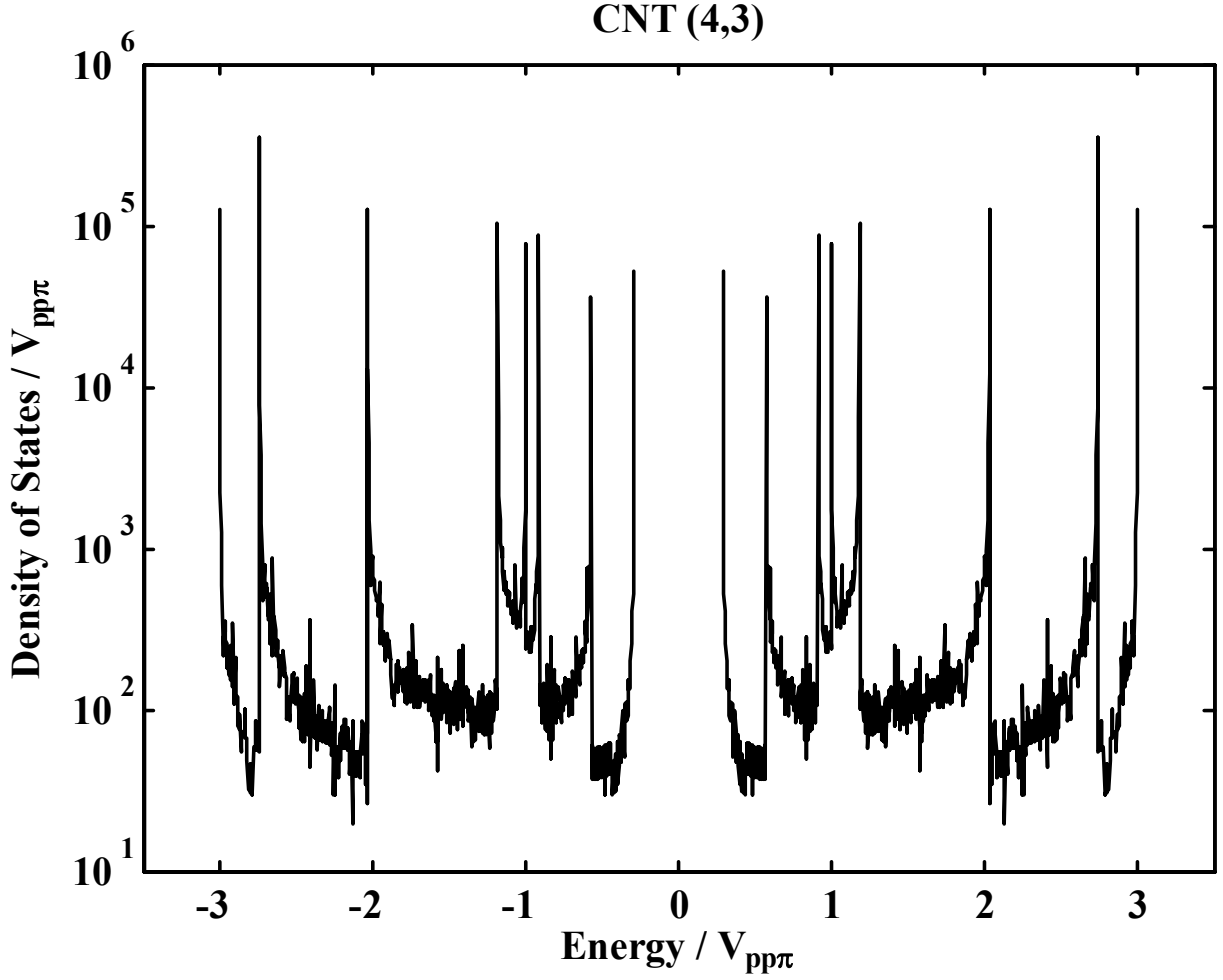

Figure 1.7: Plot of the density of states for a CNT with chiral vector (4,3).

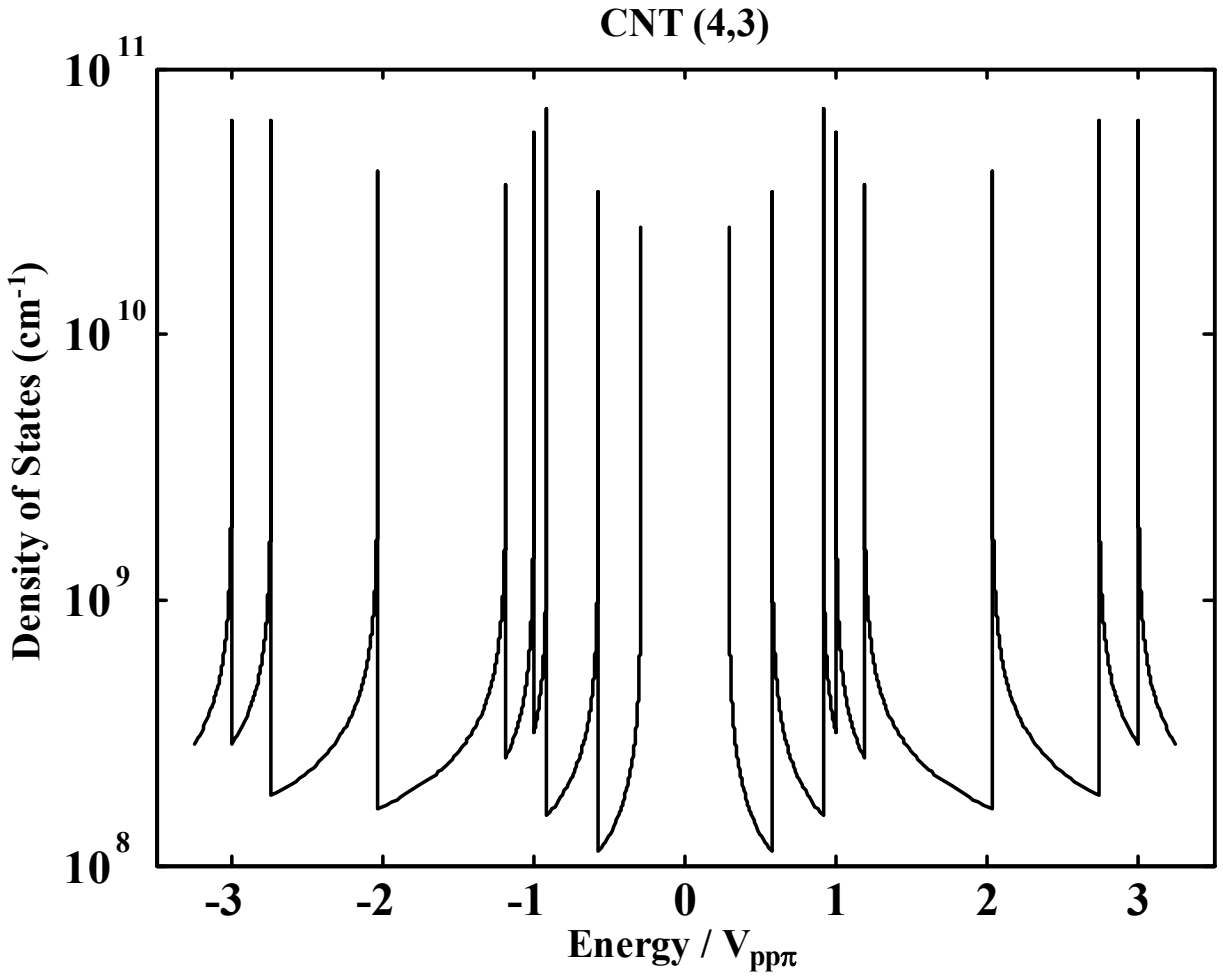

Figure 1.8: Plot of the density of states for a CNT with chiral (4,3) from the approximated equation (1.11).

of a gate voltage that causes an inverted channel underneath the gate oxide. Current can then flow between drain and source terminals. The CNT-FET works under the same principle, however, it achieves this operation by using a SWNT as the conducting channel between source and drain. The gate voltage varies the conductance of the SWNT and current can therefore flow between the drain and source. The basic structure of a CNT-FET is shown in Fig. 1.9 and the corresponding energy band diagram as a function of length (gate to substrate) is shown in Fig. 1.10.

1.7.1 Background of CNT-FETs

The first CNT-FETs were reported in 1998 by Dekker's group [34] and Martel et al. [14]. Such devices were fabricated using carbon nanotubes on top of SiO_2 and a Si-substrate that worked as a backgate, platinum (Pt) electrodes were used for the drain and the source terminals. The carbon nanotubes were produced by laser ablation synthesis and dispersed randomly on the SiO_2. This method showed poor characteristics since it was based on an undefined number of carbon nanotubes being bridged between the electrodes. Consequently, the use of chemical vapor deposition of methane on patterned substrate allowed the growth of carbon nanotubes being grown only in specific metallic catalyst islands [35].

Early CNT-FETs were fabricated on oxidized Si-substrates, the gate coupling was very poor due to the thick SiO_2 layer and back gate geometry [14,34]. In 2002, major improvement was observed after the implementation of CNT-FETs using top-gate geometry [8,36].

Transconductance of ~3.25 μS and subthreshold slope of ~130 mV/decade were observed. The transconductance was much higher in comparison to 0.3 μS of back gate geometry devices [37]. Further enhancement in performance was obtained by using a high *k*-dielectric [23] and electrolyte gating [38,39]. Javey et al., [23] reported the integration of top gated p-type CNT-FETs using the high *k*-dielectric material ZrO_2 ($k = 25$) as the gate oxide,

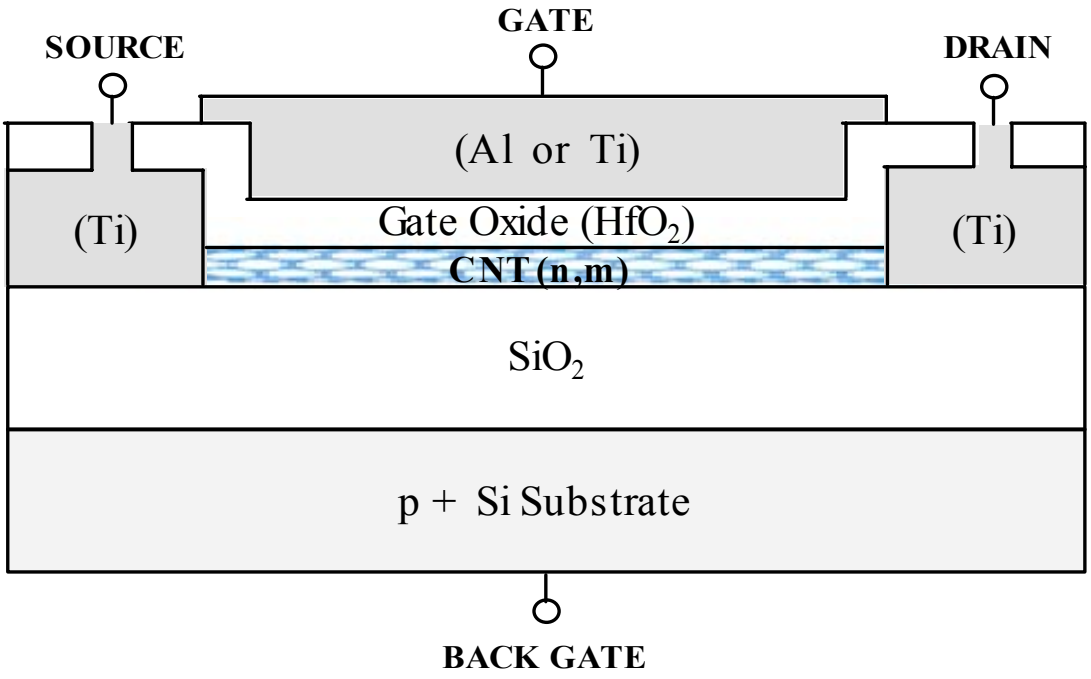

Figure 1.9: Cross-sectional view of a CNT-FET.

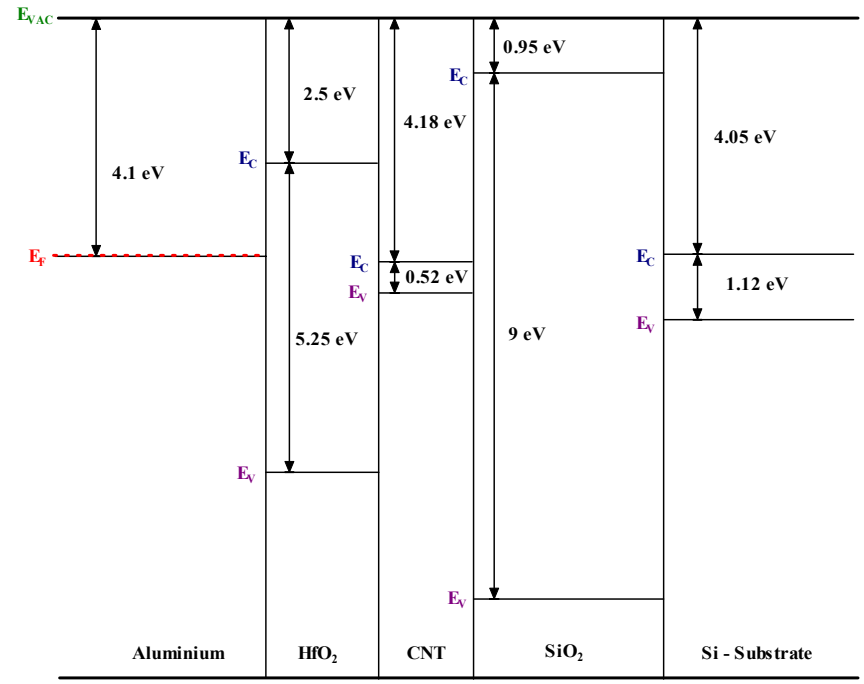

(a)

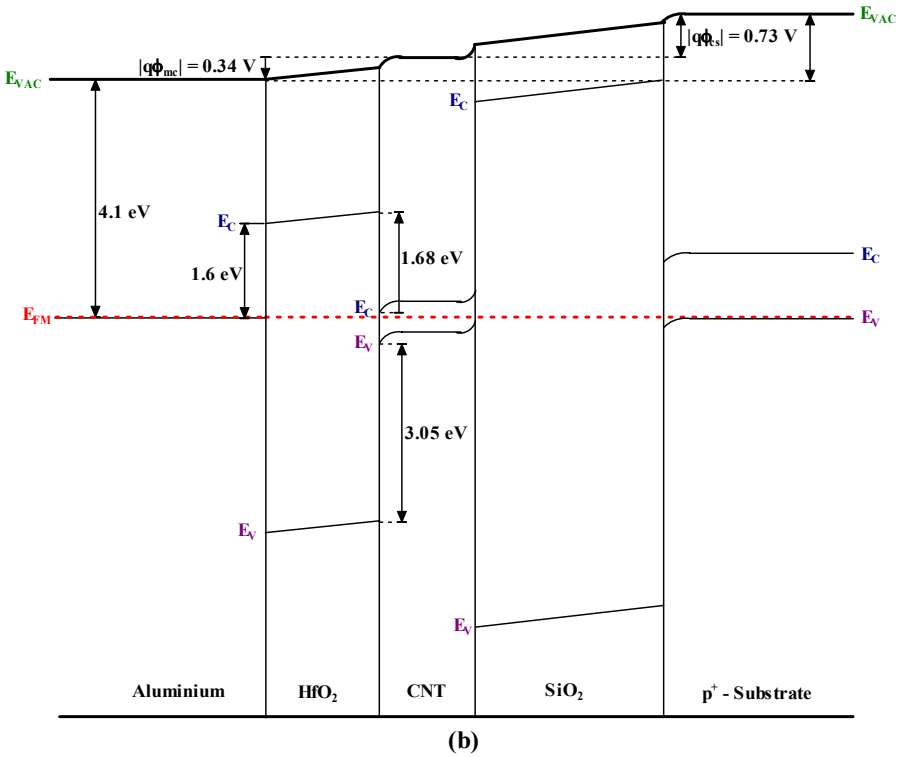

(b)

Figure 1.10: (a) Energy levels of the materials involved in manufacturing a CNT-FET and (b) energy band diagram at thermal equilibrium of a two terminal CNT-FET. Note: HfO_2 is the high *k*-dielectric hafnium oxide.

achieving a transconductance and subthreshold slope of 12 μS and 70 mV/decade, respectively. Electrolyte gating, first introduced by Kruger et al., [40] involves applying a voltage at the electrolyte gate, which creates an electrochemical potential between the electrolyte and the device. The leakage current between the electrolyte and the electrodes is negligible and the electrolyte behaves as an insulating liquid gate [38]. Subthreshold slopes of 80 mV/decade and hole mobilities of 1500 cm^2/Vsec were reported by Rosenblatt et al., [38]. Later on, hole mobilities of 2600 cm^2/Vsec and subthreshold slopes of 62 mV/decade were also reported [39].

Carbon nanotubes are conductors that fall in the ballistic operation regime [41], a feature of great interest for integrated circuits because of the long scattering lengths. Ballistic carbon nanotube have been demonstrated [12,42] and the reason behind the long scattering length is the low number of scattering events. Since carbon nanotubes are 1D conductors, there is a reduction of phase space for scattering [43] because only backscattering is possible [44,45], since only forward and backward propagation is allowed.

When CNT-FETs were first implemented, they showed a strong Schottky barrier at the electrode-nanotube interface [8,14] and current was mainly attributed to the modulation of the contact resistance at the electrode-nanotube interface rather than to the channel conductance [46]. Though characteristics of CNT-FETs resemble that of a typical MOSFET [47], the Schottky barrier still remains an important issue. Since the current is exponentially dependent, a small change in the bias voltages can cause dramatic unwanted variations in the current [48]. Nevertheless, recent improvements in fabrication of CNT-FETs have allowed the implementation of CNT-FETs with small, negative or no Schottky barriers [49-51]. Javey et al., [49] have used palladium (Pd) to eliminate the Schottky barrier for holes in the valence band in p-type CNT-FETs and Nosho et al., [50] have used calcium (Ca) to do the same for electrons in the conduction band for n-type CNT-FETs.

1.7.2 Fabrication

Carbon nanotube field effect transistors (CNT-FETs) can be fabricated with cross-sectional dimensions of the order of the quantum mechanical wavelength of electrons. Thus, the transport properties are influenced by quantum mechanical considerations and ballistic transport [52,53]. Since CNTs can be doped with n- or p-type impurities, both n- and p-type CNT-FETs have been fabricated [10,54]. The structure of a CNT-FET is similar to the structure of a typical MOSFET [7,55] where a SWNT forms the channel between two electrodes which work as the source and drain of the transistor. The structure is build on top of an insulating layer and silicon substrate which works as the back gate [14,36,56]. In the past decade, significant work on fabrication of CNT-FETs has been reported [8,14,37,55,57-59]. This includes n- and p-type CNT-FETs [50,51], multistage complementary logic gates [23,37,54,60,61], CNT-interconnections [62-64] and even SRAM cells [37].

The steps involved in fabricating a CNT-FET are as follows: the carbon nanotubes are grown using any of the methods described in Section 1.2. AFM* or TEM† is used to measure the diameter of the carbon nanotubes [65]. The catalyst pattern position is used as an alignment marker for the metal electrodes of the carbon nanotube; these metal electrodes are the source and drain contacts. Although gold (Au) or titanium (Ti) electrodes have been used, palladium (Pd) and calcium (Ca) electrodes are preferred [51] as they can remove or decrease the Schottky barriers at the drain and source contacts. The gate oxide (usually a high *k*-dielectric material as silicon nitride) [66] and the gate contacts are deposited. High *k*-dielectric materials have been employed [23] to increase the gate capacitance and gate coupling of the device.

It was mentioned above; the fabrication of n- and p-type CNT-FETs has been

* Atomic Force Microscopy.
† Transmission Electron Microscopy.

successfully achieved. When the first CNT-FETs were fabricated their I-V characteristics showed p-type behavior [34] implying a p-type doped carbon nanotube. The reason for p-type behavior was later explained by the absorption of oxygen [60,67,68], which changes the energy band level diagram at the CNT-electrode interface favoring the conduction of holes [69,70]. Consequently, n-type CNT-FETs were fabricated [55,70], Derycke et al., [70] showed the fabrication of n-type CNT-FET by annealing in vacuum for several minutes. N- and p-type CNT-FETs have also been fabricated from conventional doping. N-type devices have been fabricated [55] using potassium (K) as the donor agent and p-type devices have been fabricated [71] using boron (B) as the acceptor agent.

1.7.3 Characterization of CNT-FETs

With the advancement in fabrication technology of carbon nanotube field effect transistors, efforts have been made in modeling the transport behavior, including the models by Raychowdhury et al., [72], John et al., [73], and Guo et al., [74] and the semi-empirical SPICE compatible models for design of CNT-FET based logic devices [72,73,75-78]. Models for the high frequency behavior of CNT-FETs have also been implemented [52,79-81].

However, the current transport phenomenon in CNT-FET is not fully understood though a few additional models for characterizing the current transport in CNT-FETs have been reported based on measured device parameters [9,56,57,82]. These models, nevertheless, are still numerically based and include too many fitting parameters. This increases the complexity of simulation and limits both the compatibility with SPICE and the applicability in analysis and design of integrated circuits.

1.8 Scope of Research

In this dissertation, we first derive and analyze the carrier concentration of electrons in carbon nanotubes. A simplified density of states function for carbon nanotubes has been

experimentally demonstrated by Mintmire and White [32]. We have used these results in Chapter 2 to analytically derive the carrier concentration in carbon nanotubes. The intrinsic carrier concentration and doping effects are investigated for different carbon nanotubes. Results for varying diameters and wrapping angles are also presented.

In Chapter 3, we utilize basic physical properties of field effect transistors [83,84] and our work on carrier concentration of carbon nanotubes [85] to present analytical modeling equations describing the current transport in CNT-FETs. I-V characteristics for normal and subthreshold operation are demonstrated and their dependence on the chiral vectors and device geometries are investigated.

In deriving the I-V characteristics of CNT-FETs, analytical model equations for threshold voltage (V_{th}) and saturation voltage ($V_{ds,sat}$) are each derived in the process. In Chapter 4, these derivations are investigated in much greater detail and the respective correlation to the chiral vectors and device geometry of CNT-FETs is demonstrated.

In the remaining chapters, we focus on the applications of our derived modeled equations. In Chapter 5, the results obtained from the I-V characteristics are used to generate voltage transfer characteristics of basic logic devices based on complementary CNT-FETs. In Chapter 6, we use our small signal equivalent circuit model [86,87] and current transport model equations [86-88] for CNT-FETs to study and analyze the frequency response of CNT-FETs and CNT-based logic devices and to establish a dependence on the chiral vectors and device geometry making predictions for very high frequency behavior in integrated circuit applications.

In Chapter 7, the bio-sensing applications of SWNTs and CNT-FETs at molecular levels are reviewed involving applications in detecting traces of chemical vapors and gases such as nerve agents and explosive components [89-93]. Our presented current transport model

equations are utilized to provide a better understanding to reactions taking place in CNT and CNT-FET sensors when exposed to traces of bio- and chemical sensing agents for the detection of traces of agents at molecular levels.

Conclusion and future scope for further advancement of research conducted are summarized in Chapter 8. Appendix A provides a solution of the integral used in Chapter 2. Appendix B shows a detailed derivation of the analytical expressions for the carbon nanotube surface potential. Appendix C provides a complete list of the model parameters. Appendix D shows a copyright permission for Fig. 1.2. Appendix E summarizes a list of published/communicated research work.

1.9 References

[1] R. Bacon, "Growth, structure, and properties of graphite whiskers," *Journal of Applied Physics,* vol. 31, pp. 283-290, February 1960.

[2] A. Oberlin, M. Endo, and T. Koyama, "Filamentous growth of carbon through benzene decomposition," *J. Crystal Growth,* vol. 32, pp. 335-349, March 1976.

[3] H. W. Kroto, J. R. Heath, S. C. O'Brien, R. F. Curl, and R. E. Smalley, "C60: Buckminsterfullerene," *Nature,* vol. 318, pp. 162-163, 1985.

[4] S. Iijima, "Helical microtubules of graphitic carbon," *Nature,* vol. 354, pp. 56-58, November 1991.

[5] D. S. Bethune, C. H. Kiang, M. S. de Vries, G. Gorman, R. Savoy, J. Vazquez, and R. Beyers, "Cobalt-catalysed growth of carbon nanotubes with single-atomic-layer walls," *Nature,* vol. 363, pp. 605-607, June 1993.

[6] S. Iijima and T. Ichihashi, "Single shell carbon nanotubes of 1-nm diameter," *Nature,* vol. 363, June 1993.

[7] H. S. P. Wong, "Field effect transistors - from silicon MOSFETs to carbon nanotube FETs," *Proc. 23th International Conference on Microelectronics, (MIEL)*, vol. 1, pp. 103-107, 2002.

[8] J. Guo, S. Datta, M. Lundstrom, M. Brink, P. McEuen, A. Javey, H. Dai, H. Kim, and P. McIntyre, "Assessment of silicon MOS carbon nanotube FET perfomance limits using a general theory of ballistic transistors," *IEDM Technical Digest,* pp. 711-714, December 2002.

[9] S. J. Wind, J. Appenzeller, R. Martel, V. Derycke, and P. Avouris, "Vertical scaling of carbon nanotube field-effect transistors using top gate electrodes," *Applied Physics Letters,* vol. 80, pp. 3817-3819, 2002.

[10] H. Dai, "Carbon nanotubes: Synthesis, integration, and properties," *Accounts of Chemical Research,* vol. 35, pp. 1035-1044, August 2002.

[11] R. Saito, M. S. Dresselhaus, and G. Dresselhaus, *Physical Properties of Carbon Nanotubes*. London: Imperial College Press, 1998.

[12] P. L. McEuen, M. Bockrath, D. H. Cobden, Y.-G. Yoon, and S. G. Louie, "Disorder, pseudospins, and backscattering in carbon nanotubes," *Applied Physics Letters,* vol. 83, pp. 5098-5101, June 1999.

[13] M. S. Dresselhaus, G. Dresselhaus, and P. Avouris, *Carbon Nanotube: Synthesis, Properties, Structure, and Applications*: Springer Verlag, 2001.

[14] R. Martel, T. Schmidt, H. R. Shea, T. Hertel, and P. Avouris, "Single and multi wall carbon nanotube field effect transistors," *Applied Physics Letters,* vol. 73, pp. 2447-2449, October 1998.

[15] H. Takikawa, M. Yatsuki, T. Sakakibara, and S. Itoh, "Carbon nanoubes in cathodic vacuum are discharge," *Journal of Physics: Applied Physics,* vol. 33, pp. 826-830, 2000.

[16] C. D. Scott, S. Arepalli, P. niklaev, and R. E. Smalley, "Growh mechanism for single-wall carbon nanotubes in a laser-ablation process," *Applied Physics Letters A,* vol. 72, pp. 573-580, 2001.

[17] P. Nikolaev, M. J. Bronikowski, R. K. Bradley, F. Rohmund, D. T. Colbert, and K. A. S. E. Smalley, "Gas-phase catalytic growth of single-walled carbon nanotubes from carbon monoxide," *Chemical Physics Letters,* vol. 313, pp. 91-97, 1999.

[18] M. Jose-Yacaman, M. Miki-Yoshida, L. Rendon, and J. G. Santiesteban, "Catalytic growth of carbon microtubules with fullerene structure," *Applied Physics Letters,* vol. 62, pp. 657-659, 1993.

[19] R. L. V. Wal, L. J. Hal, and G. M. Berger, "Optimization of flame synthesis for carbon nanotubes using supported catalyst," *Journal of Physical Chemistry B,* vol. 106, pp. 13122-13132, 2002.

[20] R. L. V. Wal, G. M. Berger, and L. J. Hall, "Single-walled carbon nanotube synthesis via a multi stage flame configuration," *Journal of Physical Chemistry B,* vol. 106, pp. 3564-3567, 2002.

[21] F. Xu, X. Liu, and S. Tse, "Synthesis of carbon nanotubes in alloy substrates with voltages bias in methane inverse diffusion flames," *Carbon,* vol. 44, pp. 570-577, 2006.

[22] R. L. Vander-Wal and T. M. Ticich, "Flame and furnace synthesis of single-walled and multi-walled carbon nanotubes and nanofibers," *Journal of Physical Chemistry B,* vol. 105, pp. 10249-10256, 2001.

[23] A. Javey, H. Kim, M. Brink, Q. Wang, A. Ural, J. Guo, P. Mcientyre, P. McEuen, M. Lundstrom, and H. Dai, "High k-dielectric for advanced carbon nanotube transistors and logic gates," *Nature Materials,* vol. 1, pp. 241-246, November 2002.

[24] A. Loiseau, P. Launois, P. Petit, S. Roche, and J. P. Salvetat, *Understanding Carbon Nanotubes*. Berlin Heidelberg: Springer, 2006.

[25] J. Wildoer, L. Venema, A. Rinzler, R. Smalley, and C. Dekker, "Electronic structure of atomically resolved carbon nanotubes," *Nature,* vol. 391, pp. 59-62, January 1998.

[26] R. Saito, G. Dresselhaus, and M. S. Dresselhaus, "Trigonal warping effect of carbon nanotubes," *Physical Review Letters B,* vol. 61, pp. 2981-2990, January 2000.

[27] C. T. White and J. W. Mintmire, "Density of states reflects diameter in nanotubes," *Nature (London),* vol. 394, pp. 29-30, 1998.

[28] K. Tanaka, T. Yamabe, and K. Fukui, *The Science and Technology of Carbon Nanotubes*. Amsterdam: Elsevier, 1999.

[29] J. P. McKelvey, *Solid States Physics for Engineering and Material Sciences*. Florida: Krieger Publishing Company, 1993.

[30] S. N. Levine, *Quantum Physics of Electronics*. New York: The Macmillan Company, 1965.

[31] D. Griffiths, *Introduction to Quantum Mechanics*. Uper Saddle River, NJ: Prentice Hall, Inc., 1995.

[32] J. W. Mintmire and C. T. White, "Universal density of states for carbon nanotubes," *Physical Review Letters,* vol. 81, pp. 2506-2509, September 1998.

[33] J. Guo, M. Lundstrom, and S. Datta, "Performance projections for ballistic carbon nanotube field-effect transistors," *Applied Physics Letters,* vol. 80, pp. 3192-31942, April 2002.

[34] S. J. Tans, A. R. M. Vershueren, and C. Dekker, "Room-temperature transistor based on a single carbon nanotube," *Nature,* vol. 393, pp. 49-52, May 1998.

[35] J. Kong, H. T. Soh, A. M. Cassell, C. F. Quate, and H. Dai, "Synthesis of individual single-walled carbon nanotubes on patterned silicon wafers," *Nature,* vol. 395, pp. 878-881, October 1998.

[36] S. J. Wind, J. Appenzeller, R. Martel, V. Derycke, and P. Avouris, "Fabrication and electrical characterization of top gate single-wall CNFETs," *Journal of Vacuum Science and Technology B,* vol. 20, pp. 2798-2801, 2002.

[37] A. Bachtold, P. Hadley, T. Nakanishi, and C. Dekker, "Logic circuits with carbon nanotube transistors," *Science,* vol. 294, pp. 1317-1320, November 2001.

[38] S. Rosenblatt, Y. Yaish, J. Park, J. Gore, V. Sazonova, and P. L. McEuen, "High performance electrolyte gated carbon nanotube transistors," *Nano Letters,* vol. 2, pp. 869-872, June 2002.

[39] G. P. Siddons, D. Merchin, J. H. Back, J. K. Jeong, and M. Shim, "High efficient gating and doping of carbon nanotubes with polymer electrolytes," *Nano Letters,* vol. 4, pp. 927-931, May 2004.

[40] M. Krüger, M. R. Buitelaar, T. Nussbaumer, and C. Schönenberger, "Electrochemical carbon nanotube field-effect transistor," *Applied Physics Letters,* vol. 78, pp. 1291-1293, February 2001.

[41] P. L. McEuen, "Single-wall carbon nanotubes," *Physics World,* vol. 13, pp. 31-36, June 2000.

[42] S. Franck, P. Poncharal, Z. L. Wang, and W. A. de Heer, "Carbon nanotube quantum resistors," *Science,* vol. 280, pp. 1744-1746, June 1998.

[43] P. McEuen, M. S. Fuhrer, and H. Park, "Single-walled carbon nanotube electronics," *IEEE Transactions on Nanotechnology,* vol. 1, pp. 78-85, March 2002.

[44] Z. Yao, C. L. Kane, and C. Dekker, "High-field electrical transport in single-wall carbon nanotubes," *Physical Review Letters,* vol. 84, pp. 2941-2944, March 2000.

[45] T. Ando, H. Matsumura, and T. Nakanishi, "Theory of ballistic transport in carbon nanotubes," *Physica B,* vol. 323, pp. 44-50, April 2002.

[46] S. Heinze, J. Tersoff, R. Martel, V. Derycke, J. Appenzeller, and P. Avouris, "Carbon nanotubes as Schottky barrier transistors," *Physical Review Letters,* vol. 89, p. 106801, September 2002.

[47] P. Avouris, J. Appenzeller, R. Martel, and S. J. Wind, "Carbon nanotube electronics," *Proceedings of the IEEE*, vol. 91, pp. 1772-1784, 2003.

[48] B. G. Streetman, *Solid State Electronic Devices*, 5th Ed. India: Prentice Hall, 2000.

[49] A. Javey, J. Guo, Q. Wang, M. Lundstron, and H. Dai, "Ballistic carbon nanotube field effect transistors," *Nature,* vol. 424, pp. 654-657, August 2003.

[50] Y. Nosho, Y. Ohno, S. Kishimoto, and T. Mizutani, "N-type carbon nanotube field-effect transistors fabricated by using Ca contact electrodes," *Applied Physics Letters,* vol. 86, pp. 073105-073107, February 2005.

[51] A. Javey, Q. Wang, W. Kim, and H. Dai, "Advancements in complementary carbon nanotube field-effect transistors," *IEDM Technical Digest,* pp. 31.2.1-31.2.4, December 2003.

[52] P. J. Burke, "AC performance of nanoelectronics: towards a ballisitic THz nanotube transistor," *Solid State Electronics,* vol. 48, pp. 1981-1986, June 2004.

[53] A. Akturk, G. Pennington, and N. Goldsman, "Quantum modeling and proposed designs of CNT-embedded nanoscale MOSFETs," *IEEE Transactions on Electron Devices,* vol. 52, pp. 577-584, April 2005.

[54] A. Javey, Q. Wang, A. Ural, Y. Li, and H. Dai, "Carbon nanotube transistors arrays for multistage complementary logic and ring oscillators," *Nano Letters,* vol. 2, pp. 929-932, July 2002.

[55] A. Javey, R. Tu, D. B. Farmer, J. Guo, R. G. Gordon, and H. Dai, "High performance n-type carbon nanotube field-effect transistors with chemically doped contacts," *Nano Letters,* vol. 5, pp. 345-348, January 2005.

[56] F. Nihey, H. Hongo, Y. Ochiai, M. Yudasaka, and S. Iijima, "Carbon-nanotube field effect transistors with very high intrinsic transconductance," *Japanese Journal of Applied Physics,* vol. 42, pp. L1288-L1291, October 2003.

[57] F. Nihey, H. Hongo, M. Yudasaka, and S. Iijima, "A top-gate carbon –nanotube field-effect transistor with a titanium-dioxide insulator," *Japan Journal of Applied Physics,* vol. 41, pp. L1049-L1051, October 2002.

[58] J. Li, Q. Zhang, D. Yang, and J. Tian, "Fabrication of carbon nanotube field effect transistors by AC dielectrophoresis method," *Carbon,* vol. 42, pp. 2263-2267, June 2004.

[59] A. Javey, J. Guo, D. B. Farmer, Q. Wang, D. Wang, R. G. Gordon, M. Lundstrom, and H. Dai, "Carbon nanotube field-effect transistors with integrated ohmic contacts and high-k gate dielectrics," *Nano Letters,* vol. 4, pp. 447-450, February 2004.

[60] V. Derycke, R. Martel, J. Appenzeller, and P. Avouris, "Carbon nanotube inter- and intramolecular logic gates," *Nano Letters,* vol. 1, pp. 453-456, September 2001.

[61] R. Martel, V. Derycke, J. Appenzeller, S. Wind, and P. Avouris, "Carbon nanotube field effect transistors and logic circuits," *Proc. 39th Design Automation Conference*, pp. 94-98, 2002.

[62] A. Raychowdhury and K. Roy, "Modeling of metallic carbon-nanotube interconnects for circuit simulations and a Comparison with Cu interconnects for scaled technologies," *IEEE Transactions on Computer-Aided Design of Integrated Circuits and Systems,* vol. 25, pp. 58-65, January 2006.

[63] N. Srivastava, R. V. Joshi, and K. Banerjee, "Carbon nanotube interconnects: implications for performance, power dissipation, and thermal management," *IEDM Technical Digest,* pp. 249-252, December 5-7 2005.

[64] J. Y. Park, S. Rosenblatt, Y. Yaish, V. Sazonova, H. Üstünel, S. Braig, T. A. Arias, P. W. Brouwer, and P. L. McEuen, "Electron phonon scattering in metallic single walled carbon nanotubes," *Nano Letters,* vol. 4, pp. 517-520, 2004.

[65] C. L. Cheung, A. Kurtz, H. Park, and C. M. Lieber, "Diameter-controlled synthesis of carbon nanotubes," *Journal of Physical Chemistry B,* vol. 106, pp. 2429-2433, February 2002.

[66] S. Li, Z. Yu, and P. J. Burke, "Silicon nitride gate dielectric for top-gated carbon nanotube field effect transistors," *Journal of Vacuum Science and Technology B,* vol. 22, pp. 3112-3114, December 2004.

[67] P. G. Collins, K. Bradley, M. Ishigami, and A. Zettl, "Extreme oxygen sensitivity of electronic properties of carbon nanotubes," *Science,* vol. 287, pp. 1801-1804, March 2000.

[68] G. U. Sumanaskera, C. K. W. Adu, S. Fang, and P. C. Eklund, "Effects of gas adsorption and collisions on electrical transport in single-walled carbon nanotubes," *Physical Review Letters,* vol. 85, pp. 1096-1099, July 2000.

[69] R. Martel, V. Derycke, C. Lavoie, J. Appenzeller, K. K. Chan, J. Tersoff, and P. Avouris, "Ambipolar electrical transport in semiconducting single-wall carbon nanotubes," *Physical Review Letters,* vol. 87, p. 256805, December 2001.

[70] V. Derycke, R. Martel, J. Appenzeller, and P. Avouris, "Controlling doping and carrier injection in carbon nanotube transistors," *Applied Physics Letters,* vol. 80, pp. 2773-2775, April 2002.

[71] W. Han, Y. Bando, K. Kurashima, and T. Sato, "Boron-doped carbon nanotubes prepared through a substitution reaction," *Chemical Physics Letters,* vol. 299, pp. 368-373, 1999.

[72] A. Raychowdhury, S. Mukhopadhyay, and K. Roy, "A circuit-compatible model of ballistic carbon nanotube field effect transistors," *IEEE Transactions on Computer-Aided Design of Integrated Circuits and Systems,* vol. 23, pp. 1411-1420, October 2004.

[73] D. L. John, L. C. Castro, J. P. Clifford, and D. L. Pulfrey, "Electrostatic of coaxial Schottky barrier nanotube field effect transistors," *IEEE Transactions on Nanotechnology,* vol. 2, pp. 175-180, September 2003.

[74] J. Guo, S. Goasguen, M. Lundstrom, and S. Datta, "Metal-insulator-semiconductor electrostatics of carbon nanotubes," *Applied Physics Letters,* vol. 81, pp. 1486-1488, August 2002.

[75] C. Dwyer, M. Cheung, and D. J. Sorin, "Semi-empirical SPICE models for carbon nanotube FET logic," *Proc. 4th IEEE Conference on Nanotechnology*, pp. 386-388, 2004.

[76] A. Raychowdhury and K. Roy, "Carbon nanotube based voltage-mode multiple-valued logic design," *IEEE Transactions on Nanotechnology,* vol. 4, pp. 168 - 179, March 2005.

[77] I. O'Connor, J. Liu, F. Gaffiot, F. Prégaldiny, C. Lallement, C. Maneux, J. Goguet, S. Frégonèse, T. Zimmer, L. Anghel, T.-T. Dang, and R. Leveugle, "CNTFET modeling and reconfigurable logic circuit design," *IEEE Transactions on Circuits and Systems, Part-1,* vol. 54, pp. 2365-2379, November 2007.

[78] A. Hazeghi, T. Krishnamohan, and H.-S. P. Wong, "Schottky-barrier carbon nanotube field effect transistor modeling," *IEEE Transactions on Electron Devices,* vol. 54, pp. 439-445, March 2007.

[79] P. J. Burke, "An RF circuit model for carbon nanotubes," *IEEE Transactions on Nanotechnology,* vol. 2, pp. 55-58, March 2003.

[80] L. C. Castro and D. L. Pulfrey, "Extrapolated f_{max} for Carbon Nanotube FETs," *Nanotechnology,* vol. 17, pp. 300-304, December 2006.

[81] L. C. Castro, D. L. Pulfrey, and D. L. John, "High-frequency capability of Schottky-barrier carbon nanotube FETs," *Solid-State Phenomena,* vol. 121-123, pp. 693-696, March 2007.

[82] J. W. Park, J. B. Choi, and K.-H. Yoo, "Formation of a quantum dot in a single-walled carbon nanotube using the Al top-gates," *Applied Physics Letters,* vol. 81, pp. 2644-2646, September 2002.

[83] Y. Tsividis, *Operation and Modeling of the MOS transistor*. Singapore: McGraw-hill, 1999.

[84] P. Antognetti and G. Massobrio, *Semiconductor Device Modeling with SPICE*. Singapore: McGraw-Hill, 1988.

[85] J. M. Marulanda and A. Srivastava, "Carrier density and effective mass calculations for carbon nanotubes," *Proc. International Conference on Integrated Circuit Design & Technology (ICICDT)*, Austin, TX, pp. 234-237, 2007.

[86] J. M. Marulanda, A. Srivastava, and R. K. Nahar, "Ultra-high frequency modeling of carbon nanotube field-effect transistors," *Proc. 13th International Workshop on the Physics of Semiconductor Devices (IWPSD)*, New Delhi, pp. G-11, 2005.

[87] J. Marulanda, A. Srivastava, and A. K. Sharma, "Transfer characteristics and high frequency modeling of logic gates using carbon nanotube field effect transistors (CNT-FETs)," *Proc. of The 20th Annual Conference on Integrated Circuits and Systems Design*, Rio de Janeiro, Brazil, pp. 202-206, 2007.

[88] J. Marulanda, A. Srivastava, and A. K. Sharma, "Current transport modeling in carbon nanotube field effect transistors (CNT-FETs) and bio-sensing applications," *Proc. SPIE Smart Structures and Materials & Nondestructive Evaluation and Health Monitoring: Nanosensors and Microsensors for Bio-System*, vol. 6931, pp. 693108-1-693108-12, San Diego, CA, 2008.

[89] J. P. Novak, E. S. Snow, E. J. Houser, D. Park, J. L. Stepnowski, and R. A. McGill, "Nerve agent detection using networks of single-walled carbon nanotubes," *Applied Physics Letters,* vol. 83, pp. 4026-4028, November 2003.

[90] E. S. Snow, F. K. Perkins, E. J. Houser, S. C. Badescu, and T. L. Reinecke, "Chemical detection with a single-walled carbon nanotube capacitor," *Science,* vol. 307, pp. 1942-1945, March 2005.

[91] P. Qi, O. Vermesh, M. Grecu, A. Javey, Q. Wang, H. Dai, S. Peng, and K. J. Cho, "Toward large arrays of multiplex functionalized carbon nanotube sensors for highly sensitive and selective molecular detection," *Nano Letters,* vol. 3, pp. 347-351, January 2003.

[92] C. Staii, Johnson, Jr., A. T., M. Chen, and A. Gelperin, "DNA-decorated carbon nanotubes for chemical sensing," *Nano Letters,* vol. 5, pp. 1774-1778, August 2005.

[93] A. Star, T. R. Han, V. Joshi, J. C. P. Gabriel, and G. Grüner, "Nanoelectronic carbon dioxide sensors," *Advanced Materials,* vol. 16, pp. 2049-2052, November 2004.

CHAPTER 2

CARRIER DENSITY AND EFFECTIVE MASS CALCULATIONS IN CARBON NANOTUBES*

2.1 Introduction

Since the discovery of carbon nanotubes in 1991 [1], significant amount of research has been conducted to study its electronic properties [2-5]. Carbon nanotubes are being predicted to be the future material to substitute silicon used in CMOS technology at the end of Moore's law [6-8]. As it was explained in Chapter 1 carbon nanotubes are one-dimensional (1D) graphene sheets rolled into a tubular form [9]. Their electronic properties depend on its diameter and wrapping angle [2], which are represented by the indices (n,m) defined in the chiral vector characterizing each carbon nanotube. The electronic structure and electrical properties have been theoretically studied [3,10] based on the band theory of graphite [11,12] and have also been established experimentally [2]. The density of states has also been calculated [13,14] and is directly related to the chiral vector of the carbon nanotube [15].

Though applications of carbon nanotubes have increased over the past decade, very little work has been performed on modeling the carrier concentration. Recently, Raychowdhury et al., [16] have presented equations for the carrier concentration in carbon nanotubes in an attempt to calculate the inside charge. However, their model uses numerical curve fitting techniques. In this chapter, we have used the density of states function of Mintmire and White [14] to derive analytical equations, which predict the carrier concentration in carbon nanotubes.

* Part of the work is reported in the following publication:

1. J. M. Marulanda and A. Srivastava, "Carrier density and effective mass calculations for carbon nanotubes," *Proc. International Conference on Integrated Circuit Design and Technology*, pp. 234-237 (Austin, Texas, May 30th – June 1st, 2007).
2. J. M. Marulanda, A. Srivastava, "Carrier density and effective mass calculations in carbon nanotubes," *physica status solidi (a)*, 2008 (in press).

2.1.1 Energy Dispersion Relation

The energy dispersion relation in carbon nanotubes is calculated from the electronic structure of graphene [17,18]. The one-dimensional energy dispersion relation for single walled carbon nanotubes (SWNTs) is given by [19-21],

$$E_{1D}(k) = \pm V_{pp\pi}\left[1 + 4Cos\left(\frac{\sqrt{3}K_x}{2}a\right)Cos\left(\frac{K_y}{2}a\right) + 4Cos^2\left(\frac{K_y}{2}a\right)\right]^{1/2}, \tag{2.1}$$

where $V_{pp\pi}$ is the nearest neighbor overlap integral between carbon - carbon (C-C) atoms used in tight binding calculations of the carbon nanotube. In the present research, we have used $V_{pp\pi} = 2.5\ eV$ [17]. K_x and K_y are the wave vectors of carbon nanotubes [17,18].

2.1.2 Density of States

Numerical techniques are needed to compute the density of states from Eq. (2.1) due to its complexity. However, an approximate density of states calculation has already been found for carbon nanotubes [14,22] and is described as follows,

$$D(E)dE = 2\sum_{i}^{AllBands}\frac{4}{\pi V_{pp\pi}a\sqrt{3}}\frac{E}{\sqrt{E^2 - E_{c\min_i}^2}}dE, \tag{2.2}$$

where Ec_{min_i} is the minimum energy value for the given conduction band. Ec_{min_i} is found by determining the energy minimum value for the respective conduction band using Eq. (2.1). The first conduction band, Ec_{min} can also be obtained from the following approximated equation [17]:

$$E_{c_{\min}} = \frac{E_g}{2} = \frac{aV_{pp\pi}}{d\sqrt{3}}, \tag{2.3}$$

where d is the diameter of the carbon nanotube and E_g is the energy band gap.

2.2 Effective Mass

Given the complete description of the energy dispersion for carbon nanotubes, Eq. (2.1)

can also be used to calculate the electron effective mass for each band. We can use the effective mass relationship in a semiconductor [23] for calculating the effective electron mass in a CNT (n,m) as follows:

$$m_i^* = \frac{\hbar^2}{\left(\frac{d^2E}{dk^2}\right)}. \tag{2.4}$$

Table 2.1 summarizes the electron effective mass for various carbon nanotubes (n,m) calculated from Eqs. (2.4) and (2.1).

2.3 Carrier Concentration

The carrier concentration in a semiconductor is given by [23-25],

$$n_{cnt} = \int_{E_c}^{\infty} D(E) f(E) dE. \tag{2.5}$$

where *D(E)* is the density of states, *f(E)* is the Fermi level and E_c is the conduction band minimum value. Substituting Eq. (2.2) for the density of states in Eq. (2.5), we obtain the equation for carrier concentration given by,

$$n_{cnt} = 2 \sum_{i}^{AllBands} \left[\frac{4}{\pi V_{pp\pi} a\sqrt{3}} \int_{E_{c_i}}^{\infty} E\left(E^2 - E_{c_i}^2\right)^{-1/2} \left(1 + e^{\frac{E-E_F}{kT}}\right)^{-1} dE \right]. \tag{2.6}$$

Equation (2.6) can be further simplified and expressed in the following form:

$$n_{cnt} = \frac{8}{\pi V_{pp\pi} a\sqrt{3}} \int_{0}^{\infty} \left(E' + E_c\right)\left(E'^2 + 2E_c E'\right)^{-1/2} \left(1 + e^{\frac{E'-E_F+E_c}{kT}}\right)^{-1} dE'. \tag{2.7}$$

In deriving Eq. (2.7), the limits of integration in Eq. (2.6) have been changed by replacing the variable *E* with *(E_c + E')*. Furthermore, the summation has also been dropped as the Fermi function becomes negligible for conduction energy band minimums beyond the first band.

The integral in Eq. (2.7) is still very difficult to solve analytically, nevertheless, by

Table 2.1. Effective mass of electrons in carbon nanotubes

(n,m)	Effective mass of electrons (*m**)
(3,1)	0.507 m_0[†]
(3,2)	0.222 m_0
(4,2)	0.271 m_0
(4,3)	0.175 m_0
(5,0)	0.408 m_0
(5,1)	0.159 m_0
(5,3)	0.189 m_0
(6,1)	0.255 m_0
(7,3)	0.116 m_0
(9,2)	0.099 m_0
(11,3)	0.108 m_0

[*] m_0 is the mass of the electron (9.109×10^{-31} Kg).

putting $x = \frac{E}{kT}$ and $\eta = \frac{E_F - E_c}{kT}$, we can write Eq. (2.7) as,

$$n_{cnt} = \frac{8\sqrt{kT}}{\pi V_{pp\pi} a\sqrt{3}} \int_0^{\infty} (kTx + E_c)\left[x(kTx + 2E_c)\right]^{-1/2} \left(1 + e^{x-\eta}\right)^{-1} dx \,. \tag{2.8}$$

In addition, by defining $G(x) = \frac{(kTx + E_c)}{x^{1/2}(kTx + 2E_c)^{1/2}}$ and $F(x) = \frac{1}{1 + e^{x-\eta}}$, Eq. (2.8) can be rewritten as,

$$n_{cnt} = N_c \frac{1}{\sqrt{kT}} \int_0^{\infty} G(x)F(x)dx = N_c \frac{1}{\sqrt{kT}} \int_0^{\infty} \frac{G(x)}{1 + e^{x-\eta}} dx \,, \tag{2.9}$$

where

$$N_c = \frac{8kT}{\pi V_{pp\pi} a\sqrt{3}} \,. \tag{2.10}$$

The integral in Eq. (2.9) is similar to the Fermi integral in [24] and can be approximately integrated under two limits described as follows [23,24].

2.3.1 Limit 1: $\eta << -1$

Under this limit, it can be shown that the function *G(x)* retains a constant value of $\sqrt{kT}$ for $x >> \frac{E_c}{kT}$. Therefore, the upper limit of the integral can be replaced from infinity to $\frac{6E_c}{kT}$ since for values beyond this limit, $\frac{6E_c}{kT}$, the exponential function *F(x)* approaches zero and the integral becomes negligible. Under these conditions it is possible to write,

$$n_{cnt} = N_c I e^{\frac{E_F - E_c}{kT}} \,, \tag{2.11}$$

where

$$I = \frac{1}{\sqrt{kT}} \int_0^{\frac{6E_c}{kT}} \frac{(kTx + E_c)}{x^{1/2}(kTx + 2E_c)^{1/2}} e^{-x} dx \,. \tag{2.12}$$

In Eq. (2.12), the integral, *I*, has no definite solution. However, an approximate solution

has been found by representing the exponential function, e^{-x}, with a series of polynomial functions using the Taylor series expansion approximation [26,27] around a variable *A*.

We first represent the exponential function as:

$$e^{-x} \approx e^{-A}\left[1-(x-A)+\frac{(x-A)^2}{2}-\frac{(x-A)^3}{6}\right]. \tag{2.13}$$

Equation (2.13) is a very good approximation within the range of *A* to *A+1*. Replacing the exponential term in the integral of Eq. (2.12) we obtain:

$$I=\frac{e^{-A}}{\sqrt{kT}}\sum_{A=0}^{A_{\max}}\int_{A}^{A+1}\frac{(kTx+E_c)}{x^{1/2}(kTx+2E_c)^{1/2}}\left[1-(x-A)+\frac{(x-A)^2}{2}-\frac{(x-A)^3}{6}\right]dx, \tag{2.14}$$

where A_{max} is the maximum possible integer value of $\frac{6E_c}{KT}$. This integral can now be solved analytically. The procedure involved in solving the integral of Eq. (2.14) is a long and complicated process; however, the solution is only a polynomial expression, which can be expressed as follows:

$$\begin{aligned} I=\sum_{A=0}^{\mathrm{int}\left(6\frac{E_c}{kT}\right)}\Bigg\{ & e^{-A}\sqrt{x\left(x+2\tfrac{E_c}{kT}\right)}\Big[1-\tfrac{1}{2}x+A+\tfrac{1}{2}\tfrac{E_c}{kT}+\tfrac{1}{6}x^2-\tfrac{1}{6}\tfrac{E_c}{kT}x-\tfrac{1}{2}Ax+\tfrac{1}{2}\left(\tfrac{E_c}{kT}\right)^2+\tfrac{1}{2}A\tfrac{E_c}{kT} \\ & +\tfrac{1}{2}A^2-\tfrac{1}{4}A^2x+\tfrac{5}{16}\left(\tfrac{E_c}{kT}\right)^3+\tfrac{1}{6}A^3-\tfrac{1}{24}x^3+\tfrac{1}{24}\tfrac{Ec}{kT}x^2 \\ & -\tfrac{5}{48}\left(\tfrac{Ec}{kT}\right)^2x+\tfrac{1}{2}A\left(\tfrac{Ec}{kT}\right)^2+\tfrac{1}{2}A^2\tfrac{E_c}{kT}+\tfrac{1}{6}Ax^2-\tfrac{1}{6}A\tfrac{E_c}{kT}x\Big] \\ & +\tfrac{1}{2}\left(\tfrac{E_c}{kT}\right)^2\left[1+A+\tfrac{E_c}{kT}+\tfrac{1}{2}A^2-A\tfrac{Ec}{kT}-\tfrac{5}{8}\left(\tfrac{Ec}{kT}\right)^2\right]\ln\left[\tfrac{E_c}{\sqrt{kT}}+\sqrt{kT}x+\sqrt{kTx^2+2xE_c}\right]\Bigg\}_{x=A}^{x=A+1} \end{aligned} \tag{2.15}$$

It should be noted that this integral is independent of the Fermi energy and characteristic of the chiral vector (n,m) of any particular carbon nanotube. Thus, it will remain constant at any bias voltage but dependent only on temperature. See Appendix A for the analytical solution of the integral, *I*.

2.3.2 Limit 2: $\eta >> 1$

Under this limit, the exponential function *F(x)* of Eq. (2.9) can be approximated as

F(x) = 1, which will remain true as long as $x < \eta$. This approximation fails for $x > \eta$, which is the case of Eq. (2.9) since the upper limit of integration is infinite. However, for $x > \eta$, the exponential term in *F(x)*, $e^{x-\eta}$, becomes very large causing *F(x)* to approach zero. Therefore, *F(x)* can be considered negligible for $x > \eta$. This latter approximation allows us to change the upper limit of integration since *F(x)* vanishes for $x > \eta$. Thus, the upper limit of Eq. (2.9) can be replaced with $x = \eta$.

Under these conditions Eq. (2.9) becomes

$$n_{cnt} = N_c \frac{\left(E_F^2 - E_c^2\right)^{1/2}}{kT}. \tag{2.16}$$

For intrinsic level calculations and normal doping, Limit 1 is useful (Eq. 2.11); Limit 2 (Eq. 2.16) becomes important for heavy doping. By setting $E_F = E_i$, where E_i is the intrinsic energy level and lies in the middle of the band gap, we can obtain the intrinsic carrier concentration, $n_{cnt,i}$ and is given by

$$n_{cnt,i} = N_c I e^{\frac{-E_c}{kT}}. \tag{2.17}$$

Table 2.2 shows the intrinsic carrier concentration for different carbon nanotubes (n,m) obtained from Eq. (2.17) at room temperature (300 K). An effective carbon nanotube wall thickness of 0.617 Å [28] has been used in the calculations of Table 2.2. The 4th column in Table 2.2 summarizes intrinsic carrier concentration in carbon nanotube per unit volume for specific chiral vector (n,m), energy band gap (E_g) and diameter (d). Since single-walled carbon nanotubes can be considered true quasi-one-dimensional conductors, 5th column in Table 2.2 summarizes intrinsic carrier concentration in carbon nanotubes per unit length. It is noticed from Table 2.2 that a carbon nanotube as a quasi-one dimensional behaves as an insulator for certain combinations of chiral vectors, energy band gap and diameter. For other combinations,

Table 2.2. Energy band gap, diameter and intrinsic carrier concentration in carbon nanotubes

(n,m)	***d (nm)***	E_g **(eV)**	$n_{cnt,i}$ **(cm^{-3})**	$n_{cnt,i}$ **(cm^{-1})**
(3,2)	0.344	2.089	7.042×10^{4}	0
(4,2)	0.417	1.721	6.303×10^{6}	0
(4,3)	0.480	1.497	1.239×10^{9}	0
(5,0)	0.394	1.821	2.401×10^{5}	0
(5,1)	0.439	1.635	2.677×10^{8}	0
(5,3)	0.552	1.301	1.791×10^{10}	0
(6,1)	0.517	1.389	1.656×10^{9}	0
(7,3)	0.701	1.024	5.238×10^{12}	0
(9,2)	0.800	0.897	4.911×10^{13}	0
(9,8)	1.161	0.618	7.748×10^{15}	1.70×10^{1}
(10,8)	1.232	0.583	1.404×10^{16}	3.40×10^{1}
(10,9)	1.298	0.553	2.314×10^{16}	5.80×10^{1}
(11,3)	1.007	0.713	6.034×10^{14}	3.00×10^{0}
(11,6)	1.177	0.610	8.929×10^{15}	2.00×10^{1}
(11,10)	1.434	0.500	5.530×10^{16}	15.30×10^{1}
(12,8)	1.375	0.522	3.864×10^{16}	10.30×10^{1}
(14,13)	1.844	0.389	3.289×10^{17}	11.76×10^{2}
(20,19)	2.663	0.270	1.958×10^{18}	10.11×10^{3}
(21,19)	2.732	0.263	2.153×10^{18}	11.40×10^{3}
(40,38)	5.326	0.135	9.924×10^{18}	10.25×10^{4}

the carbon nanotube behaves as a conductor.

Equations (2.11) and (2.16) can also be used to study the effect of temperature on the intrinsic carrier concentration of carbon nanotubes. Figure 2.1 shows the dependence of intrinsic carrier concentration in carbon nanotubes obtained from Eq. (2.17) on temperature for three different chiral vectors. In Fig. 2.1, we can clearly see the strong exponential dependence of the intrinsic carrier concentration on temperature for an intrinsic carbon nanotube with chiral vectors (4,2), (4,3) and (7,3).

The carrier concentration in a doped carbon nanotube can be obtained by adding an impurity concentration in Eq. (2.17) and is given by

$$n_{cnt} = n_{cnt,i} + N, \tag{2.18}$$

where N is the ionized impurity concentration in a carbon nanotube.

Figure 2.2, which is obtained from Eq. (2.18), shows the effect of temperature for a doped carbon nanotube with a chiral vector (4,3) with 10^{15} donors. In Fig. 2.2, it is assumed that below 100 K, there is low ionization and therefore low carrier concentration is observed (a value of 100 K for the ionization temperature of CNTs has been assumed from that of silicon). As the temperature is increased more and more electrons are available in the conduction band and at about 100 K (*1000/T = 10*) [23] all donor atoms are ionized and the carrier concentration equals that of the donor atoms. This temperature range ~100 K to 500 K is the ionization region for carbon nanotubes. Beyond ~500 K, the intrinsic carrier concentration dominates as predicted by the exponential dependence shown in Fig. 2.1. The behavior is similar to carrier concentration dependence on temperature in silicon [23]. The effect of donor atoms on the Fermi energy level of carbon nanotubes has been studied using Eqs. (2.11) and (2.16). In Fig. 2.3, we can see the variation of the energy separation ($E_c - E_F$) under normal and heavy dopings

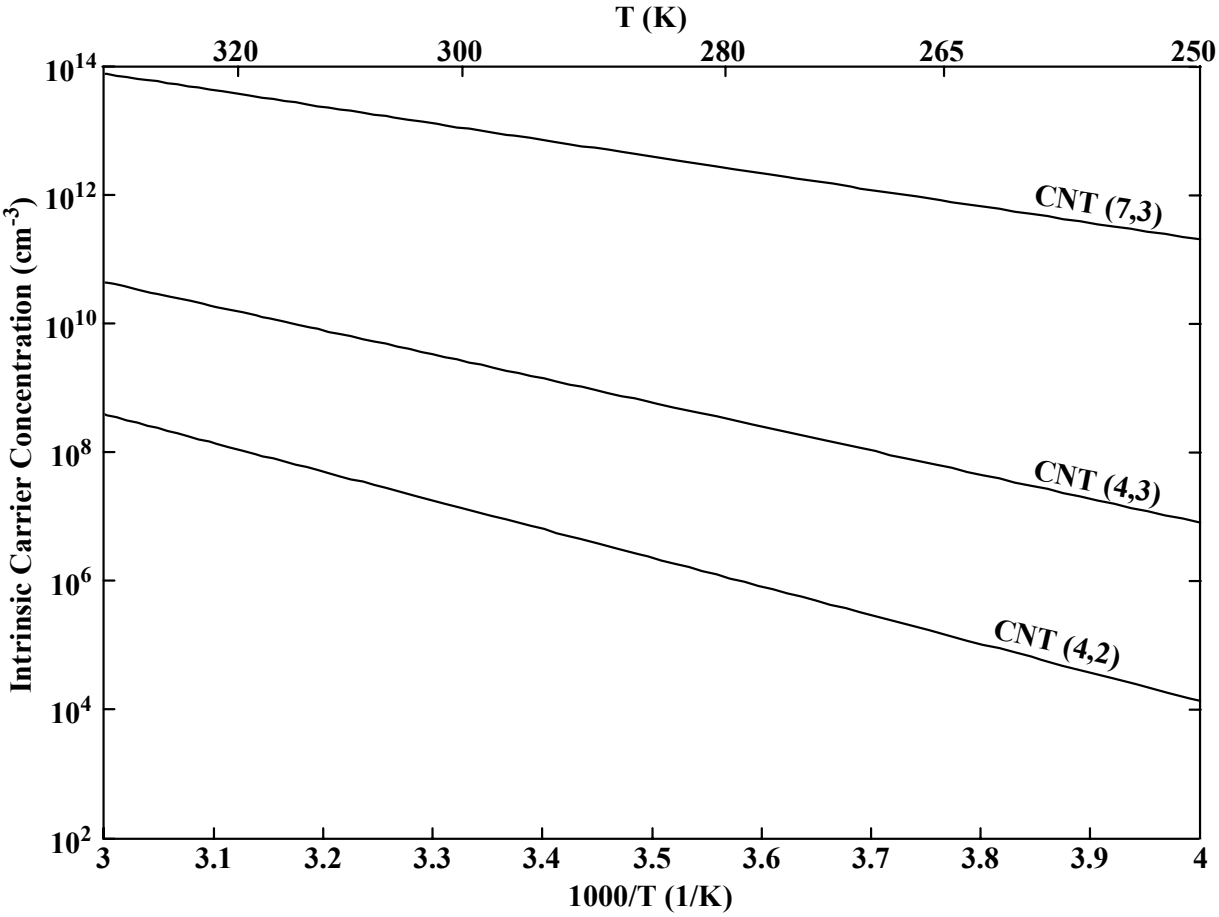

Figure 2.1: Plot of the intrinsic carrier concentration dependence on temperature for a carbon nanotube with chiral vectors (4,2), (4,3) and (7,3).

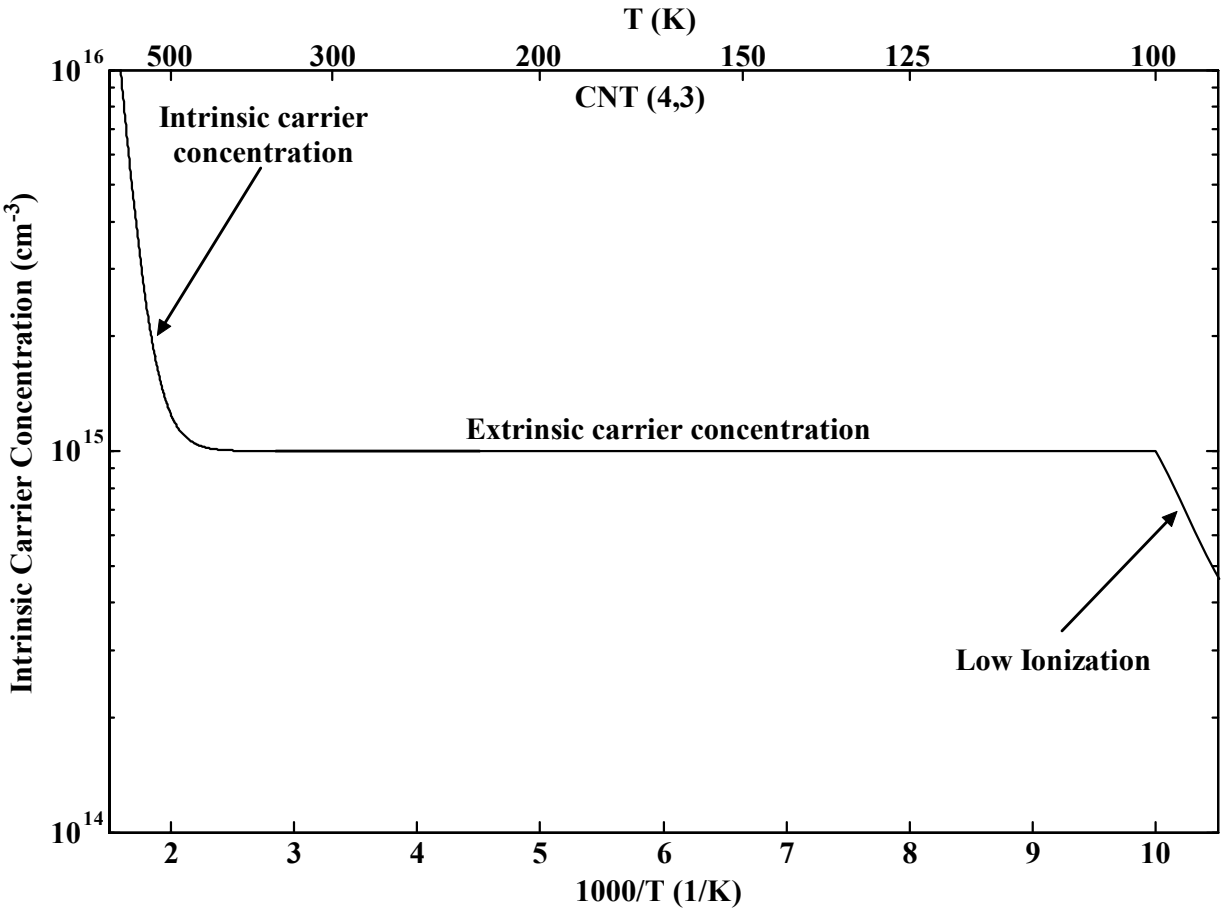

Figure 2.2: Plot of the carrier concentration dependence on temperature for a carbon nanotube with a chiral vector (4,3) and a doping concentration of 10^{15} donor atoms. Note: For high temperatures the intrinsic concentration dominates and for low temperatures (below 100 K), the concentration decreases due to the incapability of the donor atoms to become ionized.

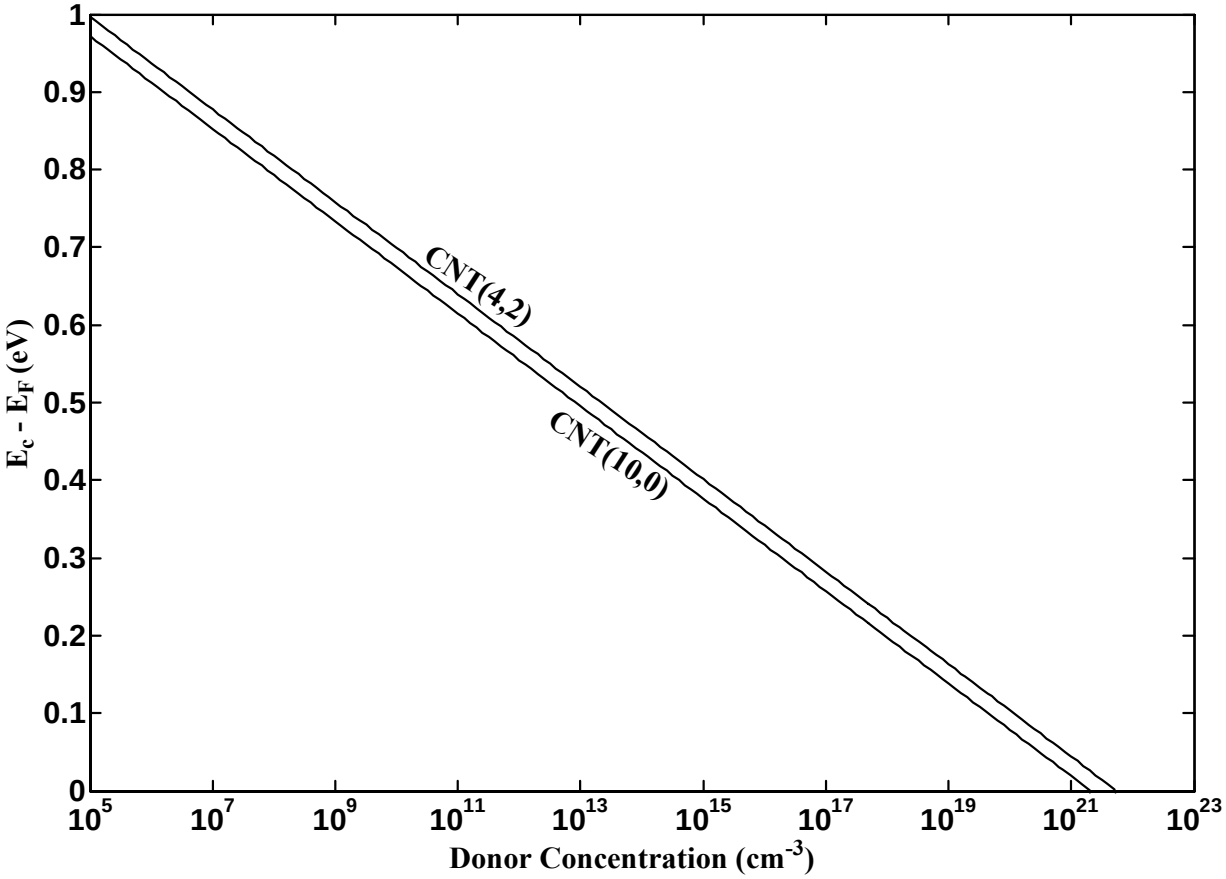

Figure 2.3: Plot of the energy separation ($E_F - E_C$) versus doping concentration for two carbon nanotubes with chiral vectors (4,2) and (10,0).

for two carbon nanotubes with chiral vectors (4,2) and (10,0). In Fig. 2.3, we can also notice the exponential dependence of the Fermi energy level on the doping concentration. This is confirmed by the linear dependence observed in the plot of the energy separation ($E_F - E_C$) versus *ln*(*doping concentration*) for carbon nanotubes.

2.4 Summary

The effective mass and carrier concentration in carbon nanotubes have been theoretically studied. A concise derivation of the carrier density under two limiting cases has been presented including analytical solutions for calculating the intrinsic carrier concentrations and effective mass in carbon nanotubes. Temperature dependences of the carrier concentration and energy band structure have been established analytically. The calculations obtained provide useful understanding of the conductivity in carbon nanotubes and electrical modeling. They represent an important contribution to this field of research; especially, when dealing with impurities, doping concentrations and its effects on the electronic band structure of hexagonal crystal lattice materials. In addition, looking ahead into the application of CNT-FETs, the analytical equations presented can also be used in calculating and deriving current transport models for these transistors. The analysis can be extended to the bundles of carbon nanotubes comparing to a bulk material for interconnect applications.

2.5 References

[1] S. Iijima, "Helical microtubules of graphitic carbon," *Nature,* vol. 354, pp. 56-58, November 1991.

[2] J. Wildoer, L. Venema, A. Rinzler, R. Smalley, and C. Dekker, "Electronic structure of atomically resolved carbon nanotubes," *Nature,* vol. 391, pp. 59-62, January 1998.

[3] N. Hamada, S. I. Sawada, and A. Oshiyama, "New one dimensional conductors: graphite microtubules," *Physical Review Letters,* vol. 68, pp. 1579-1581, 1992.

[4] J. W. Mintmire, B. I. Dunlap, and C. T. White, "Are fullerene tubules metallic?," *Physical Review Letters,* vol. 68, pp. 631-634, 1992.

[5] R. Saito, M. Fujita, G. Dresselhaus, and M. S. Dresselhaus, "Electronic structure of chiral graphene tubules," *Applied Physics Letters,* vol. 60, pp. 2204-2206, May 1992.

[6] H. S. P. Wong, "Field effect transistors - from silicon MOSFETs to carbon nanotube FETs," *Proc. 23th International Conference on Microelectronics, (MIEL)*, pp. 103-107, 2002.

[7] J. Guo, S. Datta, M. Lundstrom, M. Brink, P. McEuen, A. Javey, H. Dai, H. Kim, and P. McIntyre, "Assessment of silicon MOS carbon nanotube FET perfomance limits using a general theory of ballistic transistors," *IEDM Technical Digest,* pp. 711-714, December 2002.

[8] S. J. Wind, J. Appenzeller, R. Martel, V. Derycke, and P. Avouris, "Vertical scaling of carbon nanotube field-effect transistors using top gate electrodes," *Applied Physics Letters,* vol. 80, pp. 3817-3819, 2002.

[9] R. Martel, T. Schmidt, H. R. Shea, T. Hertel, and P. Avouris, "Single and multi wall carbon nanotube field effect transistors," *Applied Physics Letters,* vol. 73, pp. 2447-2449, October 1998.

[10] P. Avouris, "Molecular electronics with carbon nanotubes," *Accounts of Chemical Research,* vol. 35, pp. 1026-1034, December 2002.

[11] P. R. Wallace, "The band theory of graphite," *Physical Review Letters,* vol. 71, pp. 622-634, May 1947.

[12] R. Saito, M. Fujita, G. Dresselhaus, and M. S. Dresselhaus, "Electronic band structure of graphene tubules based on C_{60}," *Physical Review Letters B,* vol. 46, pp. 1804-1811, 1992.

[13] R. Martel, V. Derycke, J. Appenzeller, S. Wind, and P. Avouris, "Carbon nanotube field effect transistors and logic circuits," *Proc. 39th Design Automation Conference*, pp. 94-98, 2002.

[14] J. W. Mintmire and C. T. White, "Universal density of states for carbon nanotubes," *Physical Review Letters,* vol. 81, pp. 2506-2509, September 1998.

[15] C. T. White and J. W. Mintmire, "Density of states reflects diameter in nanotubes," *Nature (London),* vol. 394, pp. 29-30, 1998.

[16] A. Raychowdhury, S. Mukhopadhyay, and K. Roy, "A circuit-compatible model of ballistic carbon nanotube field effect transistors," *IEEE Transactions on Computer-Aided Design of Integrated Circuits and Systems,* vol. 23, pp. 1411-1420, October 2004.

[17] M. S. Dresselhaus, G. Dresselhaus, and P. Avouris, *Carbon Nanotube: Synthesis, Properties, Structure, and Applications*: Springer Verlag, 2001.

[18] R. Saito, M. S. Dresselhaus, and G. Dresselhaus, *Physical Properties of Carbon Nanotubes*. London: Imperial College Press, 1998.

[19] A. Loiseau, P. Launois, P. Petit, S. Roche, and J. P. Salvetat, *Understanding Carbon Nanotubes*. Berlin Heidelberg: Springer, 2006.

[20] K. Tanaka, T. Yamabe, and K. Fukui, *The Science and Technology of Carbon Nanotubes*. Amsterdam: Elsevier, 1999.

[21] R. Saito, G. Dresselhaus, and M. S. Dresselhaus, "Trigonal warping effect of carbon nanotubes," *Physical Review Letters B,* vol. 61, pp. 2981-2990, January 2000.

[22] J. Guo, M. Lundstrom, and S. Datta, "Performance projections for ballistic carbon nanotube field-effect transistors," *Applied Physics Letters,* vol. 80, pp. 3192-31942, April 2002.

[23] B. G. Streetman, *Solid State Electronic Devices*, 5th Ed. India: Prentice Hall, 2000.

[24] M. Shur, *Physics of Semiconductor Devices*. United States: Prentice Hall, 1990.

[25] J. P. McKelvey, *Solid States Physics for Engineering and Material Sciences*. Florida: Krieger Publishing Company, 1993.

[26] D. E. Johnson and J. R. Johnson, *Mathematical Methods in Engineering and Physics*. New York: The Ronald Press Company, 1965.

[27] J. Stewart, *Calculus Early Transcendentals*, 3th Ed. United States: Brooks/Cole Publishing Company, 1995.

[28] T. Vodenitcharova and L. C. Zhang, "Effective wall thickness of a single-walled carbon nanotube," *Physical Review Letters B,* vol. 68, p. 156401, 2003.

CHAPTER 3

CURRENT TRANSPORT IN CARBON NANOTUBE FIELD EFFECT TRANSISTORS (CNT-FETs)*

3.1 Introduction

Emerging carbon nanotube field effect transistors for very large scale integration and interconnects [1-6] have been a subject of intensive research for a wide range of applications. These CNT-FETs have been identified as one of the promising candidates substituting shrinking CMOS technology at the end of the Moore's law [7-9]. In this chapter, we use our carrier concentration model derived in Chapter 2 to investigate and derive a current transport model for CNT-FETs.

The structure of a CNT-FET is similar to the structure of a typical MOSFET [7,10], where a SWNT forms the channel between two electrodes which work as the source and drain of the transistor. The structure is built on top of an insulating layer and a substrate which works as the back gate [2,11]. Both n- and p-type CNT-FETs have been fabricated in the past decade [12,13] and multistage complementary logic gates have been demonstrated [14-18].

With the advancement in fabrication technology of carbon nanotube field effect transistors, efforts have also been made in modeling of the current transport behavior and models have been developed for the design of CNT-FET based logic circuits [19-24]. However,

---

* Part of the work is reported in the following publications:

1. J. M. Marulanda and A. Srivastava, "I-V characteristics modeling and parameter extraction for CNT-FETs," *Proc. 2005 International Semiconductor Device Research Symposium*, (Bethesda, MD, December 7-9, 2005).
2. J. M. Marulanda, A. Srivastava and A.K. Sharma, "Current transport modeling in carbon nanotube field effect transistors (CNT-FETs) and bio-sensing applications," *Proc. SPIE Smart Structures and Materials & Nondestructive Evaluation and Health Monitoring: Nanosensors and Microsensors for Bio-System*, vol. 6931, pp. 693108-1-693108-12, (San Diego, CA, March 9-13, 2008).
3. J. M. Marulanda, A. Srivastava and S. Yellampalli, "Numerical modeling of the I-V characteristics of the carbon nanotube field effect transistors," *Proc. IEEE 40th Southeastern Symposium on System Theory (SSST 2008)*, pp. 235-238 (New Orleans, LA, March 16-18, 2008).

transport modeling is limited to numerical and curve fitting techniques. In this chapter, we have attempted to develop analytical models characterizing the current transport in CNT-FETs for the analysis and design of integrated circuits. We have used these current-voltage model equations to generate I-V characteristics, under normal and subthreshold operation for CNT-FETs using different chiral vectors (n,m) for the carbon nanotube.

3.2 Current Transport Modeling

The current transport equation of a CNT-FET can be obtained by relating the carbon nanotube potential to the terminal voltages. The charge inside the carbon nanotube is described from the electronic structure of the carbon nanotube. A model for the carbon nanotube potential is then derived and the current transport equation is obtained.

3.2.1 Charge Sheet Model

Figure 3.1(a) shows the basic cross section of a CNT-FET including the charge distributions. Figure 3.1(b) shows the corresponding potential distributions between the gate and the substrate. In Fig. 3.1(a), charge distributions are explained as follows: the charge on the gate is Q_g, the charges in the oxide layers are Q_{01} and Q_{02}, the charge inside the CNT is Q_{cnt} and the charge in the substrate is Q_{subs}. In Fig. 3.1(b), six different potential distributions are shown, which are also described as follows: the voltage between the gate and the substrate (back gate) is V_{gb}, the potential drop across the oxides are ψ_{ox1} and ψ_{ox2}, the surface potential in the substrate with respect to the back gate, ψ_{subs}, the potential across the CNT, ψ_{cnt} and the work function difference between the gate and the substrate materials is ϕ_{ms}.

Using Kirchoff's voltage law, the potential balance and charge neutrality condition, we can write for the Fig. 3.1,

$$V_{gb} = \phi_{ms} + \psi_{ox1} + \psi_{cnt} + \psi_{ox2} + \psi_{subs}, \tag{3.1}$$

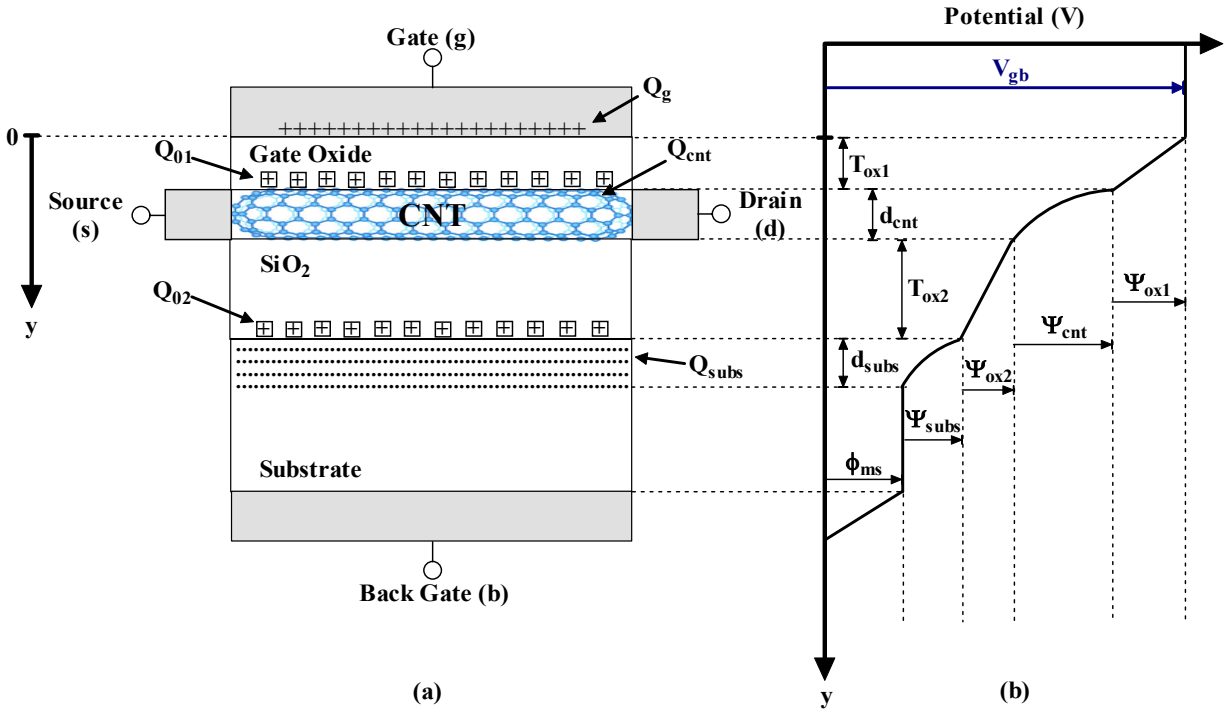

Figure 3.1: (a) Plot of the charges from gate to substrate and (b) plot of the potential distribution from gate to substrate in a CNT-FET.

$$Q'_g + Q'_{01} + Q'_{cnt} + Q'_{02} + Q'_{subs} = 0, \tag{3.2}$$

The prime in Eq. (3.2) denotes the charge per unit area. In (3.1), ϕ_{ms} is divided in two parts and expressed as follows,

$$\phi_{ms} = \phi_{mc} + \phi_{cs}, \tag{3.3}$$

where ϕ_{mc} and ϕ_{cs} are the work function differences between the metal gate and carbon nanotube materials and the carbon nanotube and substrate materials, respectively.

Combining potentials ψ_{cnt}, ψ_{ox2} , ϕ_{cs} and ψ_{subs} into a single potential, $\psi_{cnt,s}$, Eq. (3.1) can then be re-written as follows,

$$V_{gb} = \phi_{mc} + \psi_{ox1} + \psi_{cnt,s}, \tag{3.4}$$

where $\psi_{cnt,s}$ describes the surface potential at the interface of the gate oxide and the carbon nanotube with respect to the back gate.

The electric field in terms of the charge distribution can be written from the Maxwell's third equation [25] and is given by,

$$\nabla.(\varepsilon E) = \rho_v, \tag{3.5}$$

where ε is the permittivity of the material, E is the electric field, and ρ_v is the charge per unit volume. Assuming that the electric field in Fig. 3.1(a) is constant through the gate oxide region and at the bottom edge of the carbon nanotube, Eq. (3.5) can be integrated between the gate and the bottom edge of the carbon nanotube, that is in Fig. 3.1(a) from $y = 0$ to $y = T_{ox1} + d_{cnt}$, where d_{cnt} is the diameter of the carbon nanotube. In this derivation we have assumed that the carbon nanotube has a relative permittivity, ε_{cnt}. We can write Eq. (3.6) as follows,

$$\varepsilon_{cnt} E_{cnt} - \varepsilon_{ox1} E_{ox1} = Q'_{01} + Q'_{cnt}, \tag{3.6}$$

where E_{cnt} and E_{ox1} are the electric fields along the y-axis across the carbon nanotube and gate oxide, respectively.

In a typical top gated CNT-FET, the substrate oxide thickness, T_{ox2} is much greater than the gate oxide thickness, T_{ox1} [11]. We can then assume that any charge applied at the gate is compensated only by an induced charge in the carbon nanotube as follows:

$$\Delta Q'_g = -\Delta Q'_{cnt} \,. \tag{3.7}$$

Furthermore, there is a specific gate voltage, called the flat band voltage, V_{fb} [26], which when applied at the gate with respect to the back gate; it compensates for the band bending at the gate oxide and carbon interface. Under this flat band condition, the electric field at the bottom edge of the carbon nanotube, E_{cnt} in Eq. (3.6) can be neglected. Under this assumption and replacing E_{ox1} with the potential gradient $-\frac{d\psi_{ox1}(y)}{dy}$ in Eq. (3.6) we obtain,

$$\varepsilon_{ox1}\frac{d\psi_{ox1}(y)}{dy} = Q'_{01} + Q'_{cnt} \,. \tag{3.8}$$

By integrating Eq. (3.8) through the gate oxide region, that is in Fig. 3.1(a) from $y = 0$ to $y = T_{ox1}$, we can write an expression for the gate oxide potential as:

$$\psi_{ox1} = -\frac{Q'_{01} + Q'_{cnt}}{C'_{ox1}}. \tag{3.9}$$

In Eq. (3.9), C'_{ox1} is the gate oxide capacitance per unit area. Substituting Eq. (3.9) in Eq. (3.4) we obtain an expression for the gate voltage given by,

$$V_{gb} = \psi_{cnt,s} - \frac{Q_{cnt}}{C_{ox1}} + \phi_{mc} - \frac{Q_{01}}{C_{ox1}} \,. \tag{3.10}$$

In Eq. (3.10), Q_{cnt}, Q_{01} and C_{ox1} are the total charges and capacitance, respectively, which are obtained by multiplying Q'_{01}, Q'_{cnt}, and Q'_{02} with their respective areas. C_{ox1}, the capacitance between the gate and the carbon nanotube, can be redefined by considering the carbon nanotube to be a line of charge and the gate to be a planar conducting plate. Therefore, the gate

oxide capacitance of thickness T_{ox1} of a carbon nanotube of length L and radius r is given by [27,28],

$$C_{ox1} = \frac{2\pi\varepsilon_{ox1}L}{\ln\left(\frac{T_{ox1}+r+\sqrt{T_{ox1}^2+2T_{ox1}r}}{r}\right)}. \tag{3.11}$$

In Eq. (3.10), the flat band voltage, V_{fb} is:

$$V_{fb} = \phi_{mc} - \frac{Q_{01}}{C_{ox1}}. \tag{3.12}$$

The gate voltage, V_{gs} in Eq. (3.10) after combining with the Eq. (3.12) can be expressed as follows,

$$V_{gb} = \psi_{cnt,s} - \frac{Q_{cnt}}{C_{ox1}} + V_{fb}. \tag{3.13}$$

In Eq. (3.13), $\psi_{cnt,s}$ can be explained as a control potential in the carbon nanotube in charge of shifting the energy band at the interface of the gate oxide and carbon nanotube. As the gate voltage increases, we start seeing a voltage drop across the gate oxide modeled as $\frac{Q_{cnt}}{C_{ox1}}$. Equation (3.13) can be used to define the threshold voltage.

3.2.2 Charge Inside the Carbon Nanotube

In Eq. (3.13), the charge inside the carbon nanotube can be calculated using the following relation $|Q_{cnt}| = qn_{cnt}L$, where n_{cnt} is the carrier concentration per unit length inside the carbon nanotube, which we have derived in our earlier work [29] and is given by

$$n_{cnt}(\eta) = \frac{8\sqrt{kT}}{\pi\sqrt{3}V_{pp\pi}a}\int_0^\infty \frac{kTx+E_c}{\sqrt{x(kTx+2E_c)}}\left(1+e^{x-\eta}\right)^{-1}dx, \tag{3.14}$$

where a is the lattice constant, $V_{pp\pi}$ is the energy transfer integral [30,31], k is Boltzmann's constant and T is the temperature. The parameter, η is given by:

$$\eta = \frac{E_F - E_c}{kT}, \tag{3.15}$$

where E_c is the conduction band minima. It is found from the energy dispersion relation of the carbon nanotubes and is expressed as [30,31]:

$$E_{1D}(k) = \pm V_{pp\pi}\left[1 + 4Cos\left(\frac{\sqrt{3}K_x}{2}a\right)Cos\left(\frac{K_y}{2}a\right) + 4Cos^2\left(\frac{K_y}{2}a\right)\right]^{1/2}, \tag{3.16}$$

where K_x and K_y are the wave vectors of a one-dimensional (1D) carbon nanotube.

There is no reported work on finding an analytical solution of Eq. (3.14). We have reported an approximate solution under two limiting cases [29]. Under these limiting conditions, we can express the charge inside the carbon nanotube as follows:

Limit 1, $\eta << -1$:

$$\left|Q_{cnt}\right| = qLN_c I e^{\frac{E_F - E_c}{kT}}, \tag{3.17}$$

Limit 2, $\eta >> 1$:

$$\left|Q_{cnt}\right| = qLN_c \frac{\sqrt{E_F^2 - E_c^2}}{kT}, \tag{3.18}$$

where

$$I = \frac{1}{\sqrt{kT}} \int_0^{\frac{6E_c}{kT}} \frac{(kTx + E_c)}{x^{1/2}(kTx + 2E_c)^{1/2}} e^{-x} dx \tag{3.19}$$

and

$$N_c = \frac{8kT}{\pi\sqrt{3}V_{pp\pi}a}. \tag{3.20}$$

An approximate solution for the integral I of Eq. (3.19) is given in Appendix A.

3.2.3 Carbon Nanotube Surface Potential

In order to effectively describe the potential inside the carbon nanotube, we need to

determine the energy separation between the Fermi level and the conduction band at the interface of the gate oxide and carbon nanotube. Assuming a flat band energy in the carbon nanotube, we can say that the Fermi level and the conduction band at the interface of the gate oxide and carbon nanotube will be shifted by an amount determined by qV_{cb} and $q\psi_{cnt,s}$, respectively; where V_{cb} is the induced potential between the carbon nanotube and the substrate due to the drain and source terminal voltages. The potential, V_{cb} varies from V_{sb} (source to back gate potential) to V_{db} (drain to back gate potential). Figure 3.2 shows the energy band diagram of a two terminal CNT-FET when (a) $V_{gb} = |V_{fb}|$ and (b) $V_{gb} > 0$. In Fig. 3.2(a), we have used hafnium dioxide (HfO_2) as the gate oxide, which is a high k-dielectric insulator material. Furthermore, ϕ_0 in Fig. 3.2(a) is the carbon nanotube surface potential, $q\psi_{cnt,s}$ when $V_{gb} = V_{fb}$ and $\psi_{cnt} = 0$. ϕ_0 is then given by,

$$\phi_0 = \psi_{ox2} + \psi_{subs} + \phi_{cs}. \tag{3.21}$$

As it was previously done, by integrating Eq. (3.5) from $y = T_{ox1} + d_{cnt}$ to $y = T_{ox1} + d_{cnt} + T_{ox2} + d_{subs}$, where d_{subs} is the thickness of Q_{subs} in the substrate as shown in Fig. 3.1(a), we can write,

$$\varepsilon_s E_s - \varepsilon_{ox2} E_{ox2} = Q'_{02} + Q'_{subs}, \tag{3.22}$$

where ε_s is the permittivity of the substrate material. Assuming the electric field, E_s is negligible deep inside the substrate and replacing E_{ox2} with the potential gradient $-\frac{d\psi_{ox2}(y)}{dy}$ in Eq. (3.22) we have,

$$\varepsilon_{ox2} \frac{d\psi_{ox2}(y)}{dy} = Q'_{02} + Q'_{subs}. \tag{3.23}$$

By integrating Eq. (3.23) from $y = T_{ox1} + d_{cnt}$ to $y = T_{ox1} + d_{cnt} + T_{ox2}$ in Fig. 3.1(a) we can obtain an expression for the second oxide potential as:

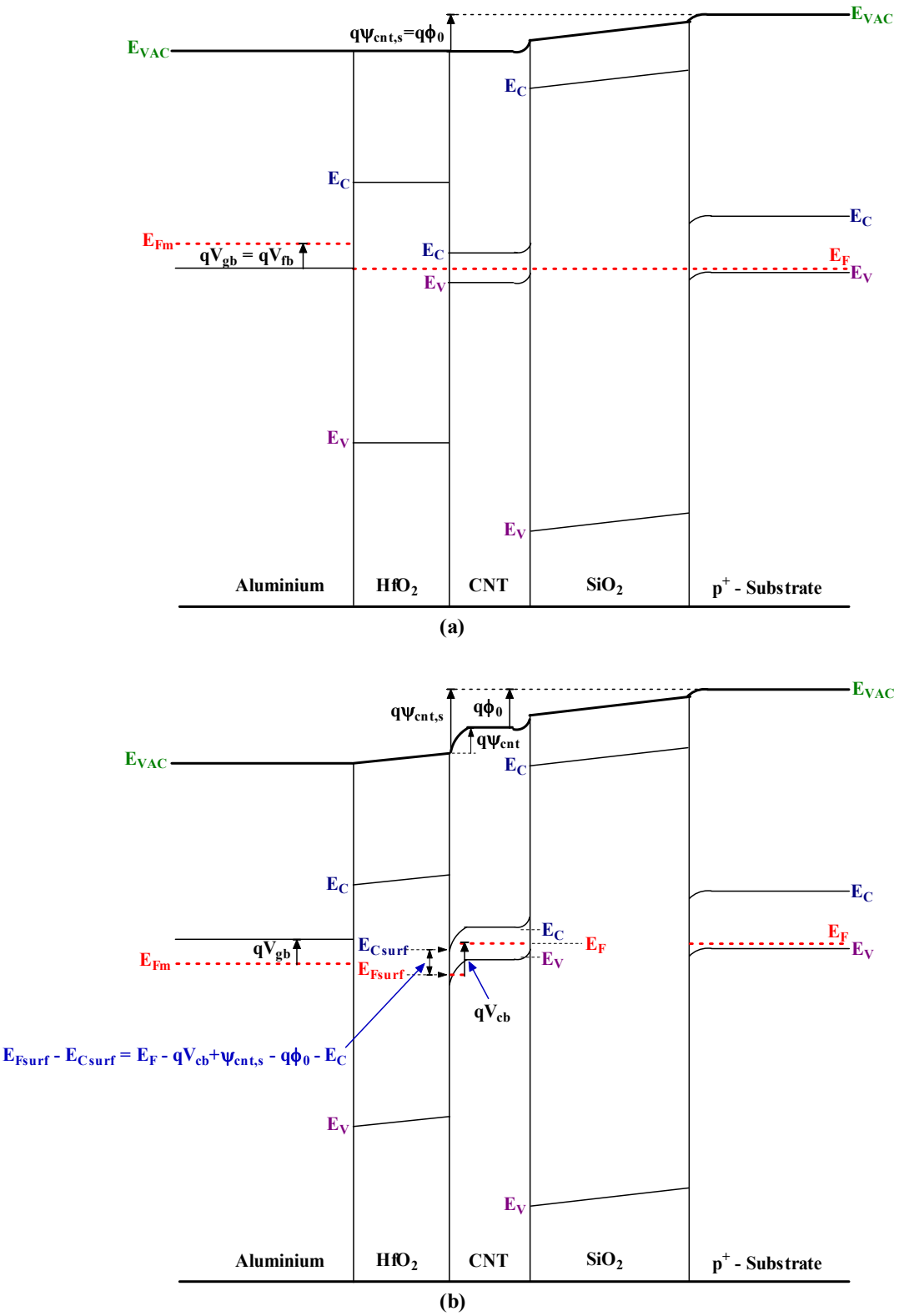

Figure 3.2: Energy band diagram of a two terminal CNT-FET for (a) $V_{gb} = V_{fb}$ and (b) $V_{gb} > 0$. Note: HfO_2 is the high *k*-dielectric hafnium oxide.

$$\psi_{ox2} = -\frac{Q'_{02} + Q'_{subs}}{C'_{ox2}}. \tag{3.24}$$

The total capacitance C_{ox2}, which is the capacitance between the carbon nanotube and the substrate and is defined as follows,

$$C_{ox2} = \frac{2\pi\varepsilon_{ox2}L}{\ln\left(\frac{T_{ox2} + r + \sqrt{T_{ox2}^2 + 2T_{ox2}r}}{r}\right)}. \tag{3.25}$$

Assuming Q_{subs} and ψ_{subs} to be small compared to Q_{02} and $\phi_{cs} + \psi_{ox2}$, we can rewrite Eq. (3.21) for ϕ_0 as follows:

$$\phi_0 = \phi_{cs} - \frac{Q_{02}}{C_{ox2}}. \tag{3.26}$$

We are interested in the separation between the Fermi level and conduction band on at the interface of the gate oxide and carbon nanotube. Following the Fig. 3.2(a) we can observe that the conduction band of the carbon nanotube is shifted by an amount of $\psi_{cnt,s} - \phi_0$ expressed as [19,26],

$$E_{Csurf} = E_c - q\left(\psi_{cnt,s} - \phi_0\right). \tag{3.27}$$

where E_{Csurf} is the conduction band energy at the interface of the gate oxide and carbon nanotube. The Fermi level at the interface, E_{Fsurf} is shifted by an amount of V_{cb} and is expressed as [19,26],

$$E_{Fsurf} = E_F - qV_{cb}. \tag{3.28}$$

From Eqs. (3.27) and (3.28) we can write:

$$E_{Fsurf} - E_{Csurf} = E_F + q\left(\psi_{cnt,s} - V_{cb} - \phi_0\right) - E_c. \tag{3.29}$$

The shift in the Fermi level of the carbon nanotube due to impurity doping can be obtained as follows. In Chapter 2, we studied the carrier concentration in carbon nanotubes, the

carrier concentration in a carbon nanotube is given by

$$n_{cnt} = N_c I e^{\frac{E_F - E_c}{kT}}. \tag{3.30}$$

The intrinsic carrier concentration can be obtained by setting the Fermi level in the middle of the band gap, that is $E_F = 0$ in Eq. (3.30) to obtain,

$$n_{cnt,i} = N_c I e^{\frac{-E_c}{kT}}. \tag{3.31}$$

Using Eq. (3.31) we can rewrite Eq. (3.30) as follows:

$$E_F = kT \ln\left(\frac{n_{cnt}}{n_{cnt,i}}\right). \tag{3.32}$$

The carrier concentration in a doped carbon nanotube can also be obtained by adding an ionized impurity doping concentration, N in Eq. (3.31) as follows:

$$n_{cnt} = n_{cnt,i} + N. \tag{3.33}$$

The ionized impurity concentration, N in Eq. (3.33) can be either donor atoms, N_D or acceptor atoms, N_A.

In an intrinsic carbon nanotube, the Fermi level lies in the middle of the band gap; we can use Eq. (3.32) to express the shift in the Fermi level depending upon the doping. Furthermore, using Eq. (3.33) we can define a parameter ΔE_F given by,

$$\Delta E_F = \pm kT \ln\left(1 + \frac{N}{n_{cnt,i}}\right), \tag{3.34}$$

where ΔE_F is positive for an n-type carbon nanotube (donors impurity concentration, $N = N_D$) and negative for a p-type carbon nanotubes (acceptors impurity concentration, $N = N_A$). Thus, using Eq. (3.34) for the shift in the Fermi level, we can rewrite Eq. (3.29) as:

$$E_{Fsurf} - E_{Csurf} = \Delta E_F + q\left(\psi_{cnt,s} - V_{cb} - \phi_0\right) - E_c. \tag{3.35}$$

Using Eq. (3.35) in the analytical expressions for the charge inside the carbon nanotube given by Eqs. (3.17) and (3.18), the gate substrate voltage, V_{gb}, in Eq. (3.10) can be rewritten as:

$$V_{gb} = \psi_{cnt,s} + \delta f\left(\psi_{cnt,s}, V_{cb}\right) + V_{fb}, \tag{3.36}$$

where

$$f\left(\psi_{cnt,s}, V_{cb}\right) = \begin{cases} Ie^{\frac{\Delta E_F + q\left(\psi_{cnt,s} - V_{cb} - \phi_0\right) - E_c}{kT}}; & for\ \psi_{cnt,s} \le V_{cb} + \phi_0 - \frac{\Delta E_F}{q} + \frac{E_c}{q} - \frac{kT}{q} \\ \frac{\sqrt{\left(\Delta E_F + q\psi_{cnt,s} - qV_{cb} - q\phi_0\right)^2 - E_c^2}}{kT}; & for\ \psi_{cnt,s} \ge V_{cb} + \phi_0 - \frac{\Delta E_F}{q} + \frac{E_c}{q} + \frac{kT}{q} \end{cases}, \tag{3.37}$$

and

$$\delta = \frac{qLN_c}{C_{ox1}}. \tag{3.38}$$

Equation (3.36) cannot be solved explicitly in terms of the terminal voltages and numerical techniques are to be used to find the exact carbon nanotube potential given a gate input voltage. Figure 3.3 shows the carbon nanotube potential versus the gate substrate voltage for varying V_{cb}.

Nevertheless, by partitioning Eq. (3.36) in three effective regions, an explicit solution in terms of the terminal voltages can be obtained: Region 1, in which the carbon nanotube surface potential has a linear and exponential dependence on the gate to substrate voltage, Region 3, in which the carbon nanotube potential does not change significantly with the gate to substrate voltage, and Region 2, in which no real dependence of the carbon nanotube potential on the gate to substrate voltage can be established and an approximate curve fitting can be obtained. The carbon nanotube potential can be found using the following equations:

Region 1, for $0 \le V_{gb} \le V_{cb} + V_{fb} + \phi_0 - \frac{\Delta E_F}{q} + \frac{E_c}{q} - \frac{kT}{q} - \frac{Ie^{-1}}{m}$:

$$\psi_{cnt,s} = V_{gb} - V_{fb}, \tag{3.39}$$

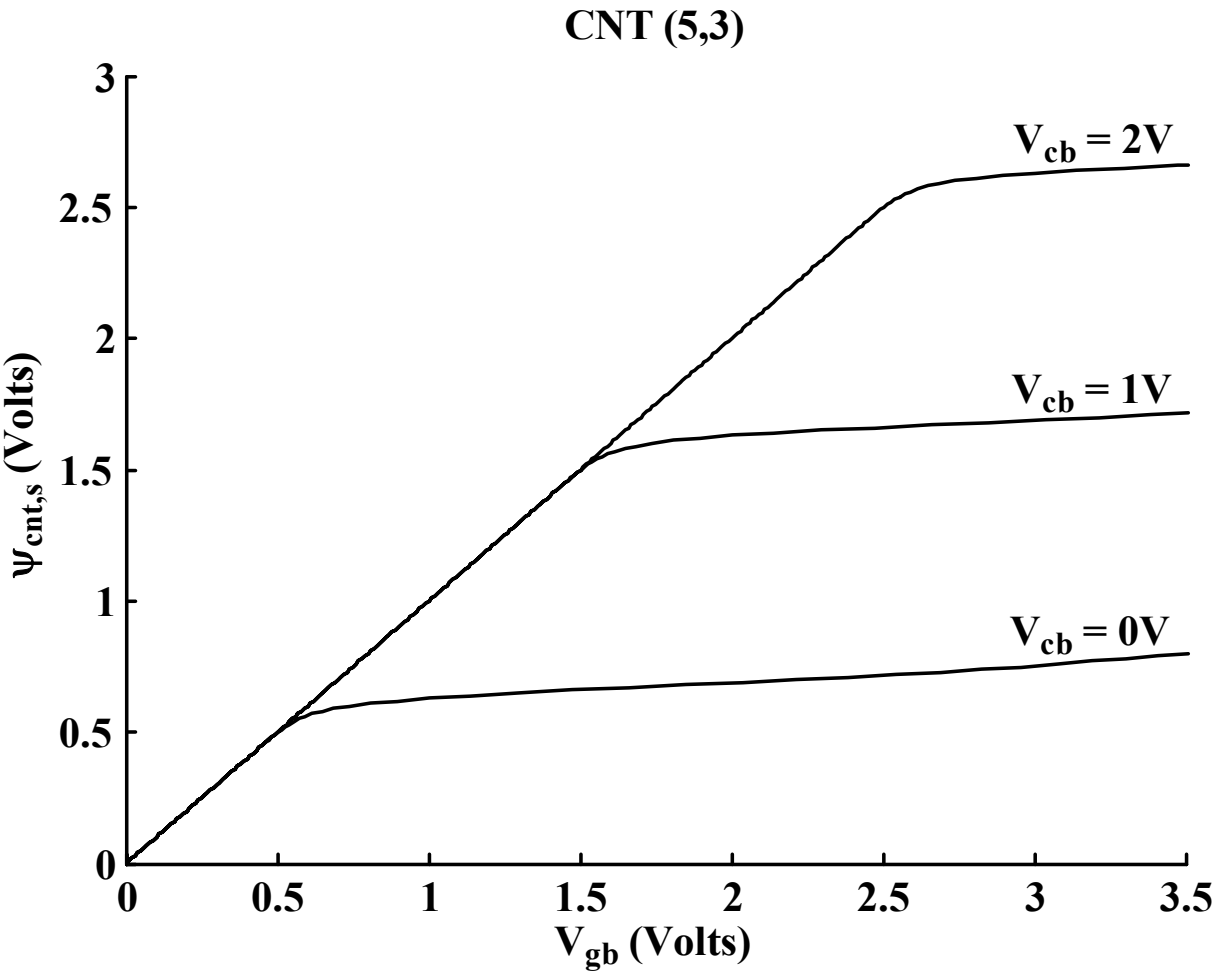

Figure 3.3: Carbon nanotube surface potential, $\psi_{cnt,s}$ versus gate substrate voltage for $V_{fb} = 0$ and $\phi_0 = 0$ for a CNT-FET (5,3) using a numerical approach. The device dimensions are: $T_{ox1} = 40\ nm$, $T_{ox2} = 400\ nm$ and $L = 50\ nm$.

Regions 2 and 3, for $V_{gb} \geq V_{cb} + V_{fb} + \phi_0 - \frac{\Delta E_F}{q} + \frac{E_c}{q} - \frac{kT}{q} - \frac{Ie^{-1}}{m}$

$$\psi_{cnt,s} = \frac{V_{gb} - \delta I e^{-1} - V_{fb} + \delta m\left(V_{cb} + \phi_0 - \frac{\Delta E_F}{q} + \frac{E_c}{q} - \frac{kT}{q}\right)}{1 + \delta m}, \tag{3.40}$$

where m is the slope of Region 2 and is of the form:

$$m = \frac{\sqrt{\frac{2E_c}{kT} + 1} - Ie^{-1}}{\frac{2kT}{q}}. \tag{3.41}$$

The slope 'm' should not be confused with the index m of the chiral vector (n,m). A complete derivation for Eqs. (3.39) and (3.40) is given in Appendix B. Figures 3.4 (a) and (b) show a plot of $\psi_{cnt,s}$ versus V_{gb} for two chiral vectors (11,3) and (7,2), respectively. The solid lines in Fig. 3.4 correspond to the analytical solution and circle markers show the numerical solution. It is clearly noticed that the analytical solution agrees closely to the numerical solution.

In Fig. 3.4, the curve fitting has been used for the Region 2 given by Eq. (3.40). The Region 2, defined by the gap predicted by the limits of Eqs. (3.17) and (3.18) is further extended to cover the Region 3. This is a very good approximation, but starts failing for gate voltages above 3 V. However, transistors will hardly operate beyond this voltage given the low power restrictions of the current technology [32-34].

3.2.4 The Current Equation

In CNT-FETs, both diffusion and drift carrier transport mechanisms contribute to the current, which is given by [26,35],

$$I_{ds} = I_{diff}(x) + I_{drift}(x) = \frac{|R|}{2L}\left[\int_{\psi_{cnt}(0)}^{\psi_{cnt}(L)} \mu\left(-Q'_{cnt}\right) d\psi_{cnt} + \frac{kT}{q}\int_{Q'_{cnt}(0)}^{Q'_{cnt}(L)} \mu dQ'_{cnt}\right]. \tag{3.42}$$

$|R|$ in Eq. (3.42) is the circumference of the nanotube and μ is the carrier mobility in a carbon nanotube. In Eq. (3.42) we have used the charge per unit area, but only to show that we have

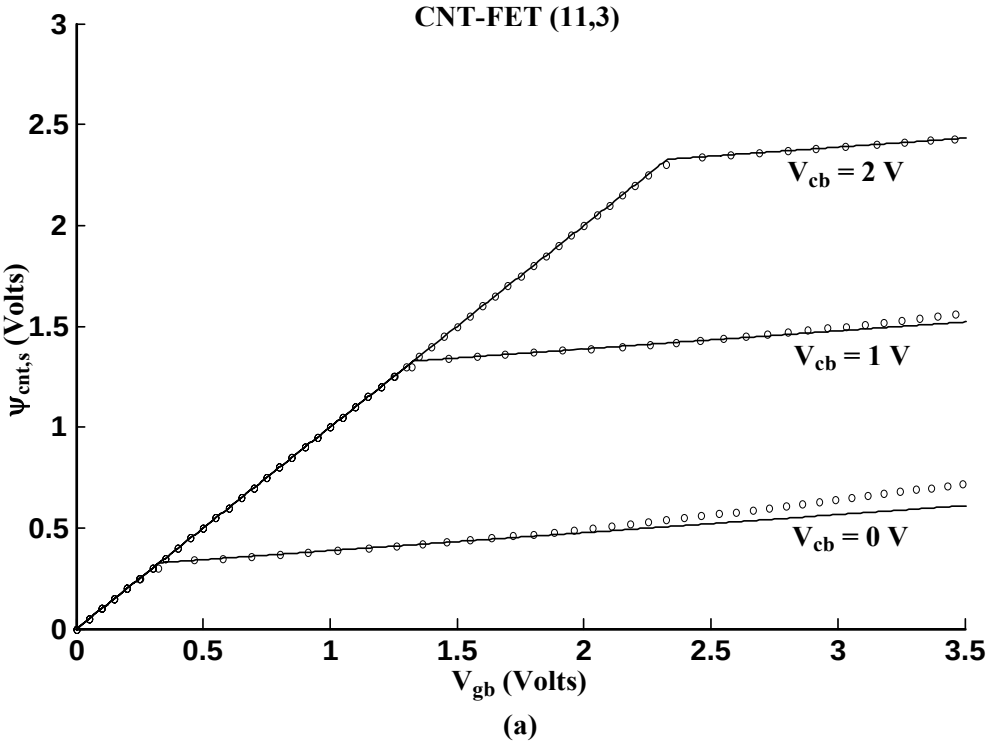

(a)

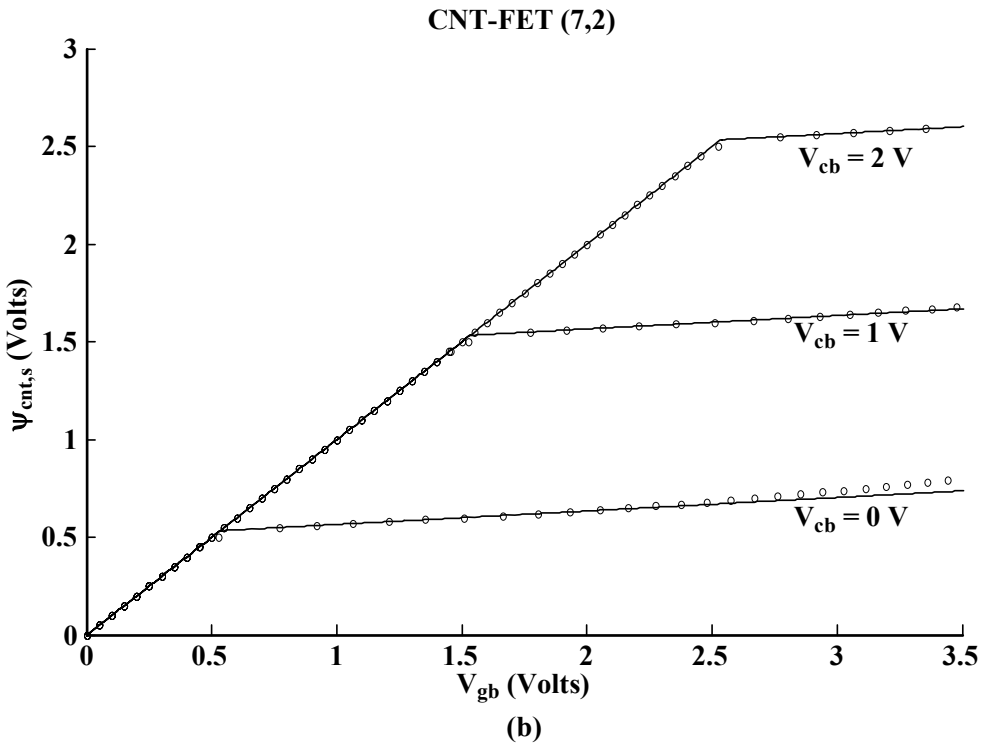

(b)

Figure 3.4: Carbon nanotube surface potential, $\psi_{cnt,s}$ versus gate substrate voltage for $V_{fb} = 0$ and ϕ_0 = for (a) CNT-FET (11,3) and (b) CNT-FET (7,2). The device dimensions are: $T_{ox1} = 40\ nm$, $T_{ox2} = 400\ nm$ and $L = 50\ nm$.

considered a surface area, $\frac{|R|L}{2}$ for the carbon nanotube. The mobility can be replaced by $\mu = \gamma \mu_{graphite}$, as each CNT (n,m) will have different values for the mobility, γ is a conversion factor for CNTs from graphite with a value varying from 0 to 1. In addition, γ can also be used to represent how much surface area of the CNT is responsible for the charge flow. The charge, Q_{cnt} can be obtained from Eq. (3.13) as follows:

$$Q_{cnt} = C_{ox1}\left(-V_{gb} + \psi_{cnt,s} + V_{fb}\right). \tag{3.43}$$

Equation (3.43) can be expressed in terms of the charge per unit area by diving it by $\frac{|R|L}{2}$ to obtain Q'_{cnt}. By substituting Eq. (3.43) in Eq. (3.42) the following expression for the current is obtained:

$$I_{ds} = \beta\left[f\left\{\psi_{cnt,s}(L), V_{gs}\right\} - f\left\{\psi_{cnt,s}(0), V_{gs}\right\}\right], \tag{3.44}$$

where

$$f\left\{\psi_{cnt,s}(x), V_{gs}\right\} = \left(V_{gs} + V_{sb} - V_{fb} + \frac{kT}{q}\right)\psi_{cnt,s}(x) - \frac{1}{2}\psi_{cnt,s}^2(x) \tag{3.45}$$

and

$$\beta = \gamma\frac{\mu C_{ox1}}{L^2}. \tag{3.46}$$

In Eq. (3.44), $\psi_{cnt,s(L)}$ is the carbon nanotube surface potential at the drain end, which can be found from Eqs. (3.39) and (3.40) by setting $V_{cb} = V_{ds} + V_{sb}$. The carbon nanotube surface potential at the source end, $\psi_{cnt(0)}$ is obtained from Eq. (3.40) by setting $V_{cb} = V_{sb}$. In order for this assumption to be valid, the gate to substrate voltage must satisfy the condition: $V_{gb} \geq V_{sb} + V_{fb} + \phi_0 - \frac{\Delta E_F}{q} + \frac{E_c}{q} - \frac{kT}{q} - \frac{Ie^{-1}}{m}$. The right hand side of this inequality equation can be recognized as the threshold voltage.

In addition, depending on which equation is to be used, either Eq. (3.39) or (3.40), to find the carbon nanotube surface potential $\psi_{cnt,s}(L)$, two regions of operation can be defined: a saturation region for $V_{ds} \geq V_{gs} - \left(V_{fb} + \phi_0 - \frac{\Delta E_F}{q} + \frac{E_c}{q} - \frac{kT}{q} - \frac{Ie^{-1}}{m}\right)$, and a linear region for $V_{ds} \leq V_{gs} - \left(V_{fb} + \phi_0 - \frac{\Delta E_F}{q} + \frac{E_c}{q} - \frac{kT}{q} - \frac{Ie^{-1}}{m}\right)$. The right hand side of this inequality equation is similar to a saturation voltage in a typical MOSFET and under parenthesis is the threshold voltage, V_{th} term. The saturation voltage, $V_{ds,sat}$ and the threshold voltage, V_{th} derivations will be addressed in more detailed in Chapter 4.

Figure 3.5 shows the I-V characteristics for two carbon nanotubes with chiral vectors (3,1) and (7,2) for different overdrive gate voltages. In Fig. 3.5(a), experimentally measured data taken from the work of Wind et al., [9] for chiral vector (3,1) are also plotted for comparison. The model equation follows closely the experimentally measured data for V_{ds} up to *1 V*. Beyond V_{ds} = *1 V*, experimental values deviate from the model equation since our model equation does not include a correction term similar to the channel length modulation parameter in a MOSFET. No experimental data could be made available for CNT-FET (7,2) for comparison with the model equation.

3.3 Subthreshold Current

In subthreshold region, the carbon nanotube surface potential is found in the same way as in normal operation, using Eqs. (3.39) and (3.40). However, we can use a different current equation for low bias conditions. The current equation per conduction band of a carbon nanotube is defined as follows [36,37]:

$$I_{ds_i} = \frac{q}{\pi\hbar}\sum_i \int_{E_{c_i}}^{E_{\max}} T_i(E)\left[f_s(E) - f_d(E)\right]dE\,, \tag{3.47}$$

where $f_s(E)$ and $f_d(E)$ are the Fermi levels at the source and drain, respectively. The total I_{ds} will

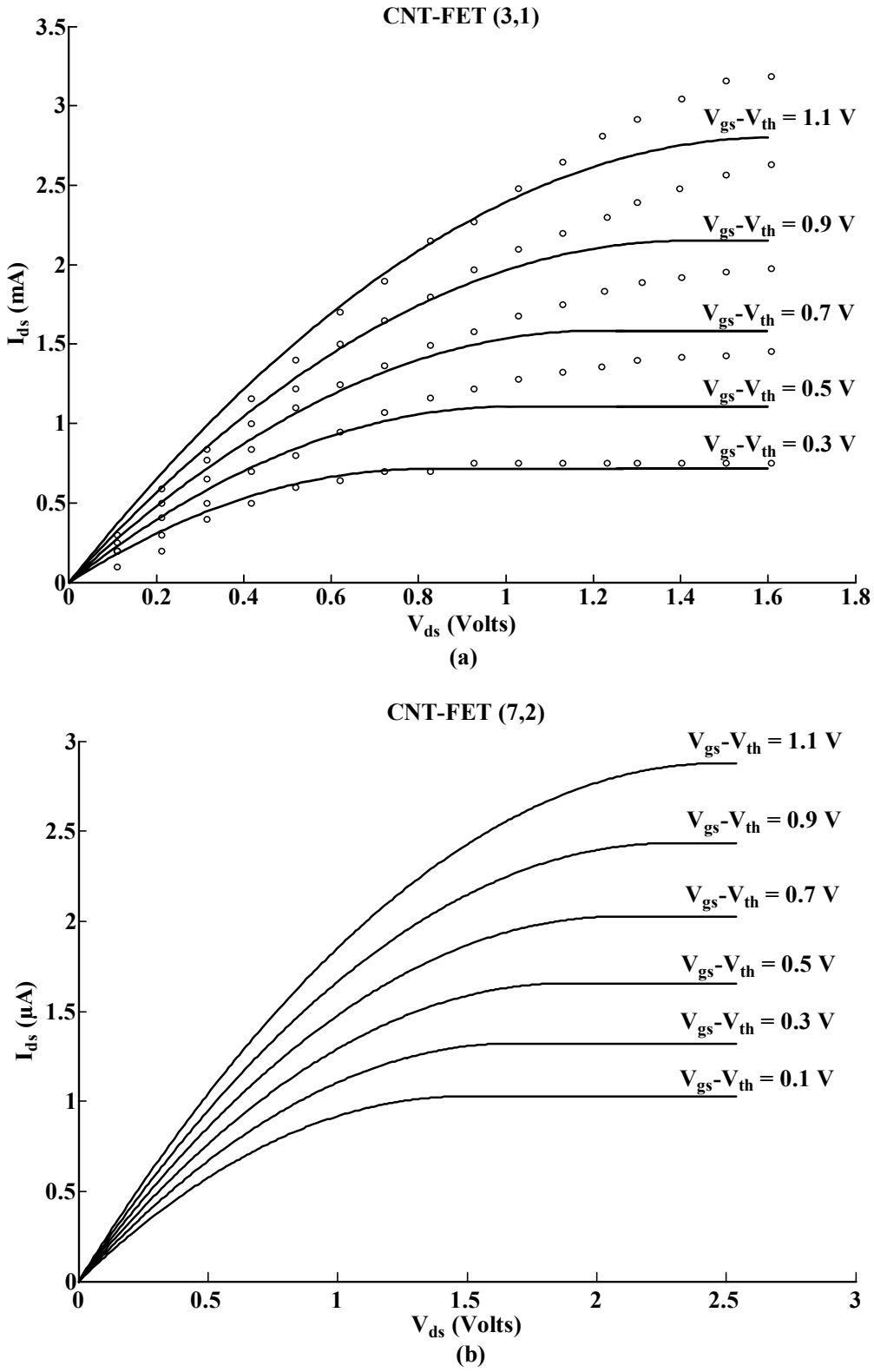

Figure 3.5: I-V characteristics of CNT-FETs with $Q_{01} = Q_{02} = 0$ for (a) CNT-FET (3,1) and (b) CNT-FET (7,2). The device dimensions are: $T_{ox1} = 15$ *nm*, $T_{ox2} = 120$ *nm* and $L = 260$ *nm*.

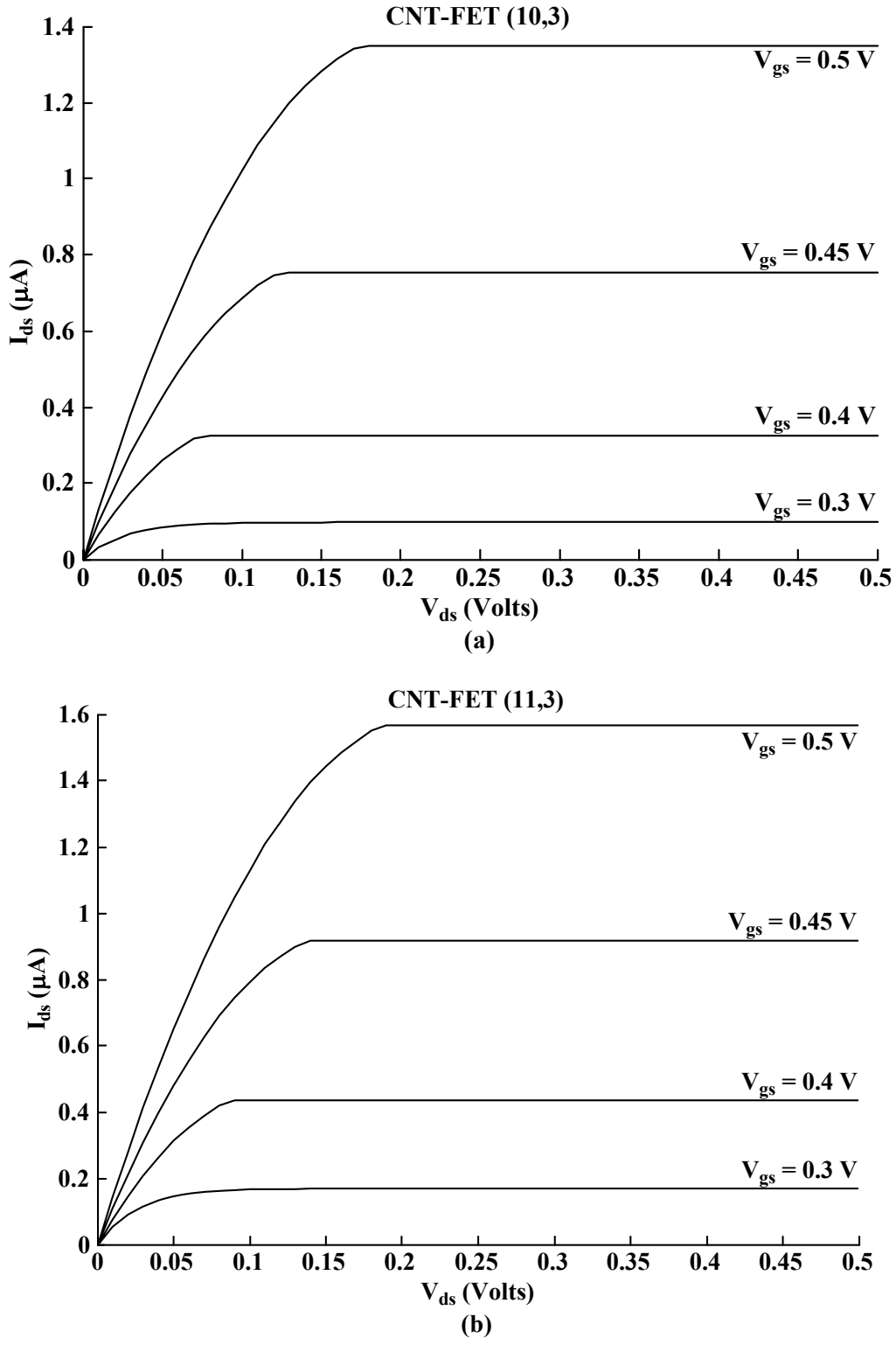

Figure 3.6: I-V characteristics of CNT-FETs in subthreshold region of operation for $Q_{01} = Q_{02} = 0$ for (a) CNT-FET (10,3) and (b) CNT-FET (11,3). The device dimensions are: $T_{ox1} = 40\ nm$, $T_{ox2} = 400\ nm$ and $L = 50\ nm$.

be the sum of I_{dsi} over all bands.

By letting the limit of E_{max} go to infinity and the transmission coefficient, $T_i\ (E) = 1$ (implies ballistic transport), for the energy range of integration, Eq. (3.47) becomes:

$$I_{ds} = \frac{qkT}{\pi\hbar}\left[\ln\left(1+e^{\frac{\Delta E_F + q\left(\psi_{cnt,s} - V_{sb} - \phi_0\right) - E_c}{kT}}\right) - \ln\left(1+e^{\frac{\Delta E_F + q\left(\psi_{cnt,s} - V_{db} - \phi_0\right) - E_c}{kT}}\right)\right], \tag{3.48}$$

where Eq. (3.35) has been used to substitute the Fermi level energies at the source and drain. In addition, the summation has been removed as higher conduction band energies will not contribute to the current under low voltages and can be neglected. Figures 3.6(a) and (b) show the I-V characteristics for the subthreshold operation of CNT-FETs with chiral vectors (11,3) and (10,3), respectively.

3.4 Summary

The charge transport in a CNT-FET, based on our reported carrier concentration model, has been used to relate the carbon nanotube potential and the gate substrate voltage. Analytical solutions have been developed relating the carbon nanotube potential and the gate substrate voltage. These solutions are then used to model analytically the current transport in a CNT-FET depending on the chiral vector and device geometry. Threshold and saturation voltage model equations are each derived in the process. CNT-FET is also modeled for subthreshold operation. The analytical transport models have been used to generate CNT-FET I-V characteristics for two different chiral vectors and compare them with the recently reported experimental data for one of the chiral vectors, CNT (11,3). A close agreement is obtained between the analytical models and the experimental observations in linear and saturation regions. Some disagreement is noted beyond V_{ds} above 1 V since the model equations do not include a term similar to the channel length modulation parameter in a typical MOSFET.

3.5 References

[1] S. J. Tans, A. R. M. Vershueren, and C. Dekker, "Room-temperature transistor based on a single carbon nanotube," *Nature,* vol. 393, pp. 49-52, May 1998.

[2] R. Martel, T. Schmidt, H. R. Shea, T. Hertel, and P. Avouris, "Single and multi wall carbon nanotube field effect transistors," *Applied Physics Letters,* vol. 73, pp. 2447-2449, October 1998.

[3] P. Avouris, J. Appenzeller, R. Martel, and S. J. Wind, "Carbon nanotube electronics," *Proceedings of the IEEE*, vol. 91, pp. 1772-1784, 2003.

[4] A. DeHon and K. K. Likharev, "Hybrid CMOS/nanoelectronic digital circuits: devices, architectures, and design automation," *Proc. ICCAD*, pp. 375-382, 2005.

[5] N. Srivastava, R. V. Joshi, and K. Banerjee, "Implications for performance, power dissipation, and thermal management," *IEDM Technical Digest,* pp. 249-252, December 5-7 2005.

[6] A. Raychowdhury and K. Roy, "Modeling of metallic carbon-nanotube interconnects for circuit simulations and a Comparison with Cu interconnects for scaled technologies," *IEEE Transactions on Computer-Aided Design of Integrated Circuits and Systems,* vol. 25, pp. 58-65, January 2006.

[7] H. S. P. Wong, "Field effect transistors - from silicon MOSFETs to carbon nanotube FETs," *Proc. 23th International Conference on Microelectronics, (MIEL)*, pp. 103-107, 2002.

[8] J. Guo, S. Datta, M. Lundstrom, M. Brink, P. McEuen, A. Javey, H. Dai, H. Kim, and P. McIntyre, "Assessment of silicon MOS carbon nanotube FET perfomance limits using a general theory of ballistic transistors," *IEDM Technical Digest,* pp. 711-714, December 2002.

[9] S. J. Wind, J. Appenzeller, R. Martel, V. Derycke, and P. Avouris, "Vertical scaling of carbon nanotube field-effect transistors using top gate electrodes," *Applied Physics Letters,* vol. 80, pp. 3817-3819, 2002.

[10] A. Javey, J. Guo, D. B. Farmer, Q. Wang, D. Wang, R. G. Gordon, M. Lundstrom, and H. Dai, "Carbon nanotube field-effect transistors with integrated ohmic contacts and high-k gate dielectrics," *Nano Letters,* vol. 4, pp. 447-450, February 2004.

[11] S. J. Wind, J. Appenzeller, R. Martel, V. Derycke, and P. Avouris, "Fabrication and electrical characterization of top gate single-wall CNFETs," *Journal of Vacuum Science and Technology B,* vol. 20, pp. 2798-2801, 2002.

[12] Y. Nosho, Y. Ohno, S. Kishimoto, and T. Mizutani, "N-type carbon nanotube field-effect transistors fabricated by using Ca contact electrodes," *Applied Physics Letters,* vol. 86, pp. 073105-073107, February 2005.

[13] A. Javey, Q. Wang, W. Kim, and H. Dai, "Advancements in complementary carbon nanotube field-effect transistors," *IEDM Technical Digest,* pp. 31.2.1-31.2.4, December 2003.

[14] A. Javey, Q. Wang, A. Ural, Y. Li, and H. Dai, "Carbon nanotube transistors arrays for multistage complementary logic and ring oscillators," *Nano Letters,* vol. 2, pp. 929-932, July 2002.

[15] A. Javey, H. Kim, M. Brink, Q. Wang, A. Ural, J. Guo, P. Mcientyre, P. McEuen, M. Lundstrom, and H. Dai, "High k-dielectric for advanced carbon nanotube transistors and logic gates," *Nature Materials,* vol. 1, pp. 241-246, November 2002.

[16] V. Derycke, R. Martel, J. Appenzeller, and P. Avouris, "Carbon nanotube inter- and intramolecular logic gates," *Nano Letters,* vol. 1, pp. 453-456, September 2001.

[17] R. Martel, V. Derycke, J. Appenzeller, S. Wind, and P. Avouris, "Carbon Nanotube Field Effect Transistors and Logic Circuits," *Proc. 39th Design Automation Conference*, pp. 94-98, 2002.

[18] A. Bachtold, P. Hadley, T. Nakanishi, and C. Dekker, "Logic circuits with carbon nanotube transistors," *Science,* vol. 294, pp. 1317-1320, November 2001.

[19] D. L. John, L. C. Castro, J. P. Clifford, and D. L. Pulfrey, "Electrostatic of coaxial Schottky barrier nanotube field effect transistors," *IEEE Transactions on Nanotechnology,* vol. 2, pp. 175-180, September 2003.

[20] C. Dwyer, M. Cheung, and D. J. Sorin, "Semi-empirical SPICE models for carbon nanotube FET logic," *Proc. 4th IEEE Conference on Nanotechnology*, pp. 386-388, 2004.

[21] A. Raychowdhury, S. Mukhopadhyay, and K. Roy, "A circuit-compatible model of ballistic carbon nanotube field effect transistors," *IEEE Transactions on Computer-Aided Design of Integrated Circuits and Systems,* vol. 23, pp. 1411-1420, October 2004.

[22] A. Raychowdhury and K. Roy, "Carbon nanotube based voltage-mode multiple-valued logic design," *IEEE Transactions on Nanotechnology,* vol. 4, pp. 168 - 179, March 2005.

[23] I. O'Connor, J. Liu, F. Gaffiot, F. Prégaldiny, C. Lallement, C. Maneux, J. Goguet, S. Frégonèse, T. Zimmer, L. Anghel, T.-T. Dang, and R. Leveugle, "CNTFET modeling and reconfigurable logic circuit design," *IEEE Transactions on Circuits and Systems, Part-1,* vol. 54, pp. 2365-2379, 2007.

[24] A. Hazeghi, T. Krishnamohan, and H.-S. P. Wong, "Schottky-barrier carbon nanotube field effect transistor modeling," *IEEE Transactions on Electron Devices,* vol. 54, pp. 439-445, March 2007.

[25] L. C. Shen and J. A. Kong, *Applied Electromagnetism*, 3th Ed. Boston, MA: PWS Foundations in Engineering Series, 1995.

[26] Y. Tsividis, *Operation and Modeling of the MOS transistor*. Singapore: McGraw-hill, 1999.

[27] W. H. Hayt, *Engineering Electro-Magnetics*, 3th Ed. New York: McGraw-Hill, 1974.

[28] J. M. Marulanda, A. Srivastava, and R. K. Nahar, "Ultra-high frequency modeling of carbon nanotube field-effect transistors," *Proc. 13th International Workshop on the Physics of Semiconductor Devices (IWPSD)*, New Delhi, pp. G-11, 2005.

[29] J. M. Marulanda and A. Srivastava, "Carrier density and effective mass calculations for carbon nanotubes," *Proc. International Conference on Integrated Circuit Design & Technology (ICICDT)*, Austin, TX, pp. 234-237, 2007.

[30] M. S. Dresselhaus, G. Dresselhaus, and P. Avouris, *Carbon Nanotube: Synthesis, Properties, Structure, and Applications*: Springer Verlag, 2001.

[31] R. Saito, M. S. Dresselhaus, and G. Dresselhaus, *Physical Properties of Carbon Nanotubes*. London: Imperial College Press, 1998.

[32] P. E. Allen and Holberg, *CMOS Analog Circuit Design*, 2nd Ed.: Oxford University Press, 2002.

[33] A. Chandrakasan and R. W. Brodersen, *Low Power CMOS Design*: John Wiley & Sons Inc., 1998.

[34] K. Roy and S. Prasad, *Low Power CMOS VLSI Circuit Design*: John Wiley & Sons Inc., 2000.

[35] B. G. Streetman, *Solid State Electronics Devices*, 5th Ed. India: Prentice Hall, 2000.

[36] S. Datta, *Electronic Transport in Mesoscopic Systems*. New York: Cambridge University Press, 1999.

[37] T.-S. Xia, L. F. Register, and S. K. Banerjee, "Quantum transport in carbon nanotube transistors: complex band structure effects," *Journal of Applied Physics,* vol. 95, pp. 1597-1599, February 2004.

CHAPTER 4

THRESHOLD AND SATURATION VOLTAGES MODELING OF CARBON NANOTUBE FIELD EFFECT TRANSISTORS (CNT-FETs)

4.1 Introduction

As we already know carbon nanotubes are one-dimensional (1D) graphene sheets rolled in a tubular form [1] with electronic properties described by the chiral vector (n,m) [2,3]. In Chapter 3, we have studied the structure of CNT-FET and derived an analytical model for the current transport. In this chapter, we focus our attention on the threshold and saturation voltages modeling using our analytical equations for the charge and current transport in carbon nanotube field effect transistors.

In the past decade, several CNT-FETs have been fabricated [4-8] and their transfer characteristics have been characterized experimentally [9-11]. Although threshold and saturation voltages of the CNT-FET have also been reported [1,12,13], these are still graphically extrapolated from the experimental measurements. However, not much effort has been focused on establishing any theoretical relationship with the properties of the carbon nanotubes. The present work focuses on threshold and saturation voltages modeling of CNT-FETs based on the properties of the carbon nanotube. For better understanding, part of the work described in Chapter 3 is repeated here in brief for completeness.

Figure 4.1(a) shows the basic cross section of a CNT-FET including the charge distributions. Figure 4.1(b) shows the corresponding potential distributions between the gate and substrate. In Fig. 4.1(a), charge distributions are explained as follows. The charge on the gate is Q_g, charges in oxide layers are Q_{01} and Q_{02}, charge inside the CNT is Q_{cnt} and the charge in the substrate is Q_{subs}. In Fig. 4.1(b), six different potential distributions are shown, which are

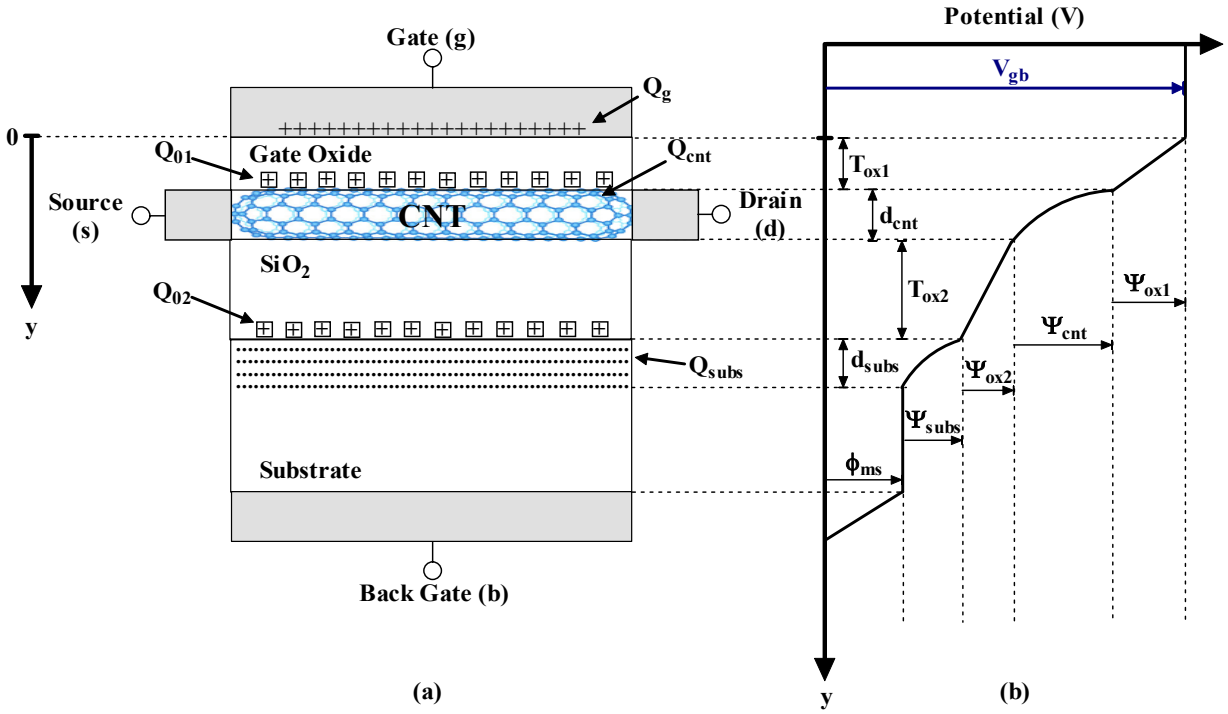

Figure 4.1: (a) Plot of the charges from the gate to the substrate and (b) plot of the potential distribution from the gate to the substrate in a CNT-FET.

also described as follows. The voltage between the gate and the substrate (back gate) is V_{gb}, the potential drop across the oxides are ψ_{ox1} and ψ_{ox2}, the surface potential in the substrate with respect to the back gate is ψ_{subs}, the potential across the CNT is ψ_{cnt} and the work function difference between the gate and the substrate materials is ϕ_{ms}. The work function, ϕ_{ms} can be divided in two parts and is expressed as follows,

$$\phi_{ms} = \phi_{mc} + \phi_{cs}\,, \tag{4.1}$$

where ϕ_{mc} and ϕ_{cs} are the work function differences between the metal gate and carbon nanotube materials and the carbon nanotube and substrate materials, respectively. We can also combine potentials ψ_{cnt}, ψ_{ox2}, ϕ_{cs} and ψ_{subs} into a single potential, $\psi_{cnt,s}$, which describes the potential at the interface of the gate oxide and carbon nanotube with respect to the back gate.

In a recent work [14], we have reported a method for calculating the carrier concentration in a carbon nanotube under two limits: Limit 1 for $\eta << -1$ and Limit 2 for $\eta >> 1$, where $\eta = \frac{E_F - E_c}{kT}$. As a result, using the relation $|Q_{cnt}| = qn_{cnt}L$, where n_{cnt} is the carrier concentration and L is the length of the carbon nanotube, the charge inside the carbon nanotube can be written as follows:

Limit 1, $\eta << -1$:

$$\left|Q_{cnt}\right| = qLN_c I e^{\frac{E_F - E_c}{kT}}\,, \tag{4.2}$$

Limit 2, $\eta >> 1$:

$$\left|Q_{cnt}\right| = qLN_c \frac{\sqrt{E_F^2 - E_c^2}}{kT}, \tag{4.3}$$

where

$$I = \frac{1}{\sqrt{kT}} \int_0^{\frac{6E_c}{kT}} \frac{(kTx + E_c)}{x^{1/2}(kTx + 2E_c)^{1/2}} e^{-x} dx \tag{4.4}$$

and

$$N_c = \frac{8kT}{\pi\sqrt{3}V_{pp\pi}a}. \tag{4.5}$$

An approximate solution for the integral *I* is given in Appendix A.

Using the potential balance and charge neutrality conditions for the field effect transistors [15], the gate to substrate voltage is given by,

$$V_{gb} = \psi_{cnt,s} - \frac{Q_{cnt}}{C_{ox1}} + V_{fb}, \tag{4.6}$$

where V_{fb} is the flat band voltage given by,

$$V_{fb} = \phi_{mc} - \frac{Q_{01}}{C_{ox1}}. \tag{4.7}$$

The carbon nanotube potentials under the same limits are given below[16],

Limit 1: $\eta << -1$:

$$\psi_{cnt,s} = V_{gb} - V_{fb}, \tag{4.8}$$

Limit 2: $\eta >> 1$:

$$\psi_{cnt,s} = \frac{V_{gb} - \delta I e^{-1} - V_{fb} + \delta m\left(V_{cb} + \phi_0 - \frac{\Delta E_F}{q} + \frac{E_c}{q} - \frac{kT}{q}\right)}{1+\delta m}, \tag{4.9}$$

where

$$m = \frac{\sqrt{\frac{2E_c}{kT}+1} - Ie^{-1}}{\frac{2kT}{q}} \tag{4.10}$$

and

$$\delta = \frac{qLN_c}{C_{ox1}}. \tag{4.11}$$

In Eq. (4.9), ϕ_0 and ΔE_F are given as follows:

$$\phi_0 = \phi_{cs} - \frac{Q_{02}}{C_{ox2}} \tag{4.12}$$

and

$$\Delta E_F = \pm kT \ln\left(1 + \frac{N}{n_{cnt,i}}\right). \tag{4.13}$$

In Eq. (4.13), $n_{cnt,i}$ is the intrinsic carrier concentration given by $n_{cnt,i} = N_c I e^{\frac{-E_c}{kT}}$ and N is the ionized impurity concentration. Furthermore, ΔE_F is positive for n-type carbon nanotubes (donor atoms $N = N_D$) and negative for p-type carbon nanotubes (acceptor atoms $N = N_A$), and C_{ox2} is the oxide capacitance between the carbon nanotube and the surface of the substrate given by,

$$C_{ox2} = \frac{2\pi\varepsilon_{ox2}L}{\ln\left(\frac{T_{ox2} + r + \sqrt{T_{ox2}^2 + 2T_{ox2}r}}{r}\right)}. \tag{4.14}$$

The charge inside the carbon nanotube, Q_{cnt} can be obtained from Eq. (4.6) and is given as follows,

$$Q_{cnt} = -C_{ox1}\left(V_{gb} - \psi_{cnt,s} - V_{fb}\right). \tag{4.15}$$

Under Limit 1, $Q_{cnt} = 0$ for $\psi_{cnt,s} = V_{gb} - V_{fb}$. For the Limit 2, substituting Eq. (4.9) in Eq. (4.15), Q_{cnt} can be put in the following form:

$$Q_{cnt} = -C_{ox1}\left(\frac{\delta m\left(V_{gb} - V_{fb} - V_{cb} - \phi_0 + \frac{\Delta E_F}{q} - \frac{E_c}{q} + \frac{kT}{q}\right) + \delta I e^{-1}}{1 + \delta m}\right). \tag{4.16}$$

4.2 Threshold Voltage (V_{th})

The threshold voltage, V_{th} in a metal oxide semiconductor is, by definition, the voltage at which a conducting channel begins to form [17-20], the same definition can be applied in

determining V_{th} of a CNT-FET. Therefore, we can assume that $Q_{cnt} = 0$ at V_{th}.

By setting $Q_{cnt} = 0$ in Eq. (4.16) and solving for the gate voltage, we obtain an expression for the gate voltage with respect to the substrate and is given by,

$$V_{gb} = V_{fb} + V_{cb} + \phi_0 - \frac{\Delta E_F}{q} + \frac{E_c}{q} - \frac{kT}{q} - \frac{Ie^{-1}}{m} . \tag{4.17}$$

Equating Eq. (4.17) with V_{gb} as $V_{gs} + V_{cb}$ at the source end, we obtain an expression for the threshold voltage, V_{th}, which is given by,

$$V_{th} = V_{fb} + \phi_0 - \frac{\Delta E_F}{q} + \frac{E_c}{q} - \frac{kT}{q} - \frac{Ie^{-1}}{m} . \tag{4.18}$$

At the source end, V_{cb} becomes V_{sb}, the channel to substrate potential. Equation (4.18) for V_{th} is the gate to source voltage, V_{gs} at which transistor begins to conduct. Equations (4.2) and (4.3) can be used to plot the charge inside the carbon nanotube with respect to the gate voltage as shown in Fig. 4.2(a) and (b) for two CNT-FETs with chiral vectors (3,1) and (7,2), respectively. The solid line in Fig. 4.2 shows the variation of Q_{cnt} versus V_{gb} corresponding to Eqs. (4.2) and (4.3) following the numerical approach. The dotted line in Fig. 4.2 shows the variation of Q_{cnt} versus V_{gb} following the analytical approach corresponding to Eq. (4.16) for the carbon nanotube potential and its extrapolation to V_{gb}-axis gives the threshold voltage, V_{th} considering source and substrate to be at the same potential. The threshold voltage can also be obtained graphically by drawing a tangent to the solid line in the Q_{cnt} versus V_{gb} curve in Fig. 4.2. The intersection with the V_{gb}-axis gives the threshold voltage.

4.3 Saturation Voltage ($V_{ds,sat}$)

In a CNT-FET, the saturation voltage, $V_{ds,sat}$ can be defined as the voltage at which the charge inside the carbon nanotube becomes independent of V_{ds}. It results for the current becoming independent of V_{ds} in the I-V characteristics of the CNT-FET beyond $V_{ds,sat}$. Equation (4.16) can be used to solve for the drain to source voltage V_{ds}. Since at the drain of the carbon

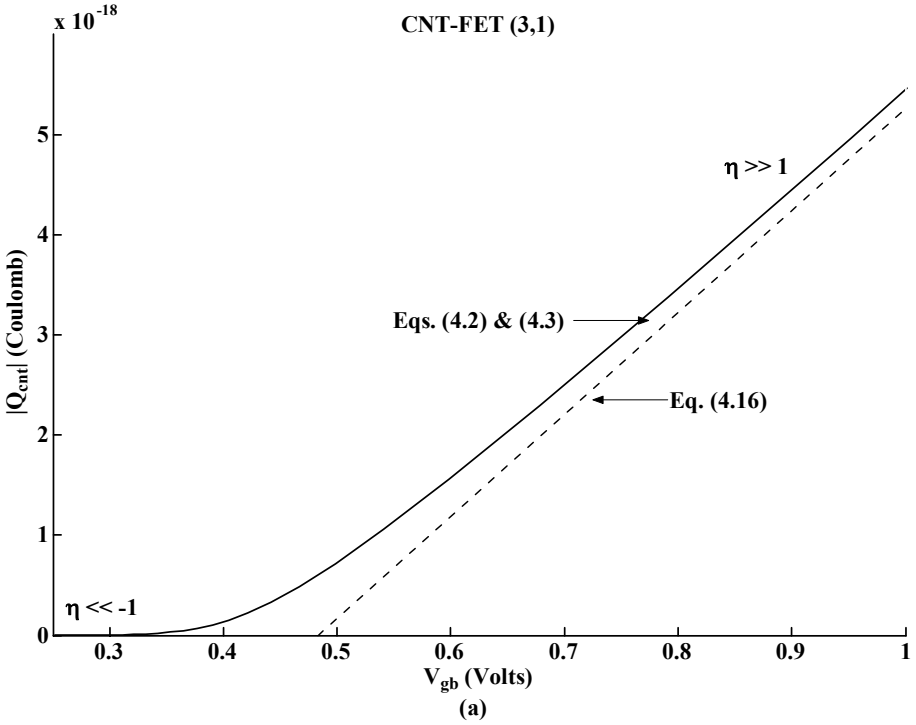

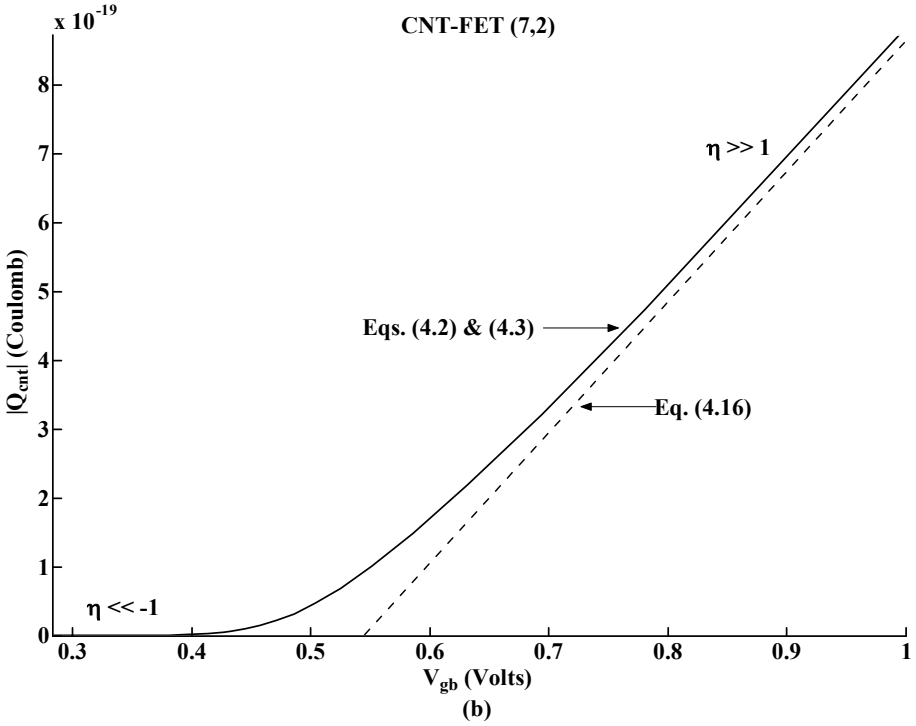

Figure 4.2: CNT charge, Q_{cnt} versus gate voltage, V_{gb}, for (a) CNT-FET of chiral vector (3,1) with $L=260\ nm$, $T_{ox1}=15\ nm$, $T_{ox2}=120\ nm$ and $V_{fb}=-0.79\ V$ and (b) CNT-FET of chiral vector (7,2) with $L=50\ nm$, $T_{ox1}=40\ nm$, and $T_{ox2}=400\ nm$ and $V_{fb}=0\ V$.

nanotube field effect transistor (CNT-FET), Q_{cnt} = 0, we can derive from Eq. (4.16) an expression for the channel to substrate voltage at the drain, V_{db}. The expression for V_{db} is obtained by replacing V_{cb} with V_{db} at the drain end and is given by,

$$V_{db} = V_{gb} - V_{fb} - \phi_0 + \frac{\Delta E_F}{q} - \frac{E_c}{q} + \frac{kT}{q} + \frac{Ie^{-1}}{m}. \tag{4.19}$$

From the Fig. 4.1(a) V_{db} is equal to $V_{ds} + V_{sb}$. In Eq. (4.19), substituting $V_{gb} = V_{gs} + V_{sb}$ and $V_{db} = V_{ds} + V_{sb}$, we obtain an expression for the drain to source voltage in saturation, $V_{ds,sat}$ as follows,

$$V_{ds,sat} \geq V_{gs} - V_{th} = V_{gs} - \left(V_{fb} + \phi_0 - \frac{\Delta E_F}{q} + \frac{E_c}{q} - \frac{kT}{q} - \frac{Ie^{-1}}{m}\right). \tag{4.20}$$

Figures 4.3(a) and (b) show a plot for the charge inside the carbon nanotube (Q_{cnt}) at the drain versus the drain to bulk voltage (V_{db}) for two CNT-FETs with chiral vectors (3,1) and (7,2), respectively. The solid line in Fig. 4.3 represents a numerical approach using Eqs. (4.2) and (4.3). The dotted line represents an analytical approach following the Eq. (4.16) and its extrapolation to V_{db}-axis gives $V_{ds,sat}$. It should be noted that in Fig. 4.3, $Q_{cnt} = 0$ at the drain under the Limit 1 ($\eta << -1$).

In a manner similar to the threshold voltage derivation, a tangent line to the solid line in Fig. 4.3 can also be drawn and the saturation voltage can be obtained from the intersection of the drawn tangent line with the V_{db}-axis considering source and substrate to be at the same potential.

4.4 Results

Table 4.1 summarizes the results of threshold and saturation voltages for different CNT-FETs using Eqs. (4.18) and (4.20). The same device geometries used by Wind et al., [13] have been utilized in these calculations. The modeled threshold voltage for the CNT-FET (3,1) closely matches the experimentally measured threshold voltage in [13] ($|V_{th}| \sim 0.5$ V). It is also

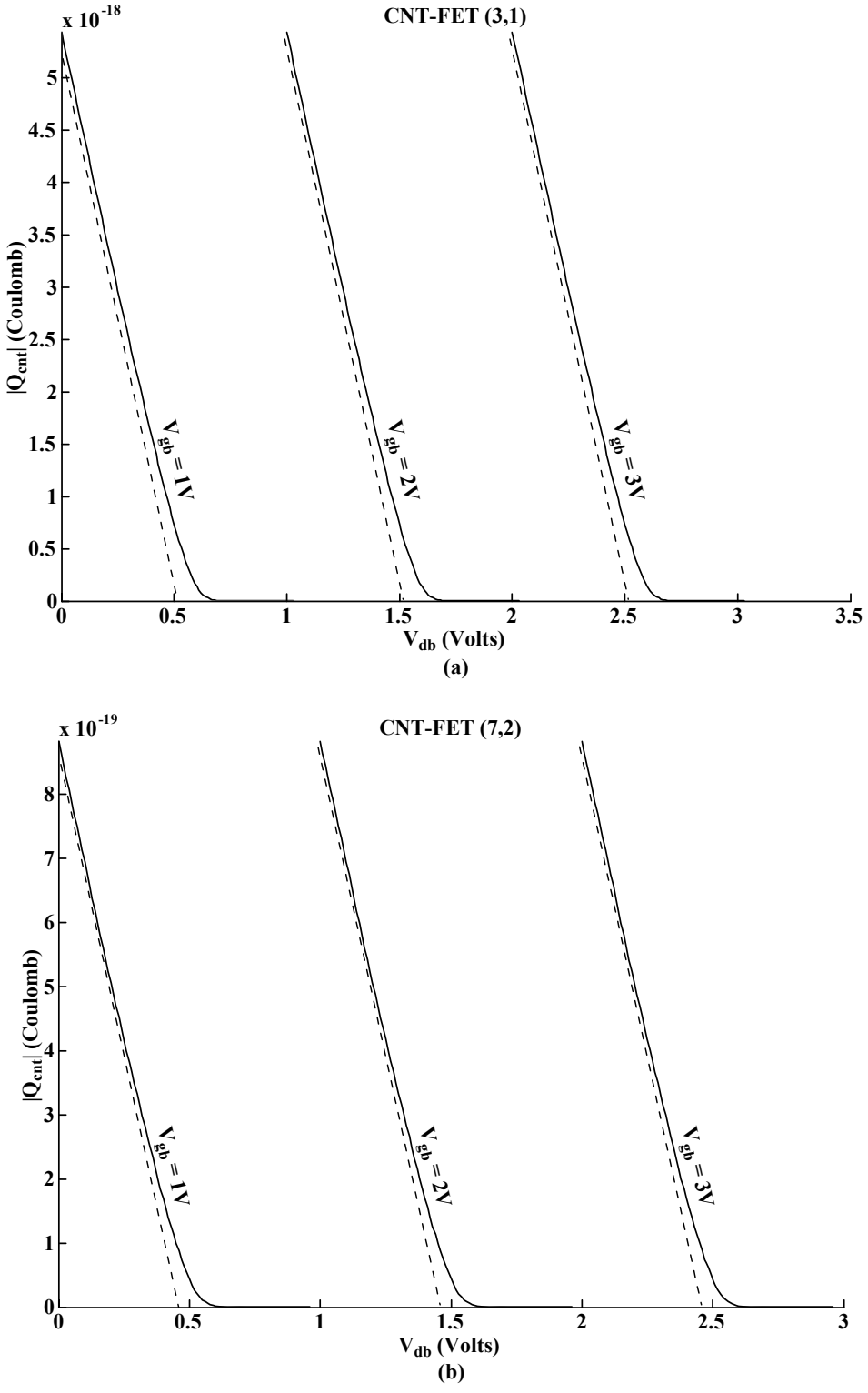

Figure 4.3: CNT charge, $|Q_{cnt}|$ at the drain versus drain to bulk voltage, V_{db}, for (a) CNT-FET of chiral vector (3,1) with $L = 260\ nm$, $T_{ox1} = 15\ nm$, $T_{ox2} = 120\ nm$ and $V_{fb} = -0.79\ V$ and (b) CNT-FET of chiral vector (7,2) with $L = 50\ nm$, $T_{ox1} = 40\ nm$, $T_{ox2} = 400\ nm$ and $V_{fb} = 0\ V$.

Table 4.1. Calculated threshold voltage (V_{th}) and saturation voltage ($V_{ds,sat}$) of CNT-FETs from the model equations for different carbon nanotubes

CNT-FET (n,m)	**V_{th} (V)**	**$V_{ds,sat}$ (V)**	
		V_{gs} = 1.5 V	**V_{gs} = 2 V**
(3,1)	0.469	1.031	1.531
(3,2)	0.154	1.346	1.846
(4,2)	0.040	1.460	1.960
(4,3)	-0.107	1.607	2.107
(5,0)	0.143	1.357	1.857
(5,1)	-0.066	1.566	2.066
(5,3)	-0.176	1.676	2.176
(6,1)	-0.105	1.605	2.105
(7,3)	-0.333	1.833	2.333
(9,2)	-0.393	1.893	2.393
(11,3)	-0.462	1.962	2.462

observable from the Table 4.1 that both V_{th} and $V_{ds,sat}$ are dependent on the chiral vector (n,m). Furthermore, negative threshold voltages are pointing toward the depletion mode behavior.

4.5 Summary

Model equations for threshold and saturation voltages in CNT-FETs have been derived, which are dependent on chiral vectors of carbon nanotubes. These model equations provide designers with useful mathematical expressions relating the properties of conductivity of carbon nanotubes and their response in circuit applications. The theoretical results show agreement with graphically extrapolated threshold and saturation voltages. The model equations in this work provide a better understanding of device modeling of carbon nanotube field effect transistors (CNT-FETs).

4.6 References

[1] R. Martel, T. Schmidt, H. R. Shea, T. Hertel, and P. Avouris, "Single and multi wall carbon nanotube field effect transistors," *Applied Physics Letters,* vol. 73, pp. 2447-2449, October 1998.

[2] K. Tanaka, T. Yamabe, and K. Fukui, *The Science and Technology of Carbon Nanotubes*. Amsterdam: Elsevier, 1999.

[3] P. R. Wallace, "The band theory of graphite," *Physical Review Letters,* vol. 71, pp. 622-634, May 1947.

[4] S. Heinze, J. Tersoff, R. Martel, V. Derycke, J. Appenzeller, and P. Avouris, "Carbon nanotubes as Schottky barrier transistors," *Physical Review Letters,* vol. 89, p. 106801, September 2002.

[5] J. Guo, S. Datta, and M. Lundstrom, "A numerical study of scaling issues for schottky barrier CNFETs," *IEEE Transactions on Electron Devices,* vol. 51, pp. 172-177, February 2004.

[6] A. Javey, J. Guo, Q. Wang, M. Lundstron, and H. Dai, "Ballistic carbon nanotube field effect transistors," *Nature,* vol. 424, pp. 654-657, August 2003.

[7] Y. Nosho, Y. Ohno, S. Kishimoto, and T. Mizutani, "N-type carbon nanotube field-effect transistors fabricated by using Ca contact electrodes," *Applied Physics Letters,* vol. 86, pp. 073105-073107, February 2005.

[8] A. Javey, Q. Wang, W. Kim, and H. Dai, "Advancements in complementary carbon nanotube field-effect transistors," *IEDM Technical Digest,* pp. 31.2.1-31.2.4, December 2003.

[9] A. Bachtold, P. Hadley, T. Nakanishi, and C. Dekker, "Logic circuits with carbon nanotube transistors," *Science,* vol. 294, pp. 1317-1320, November 2001.

[10] A. Javey, R. Tu, D. B. Farmer, J. Guo, R. G. Gordon, and H. Dai, "High performance n-type carbon nanotube field-effect transistors with chemically doped contacts," *Nano Letters,* vol. 5, pp. 345-348, January 2005.

[11] J. Li, Q. Zhang, D. Yang, and J. Tian, "Fabrication of carbon nanotube field effect transistors by AC dielectrophoresis method," *Carbon,* vol. 42, pp. 2263-2267, June 2004.

[12] A. Javey, J. Guo, D. B. Farmer, Q. Wang, D. Wang, R. G. Gordon, M. Lundstrom, and H. Dai, "Carbon nanotube field-effect transistors with integrated ohmic contacts and high-k gate dielectrics," *Nano Letters,* vol. 4, pp. 447-450, February 2004.

[13] S. J. Wind, J. Appenzeller, R. Martel, V. Derycke, and P. Avouris, "Vertical scaling of carbon nanotube field-effect transistors using top gate electrodes," *Applied Physics Letters,* vol. 80, pp. 3817-3819, 2002.

[14] J. M. Marulanda and A. Srivastava, "Carrier density and effective mass calculations for carbon nanotubes," *Proc. International Conference on Integrated Circuit Design & Technology (ICICDT)*, Austin, TX, pp. 234-237, 2007.

[15] J. M. Marulanda and A. Srivastava, "I-V characteristic modeling and parameter extraction for CNT-FETs," *Proc. International Semiconductor Device Research Symposium (ISDRS)*, Bethesda, MD, pp. 38-39, 2005.

[16] J. Marulanda, A. Srivastava, and A. K. Sharma, "Transfer characteristics and high frequency modeling of logic gates using carbon nanotube field effect transistors (CNT-FETs)," *Proc. of The 20th Annual Conference on Integrated Circuits and Systems Design*, Rio de Janeiro, Brazil, pp. 202-206, 2007.

[17] Y. Tsividis, *Operation and Modeling of the MOS transistor*. Singapore: McGraw-hill, 1999.

[18] P. Antognetti and G. Massobrio, *Semiconductor Device Modeling with SPICE*. Singapore: McGraw-Hill, 1988.

[19] B. G. Streetman, *Solid State Electronic Devices*, 5th Ed. India: Prentice Hall, 2000.

[20] M. Horenstein, *Microlectronics Circuits and Devices*, 2nd Ed. New Jersey: Prentice Hall, 1995.

CHAPTER 5

VOLTAGE TRANSFER CHARACTERISTICS OF LOGIC GATES USING CARBON NANOTUBE FIELD EFFECT TRANSISTORS (CNT-FETS)*

5.1 Introduction

In previous chapters, we have seen how carbon nanotubes have been the primary focus of many researchers, and many applications have been proposed over the past decade including nanometer-sized semiconductor devices [1-3]. The first fabricated CNT-FETs, as it was described in Chapter 1, showed a Schottky barrier phenomena, resembling Schottky diode characteristics at the electrode contacts [4-6], a fact that had been a real disadvantage since MOSFETs do not show these Schottky barriers [7,8]. However, with latter CNT-FETs fabricated in 2004 [1,9] without any of this barrier characteristic, carbon nanotube based technology has successfully arisen closer to replacing current CMOS technology especially with the end of Moore's law in sight [10-12]. Logic gates using CNT-FETs have already been fabricated [13-15] and their transfer characteristics have also been presented [14-17]. In this chapter, our previous analytical models for the current transport (Chapters 3 and 4) have been utilized to derive and present the transfer characteristics of basic logic gates needed to build systems and to show the variation of the chiral vectors (n,m) of carbon nanotubes on these voltage transfer characteristics.

5.2 Current Equation

Although the computer simulations performed in this work were done using intrinsic

* Part of the work is reported in the following publication:
J. M. Marulanda, A. Srivastava and A.K. Sharma, "Transfer characteristics and high frequency modeling of logic gates using carbon nanotube field effect transistors (CNT-FETs)," *Proc. of The 20th Annual Conference on Integrated Circuits and Systems Design (SBCCI 2007)*, pp. 202-206, (Rio de Janeiro, Brazil, September 3-6, 2007).

carbon nanotubes, CNT-FETs work under the same conditions as in CMOS [10] and therefore, can be classified as n-type and p-type transistors [9]. Figure 5.1 shows the basic cross sectional view of a CNT-FET. Relevant current transport modeling equations from Chapters 3 and 4 are given below for completeness and clarity in presentation. Even though the model equations described in this section are for n-type transistors, the same model equations can be applied for p-type transistors by changing the respective parameters and voltage polarities.

The current model equation for CNT-FETs is described as:

$$I_{ds} = \beta\left[f\left\{\psi_{cnt,s}(L), V_{gs}\right\} - f\left\{\psi_{cnt,s}(0), V_{gs}\right\}\right], \tag{5.1}$$

where

$$f\left\{\psi_{cnt,s}(x), V_{gs}\right\} = \left(V_{gs} + V_{sb} - V_{fb} + \tfrac{kT}{q}\right)\psi_{cnt,s}(x) - \tfrac{1}{2}\psi_{cnt,s}^2(x) \tag{5.2}$$

and

$$\beta = \frac{\gamma \mu C_{ox1}}{L^2}. \tag{5.3}$$

In Eq. (5.3), L is the gate length, μ is the carrier mobility, γ is a conversion factor for the carrier mobility in CNT from the graphite with a value ranging from 0 to 1 and can also be used to represent how much surface area of the CNT is responsible for the charge flow. In the present work $\gamma = 1$. K is Boltzmann's constant, T is temperature, V_{fb} is the flat band voltage given by

$$V_{fb} = \phi_{mc} - \frac{Q_{01}}{C_{ox1}}, \tag{5.4}$$

where ϕ_{mc} is the contact potential difference between the gate and the carbon nanotube, Q_{01} is the trapped charge in the gate oxide (Fig. 5.1) and C_{ox1} is the gate oxide capacitance given by [18,19]

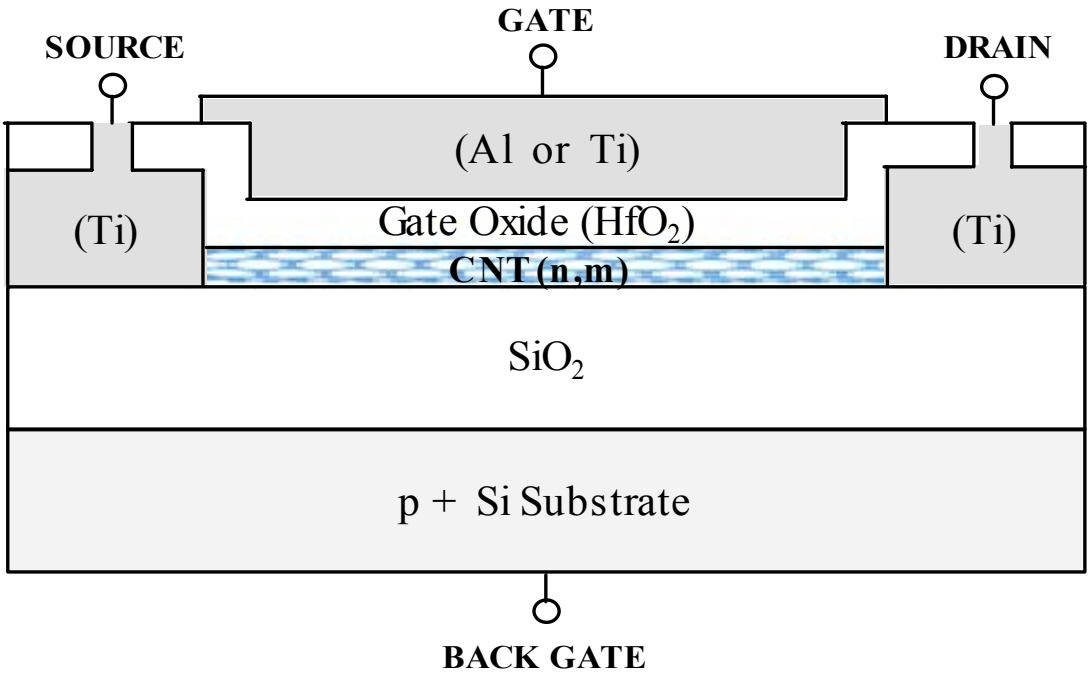

Figure 5.1: Cross sectional view of a CNT-FET.

$$C_{ox1} = \frac{2\pi\varepsilon_{ox1}L}{\ln\left(\frac{T_{ox1}+r+\sqrt{T_{ox1}^2+2T_{ox1}r}}{r}\right)}, \tag{5.5}$$

where T_{ox1} is the thickness of the gate oxide, r is the carbon nanotube radius and ε_{ox1} is the permittivity constant of the gate oxide.

The transistor turns-on when the carbon nanotube has become significantly conductive. This condition occurs when the gate to source voltage, $V_{gs} \geq$ threshold voltage, V_{th}, given by the equation,

$$V_{gs} \geq V_{th} = V_{fb} + \phi_0 - \tfrac{\Delta E_F}{q} + \tfrac{E_c}{q} - \tfrac{kT}{q} - \tfrac{Ie^{-1}}{m}, \tag{5.6}$$

where $m = \frac{\sqrt{\frac{2E_c}{kT}+1} - Ie^{-1}}{\frac{2kT}{q}}$ and I is a specific integral of each carbon nanotube defined by

$$I = \frac{1}{\sqrt{kT}} \int_0^{\frac{6E_c}{kT}} \frac{(kTx + E_c)}{x^{1/2}(kTx + 2E_c)^{1/2}} e^{-x} dx, \tag{5.7}$$

where E_c is the energy conduction band minimum. An approximate solution for the integral I is given in Appendix A. Under this condition $V_{gs} \geq V_{th}$, Eq. (5.1) can be used.

In Eq. (5.6), ϕ_0 and ΔE_F are defined as follows:

$$\phi_0 = \phi_{cs} - \frac{Q_{02}}{C_{ox2}}, \tag{5.8}$$

where Q_{02} is the trapped charge in the SiO_2 (Fig. 5.1).

$$\Delta E_F = \pm kT \ln\left(1 + \frac{N}{n_{cnt,i}}\right), \tag{5.9}$$

where $n_{cnt,i}$ is the intrinsic carrier concentration given by,

$$n_{cnt,i} = N_c I e^{\frac{-E_c}{kT}}, \tag{5.10}$$

where $N_c = \dfrac{8kT}{\pi\sqrt{3}V_{pp\pi}a}$ and N is the ionized impurity concentration.

Furthermore, ΔE_F is positive for n-type carbon nanotubes (donor atoms $N = N_D$) and negative for p-type carbon nanotubes (acceptor atoms $N = N_A$). C_{ox2} is the oxide capacitance between the carbon nanotube and the surface of the substrate given by

$$C_{ox2} = \frac{2\pi\varepsilon_{ox2}L}{\ln\left(\dfrac{T_{ox2} + r + \sqrt{T_{ox2}^2 + 2T_{ox2}r}}{r}\right)}. \tag{5.11}$$

where T_{ox1} is the thickness of the SiO_2 and ε_{ox2} is the permittivity constant of the oxide.

Under the condition $V_{gs} \geq V_{th}$ described by the Eq. (5.6), the carbon nanotube potential at the source end, $\psi_{cnt,s}(0)$ can be obtained, which is given by,

$$\psi_{cnt,s}(0) = \frac{V_{gs} + V_{sb} - \delta I e^{-1} - V_{fb} + \delta m\left(V_{sb} + \phi_0 - \frac{\Delta E_F}{q} + \frac{E_c}{q} - \frac{kT}{q}\right)}{1 + \delta m}. \tag{5.12}$$

Equation (5.12) is obtained from Eq. (3.40) after substituting $V_{gb} = V_{gs} + V_{sb}$ and $V_{cb} = V_{sb}$ at the source. Furthermore, in Eq. (5.12), 'm' is defined for the slope as in Chapter 3.

Similarly the carbon nanotube potential at the drain end, $\psi_{cnt,s}(L)$ can be obtained in two regions of operation of the CNT-FET depending on the drain to source voltage, V_{ds}. These two regions are: linear region $\left(V_{ds} \leq V_{gs} - V_{th}\right)$ and saturation region $\left(V_{ds} \geq V_{gs} - V_{th}\right)$. The carbon nanotube potential in these two regions is given by,

Linear Region $\left(V_{ds} \leq V_{gs} - V_{th}\right)$:

$$\psi_{cnt,s}(L) = \frac{V_{gs} + V_{sb} - \delta I e^{-1} - V_{fb} + \delta m\left(V_{ds} + V_{sb} + \phi_0 - \frac{\Delta E_F}{q} + \frac{E_c}{q} - \frac{kT}{q}\right)}{1 + \delta m}, \tag{5.13}$$

Equation (5.13) is obtained from Eq. (3.40) after substituting $V_{gb} = V_{gs} + V_{sb}$ and $V_{cb} = V_{db} = V_{ds} + V_{sb}$ at the drain.

Saturation Region $\left(V_{ds} \geq V_{gs} - V_{th}\right)$:

$$\psi_{cnt,s}(L) = V_{gb} - V_{fb} = V_{gs} + V_{sb} - V_{fb}, \tag{5.14}$$

where

$$\delta = \frac{qLN_c}{C_{ox1}}. \tag{5.15}$$

5.3 Logic Gates Modeling

CNT-FETs can be made both n- and p-type as in CMOS [10], making possible the implementation of CNT-FETs as fully complementary logic, such as the inverters, NOR and NAND gates as shown in Fig. 5.2. These are the basic building blocks needed for building any digital system.

As stated earlier, the model equations characterizing current voltage transport described in Section 5.2 are for the n-type CNT-FET but can also be used for the p-type CNT-FET by changing the polarities of the voltages as in standard CMOS. In generating voltage transfer characteristics, we have used Eqs. (5.1), (5.13) and (5.14) and two complementary CNT-FETs with two different chiral vectors.

Figures 5.3 shows the voltage transfer characteristics of an inverter and a two input NAND gate for a chiral vector (5,3). Figure 5.4 shows the voltage transfer characteristics of an inverter and a two input NOR gate for a chiral vector (7,3). In NAND and NOR gates, transfer characteristics have been obtained for varying input conditions as shown in both Figs. 5.3 and 5.4. The transfer characteristics of the CNT-FET inverter are similar to the transfer characteristics of a typical CMOS inverter and show a sharp transition at the inverter logic threshold voltage, 1.5 V for a 3 V operation. The gates, NAND and NOR also show a sharp transition in their transfer characteristics for a 3 V operation.

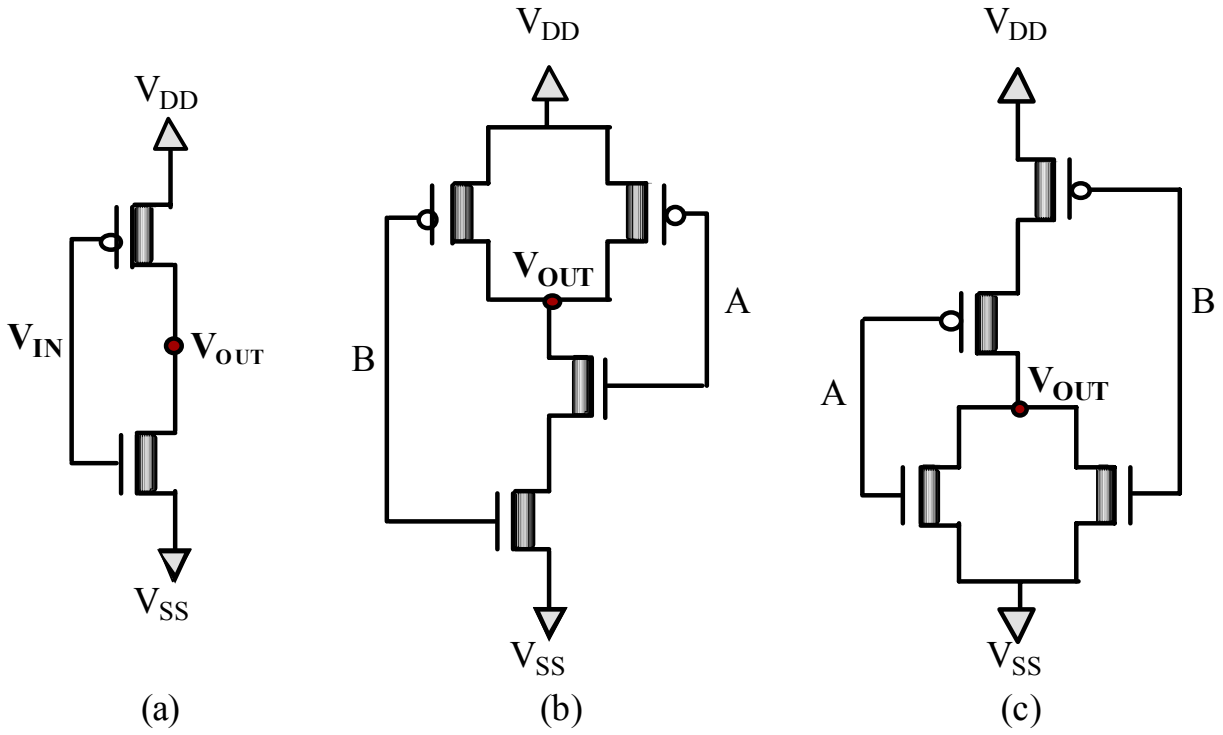

Figure 5.2: CNT-FET logic: (a) Inverter, (b) two input NAND gate and (c) two input NOR gate.

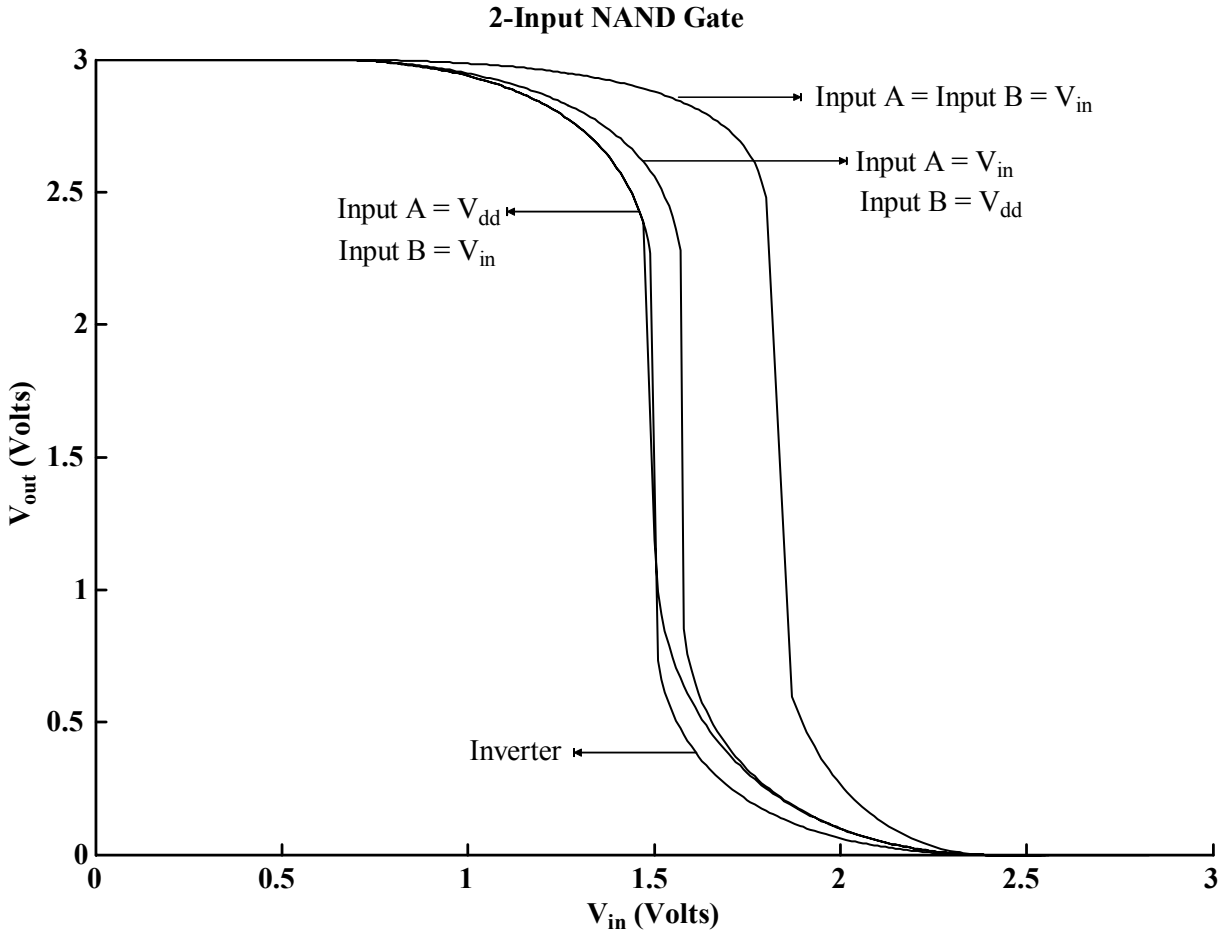

Figure 5.3: Voltage transfer characteristics of an inverter and a NAND gate using CNT-FETs (5,3). The dimensions of both the n-type CNT-FET and p-type CNT-FET are: $T_{ox1} = 40\ nm$, $T_{ox2} = 400\ nm$ and $L = 50\ nm$.

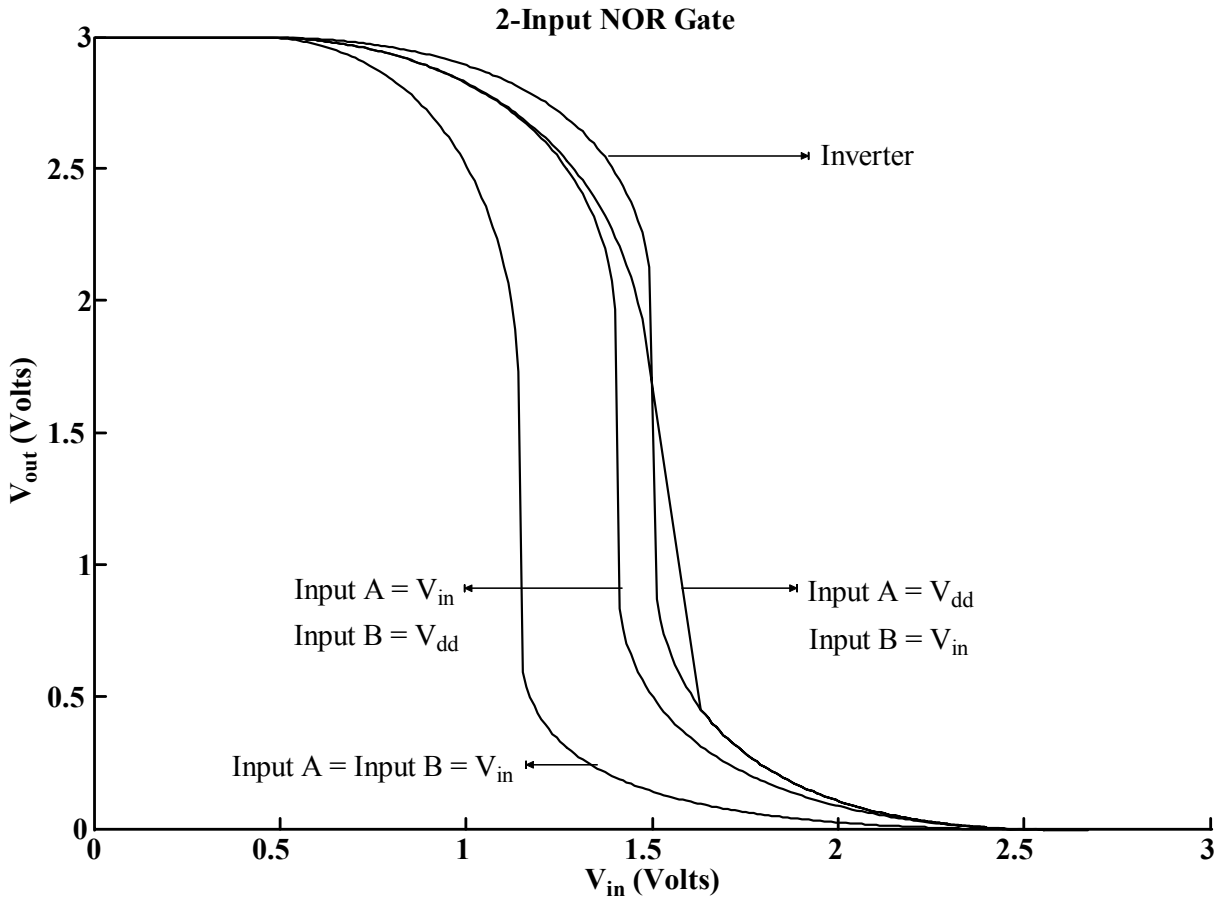

Figure 5.4: Voltage transfer characteristics of an inverter and a NOR gate using CNT-FETs (7,3). The dimensions of both the n-type CNT-FET and p-type CNT-FET are: $T_{ox1} = 40\ nm$, $T_{ox2} = 400\ nm$ and $L = 50\ nm$.

5.4 Summary

Analytical model equations for the current transport in a CNT-FET have been used to characterize voltage transfer characteristics of complementary logic devices such as the inverter, NAND and NOR gates. The voltage transfer characteristics of the CNT-FET inverter are similar to the voltage transfer characteristics of a typical CMOS inverter and show a sharp transition at the inverter logic threshold voltage, 1.5 V for a 3 V operation. The gates, NAND and NOR also show a sharp transition in their transfer characteristics for a 3 V operation. The results presented provide designers with a better understanding of carbon nanotubes and their potential for use in designing of integrated circuits for a wide range of applications.

5.5 References

[1] Y. Nosho, Y. Ohno, S. Kishimoto, and T. Mizutani, "N-type carbon nanotube field-effect transistors fabricated by using Ca contact electrodes," *Applied Physics Letters,* vol. 86, pp. 073105-073107, February 2005.

[2] X. Zhou, J.-Y. Park, S. Huan, J. Liu, and P. McEuen, "Band strucutre, phonon scattering, and the performance limit of single-walled carbon nanotube transistors," *Physical Review Letters,* vol. 95, pp. 1468051-1468052, September 2005.

[3] R. H. Baughman, A. A. Zakhidov, and W. A. d. Heer, "Carbon nanotubes – the route toward applications," *Science,* vol. 297, pp. 787-792, August 2002.

[4] S. Heinze, J. Tersoff, R. Martel, V. Derycke, J. Appenzeller, and P. Avouris, "Carbon nanotubes as Schottky barrier transistors," *Physical Review Letters,* vol. 89, p. 106801, September 2002.

[5] J. Guo, S. Datta, and M. Lundstrom, "A numerical study of scaling issues for schottky barrier CNFETs," *IEEE Transactions on Electron Devices,* vol. 51, pp. 172-177, February 2004.

[6] A. Javey, J. Guo, Q. Wang, M. Lundstron, and H. Dai, "Ballistic carbon nanotube field effect transistors," *Nature,* vol. 424, pp. 654-657, August 2003.

[7] Y. Tsividis, *Operation and Modeling of the MOS transistor*. Singapore: McGraw-hill, 1999.

[8] P. Antognetti and G. Massobrio, *Semiconductor Device Modeling with SPICE*. Singapore: McGraw-Hill, 1988.

[9] A. Javey, Q. Wang, W. Kim, and H. Dai, "Advancements in complementary carbon nanotube field-effect transistors," *IEDM Technical Digest,* pp. 31.2.1-31.2.4, December 2003.

[10] H. S. P. Wong, "Field effect transistors - from silicon MOSFETs to carbon nanotube FETs," *Proc. 23th International Conference on Microelectronics, (MIEL)*, vol. 1, pp. 103-107, 2002.

[11] J. Guo, S. Datta, M. Lundstrom, M. Brink, P. McEuen, A. Javey, H. Dai, H. Kim, and P. McIntyre, "Assessment of silicon MOS carbon nanotube FET perfomance limits using a general theory of ballistic transistors," *IEDM Technical Digest,* pp. 711-714, December 2002.

[12] S. J. Wind, J. Appenzeller, R. Martel, V. Derycke, and P. Avouris, "Vertical scaling of carbon nanotube field-effect transistors using top gate electrodes," *Applied Physics Letters,* vol. 80, pp. 3817-3819, 2002.

[13] A. Javey, Q. Wang, A. Ural, Y. Li, and H. Dai, "Carbon nanotube transistors arrays for multistage complementary logic and ring oscillators," *Nano Letters,* vol. 2, pp. 929-932, July 2002.

[14] V. Derycke, R. Martel, J. Appenzeller, and P. Avouris, "Carbon nanotube inter- and intramolecular logic gates," *Nano Letters,* vol. 1, pp. 453-456, September 2001.

[15] A. Javey, H. Kim, M. Brink, Q. Wang, A. Ural, J. Guo, P. Mcientyre, P. McEuen, M. Lundstrom, and H. Dai, "High k-dielectric for advanced carbon nanotube transistors and logic gates," *Nature Materials,* vol. 1, pp. 241-246, November 2002.

[16] A. Bachtold, P. Hadley, T. Nakanishi, and C. Dekker, "Logic circuits with carbon nanotube transistors," *Science,* vol. 294, pp. 1317-1320, November 2001.

[17] R. Martel, V. Derycke, J. Appenzeller, S. Wind, and P. Avouris, "Carbon nanotube field effect transistors and logic circuits," *Proc. 39th Design Automation Conference*, pp. 94-98, 2002.

[18] W. B. Cheston, *Elementary Theory of Electric and Magnetic Fields*. United States: John Wiley Sons Inc., 1964.

[19] W. H. Hayt, *Engineering Electro-Magnetics*, 3th Ed. New York: McGraw-Hill, 1974.

CHAPTER 6

HIGH FREQUENCY RESPONSE*

6.1 Introduction

As we already know carbon nanotubes are basically one-dimensional graphene sheets rolled into a tubular structure [1]. Their properties depend on the chiral vector and are represented by the indices (n,m) [2,3]. CNT-FETs are being explored extensively as the structure material for making future CMOS devices and circuits [4-6]. Efforts have been made in modeling their current transport behavior. The current transport models including analytical models presented in Chapters 3 and 4 have been developed for the design of CNT-FET based logic devices [7-12]. High frequency CNT-FET models have also been realized [13-16]. In this chapter, we present a small signal rf equivalent circuit model of the CNT-FET to study its high frequency response and the effect of the variation of the chiral vectors (n,m) of carbon nanotubes on small signal parameters and high frequency response for logic devices.

6.1.1 Small Signal RF Equivalent Circuit Model

The small signal high frequency model for CNT-FETs is shown in Fig. 6.1, where C_{gs} is the gate to source capacitance. The parasitic gate capacitances between gate to source and gate to drain are characterized by $C_{par,gs}$ and $C_{par,gd}$, respectively. I_{ds}(n,m) is the drain current depending on the chiral vector (n,m). R_s and R_d are the source and drain resistances.

R_{ds} represents drain to source resistance. C_{ox2} is the substrate oxide capacitance. The small

---

* Part of the work is reported in the following publications:

1. J. M. Marulanda, A. Srivastava and R.K. Nahar, "Ultra-high frequency modeling of carbon nanotube field-effect transistors (CNT-FETs), *Proc. 13th International Workshop on the Physics of Semiconductor Devices (IWPSD)*, (Delhi, India, December 13-17, 2005).
2. J. M. Marulanda, A. Srivastava and A.K. Sharma, "Transfer characteristics and high frequency modeling of logic gates using carbon nanotube field effect transistors (CNT-FETs)," *Proc. of The 20th Annual Conference on Integrated Circuits and Systems Design (SBCCI 2007)*, pp. 202-206, (Rio de Janeiro, Brazil, September 3-6, 2007).

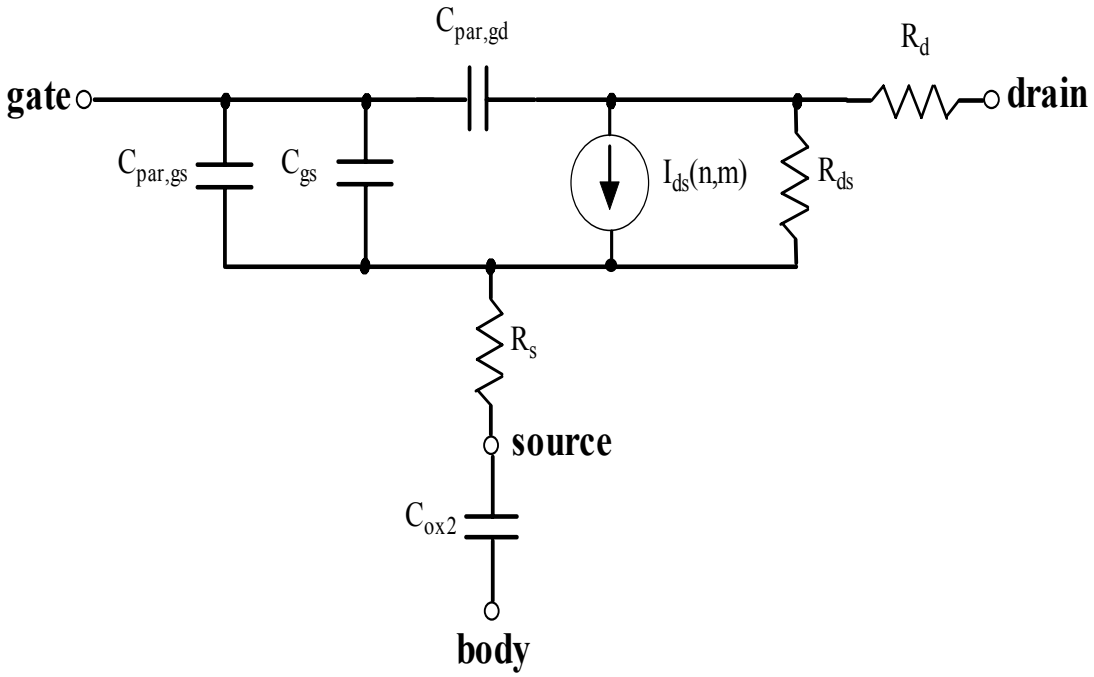

Figure 6.1: Small signal high frequency equivalent circuit model of a CNT-FET.

signal model parameters are obtained as follows.

6.1.2 Resistance and Capacitance Models

The resistance of a conductive CNT can be expressed as [13,21,22],

$$R_{cnt} = R_c + R_{ch} = \left(\frac{h}{4q^2}\right) + \left(\frac{h}{4q^2}\frac{L}{L_0}\right), \tag{6.1}$$

where h is Planck's constant, R_c and R_{ch} are the contact and channel resistances, respectively. R_{ch} is basically the equivalent drain to source resistance, R_{ds}. L_0 is a parameter that models the mean free path of an electron in a CNT. The total mean free path L_0, in a CNT is given by [23-25],

$$L_0 = \frac{L}{qV_{ds}}\left(\sum_n \frac{1}{\hbar\Omega_n}\right)^{-1}, \tag{6.2}$$

where scattering mechanisms such as phonons, noise, and impurities are modeled using the summation factor; $\hbar\Omega_n$ represents the energy of the n_{th} scattering mechanism and $\hbar = \frac{h}{2\pi}$.

The contact resistance, R_c in Eq. (6.1) can be divided in two equal parts corresponding to the source and drain resistances as shown in Fig. 6.1. Using Eq. (6.2) we obtain the resistances, R_s and R_d of a CNT-FET as follows:

$$R_s = R_d = \frac{R_c}{2} = \frac{h}{8q^2}. \tag{6.3}$$

Substituting Eq. (6.2) in R_{ch} of Eq. (6.1), which is the equivalent drain to source resistance; R_{ds} is obtained as follows,

$$R_{ds} = \frac{h}{4q}V_{ds}\sum_n \frac{1}{\hbar\Omega_n}. \tag{6.4}$$

In Fig. 6.1, C_{ox2}, the oxide capacitance between the carbon nanotube and the surface of the substrate is described in Chapter 5 by the Eq. (5.11) and repeated here,

$$C_{ox2} = \frac{2\pi\varepsilon_{ox2}L}{\ln\left(\frac{T_{ox2}+r+\sqrt{T_{ox2}^2+2T_{ox2}r}}{r}\right)}. \tag{6.5}$$

As described in Chapter 4, the charge inside the carbon nanotube is given by,

$$Q_{cnt} = -C_{ox1}\left(V_{gb} - \psi_{cnt,s} - V_{fb}\right). \tag{6.6}$$

where $\psi_{cnt}(0)$ is given by the Eq. (5.12) in Chapter 5 and repeated here,

$$\psi_{cnt,s}(0) = \frac{V_{gs}+V_{sb}-\delta Ie^{-1}-V_{fb}+\delta m\left(V_{sb}+\phi_0-\frac{\Delta E_F}{q}+\frac{E_c}{q}-\frac{kT}{q}\right)}{1+\delta m}, \tag{6.7}$$

where

$$\delta = \frac{qLN_c}{C_{ox1}}. \tag{6.8}$$

Using Eq. (6.7) for the carbon nanotube potential, $\psi_{cnt}(0)$ and substituting $V_{gb} = V_{gs} + V_{sb}$ in Eq. (6.6) we can find the total gate to source capacitance, C_{gs} of Fig. 6.1 by differentiating with respect to V_{gs}. C_{gs} is then given by,

$$C_{gs} = C_{ox1}\left(\frac{\delta m}{1+\delta m}\right). \tag{6.9}$$

The parasitic capacitances, $C_{par,gs}$ and $C_{par,gd}$ are given by [26,27]

$$C_{par} = C_{par,gs} = C_{par,gd} = \frac{\varepsilon_o\varepsilon_{ox}W}{\pi/2}\ln\left(1+\frac{T_{poly}}{T_{ox}}\right), \tag{6.10}$$

where T_{poly} and W are respectively the thickness and width of the gate.

6.1.3 Transconductance and Discussion

The transconductance, g_m is defined as follows:

$$g_m = \left.\frac{\partial I_{ds}}{\partial V_{gs}}\right|_{V_{ds}=constant}, \tag{6.11}$$

where I_{ds} in Eq. (6.11) is given in Chapter 3 by Eq. (3.44) and is repeated below,

$$I_{ds} = \beta\left[f\left\{\psi_{cnt,s}(L), V_{gs}\right\} - f\left\{\psi_{cnt,s}(0), V_{gs}\right\}\right], \tag{6.12}$$

where

$$f\left\{\psi_{cnt,s}(x), V_{gs}\right\} = \left(V_{gs} + V_{sb} - V_{fb} + \tfrac{kT}{q}\right)\psi_{cnt,s}(x) - \tfrac{1}{2}\psi_{cnt,s}^2(x) \tag{6.13}$$

and

$$\beta = \frac{\gamma \mu C_{ox1}}{L^2}. \tag{6.14}$$

Substituting Eq. (6.12) in Eq. (6.13), we obtain,

$$I_{ds} = \beta\left[\left(V_{gs} + V_{sb} - V_{fb} + \tfrac{kT}{q}\right)\psi_{cnt,s}(L) - \frac{\psi_{cnt,s}^2(L)}{2} - \left(V_{gs} + V_{sb} - V_{fb} + \tfrac{kT}{q}\right)\psi_{cnt,s}(0) - \frac{\psi_{cnt,s}^2(0)}{2}\right]. \tag{6.15}$$

Differentiating Eq. (6.15) with respect to V_{gs}, we obtain,

$$\begin{aligned}\frac{\partial I_{ds}}{\partial V_{gs}} = \beta\Bigg[& \psi_{cnt,s}(L) + \left(V_{gs} + V_{sb} - V_{fb} + \tfrac{kT}{q}\right)\frac{\partial \psi_{cnt,s}(L)}{\partial V_{gs}} - \psi_{cnt,s}(L)\frac{\partial \psi_{cnt,s}(L)}{\partial V_{gs}} \\ & - \psi_{cnt,s}(0) - \left(V_{gs} + V_{sb} - V_{fb} + \tfrac{kT}{q}\right)\frac{\partial \psi_{cnt,s}(0)}{\partial V_{gs}} - \psi_{cnt,s}(0)\frac{\partial \psi_{cnt,s}(0)}{\partial V_{gs}}\Bigg].\end{aligned} \tag{6.16}$$

In saturation region *($V_{ds} \geq V_{gs} - V_{th}$)*,

$$\psi_{cnt,s}(L) = V_{gs} + V_{sb} - V_{fb}. \tag{6.17}$$

Differentiating Eq. (6.7) for $\psi_{cnt}(0)$ and Eq. (6.17) for $\psi_{cnt}(L)$ with respect to V_{gs}, we obtain,

$$\frac{\partial \psi_{cnt,s}(0)}{\partial V_{gs}} = \frac{1}{1 + \delta m} \tag{6.18}$$

and

$$\frac{\partial \psi_{cnt,s}(L)}{\partial V_{gs}} = 1. \tag{6.19}$$

Combining Eqs. (6.16), (6.18) and (6.19) we obtain,

$$g_m = \beta\left[\left(V_{gs} + V_{sb} - V_{fb} + \tfrac{KT}{q}\right)\frac{\delta m}{1+\delta m} - \psi_{cnt,s}(0)\frac{2+\delta m}{1+\delta m}\right]. \quad (6.20)$$

Substituting Eq. (6.7) for $\psi_{cnt}(0)$ in Eq. (6.20), we obtain,

$$g_m = \beta\left[\left(V_{gs} + V_{sb} - V_{fb} + \tfrac{KT}{q}\right)\frac{\delta m}{1+\delta m} - \frac{V_{gs} + V_{sb} - \delta I e^{-1} - V_{fb} + \delta m\left(V_{sb} + \phi_0 - \frac{\Delta E_F}{q} + \frac{E_c}{q} - \frac{kT}{q}\right)(2+\delta m)}{(1+\delta m)^2}\right]. \quad (6.21)$$

6.2 Results

Table 6.1 shows the calculated small signal model parameters (g_m, R_{ds}, C_{gs}) corresponding to the equivalent circuit of a CNT-FET shown in Fig. 6.1 for different chiral vectors (n,m). The model parameters have been calculated as follows. The transconductance, g_m has been calculated using the Eq. (6.21). The resistances and capacitances have been calculated from Eqs. (6.3) - (6.10) for $Q_{01} = Q_{02} = 0$, $V_{fb} = 0$, $L = 50\ \mu m$, $T_{poly} = 1000\ Å$, $W = 0.5\ \mu m$, $T_{ox1} = 40\ nm$ and $T_{ox2} = 400\ nm$. The parasitic capacitances are common to all values of chiral vectors in Table 6.1 and are as follows: $C_{gs,par} = C_{gd,par} = 13.763\ aF$. The small signal parameters are very dependent on the chiral vector of the carbon nanotube as noticed from Table 6.1.

The cut-off frequency of a CNT-FET can be examined analytically from Fig. 6.1 using an equation of the form [13,28]:

$$f_T = \frac{1}{2\pi}\frac{g_m}{\left[C_{gs}(1 + R_c g_{ds}) + C_{par}(2 + 2R_c g_{ds} + R_c g_m)\right]}. \quad (6.22)$$

In order to calculate the cut-off frequency for a CNT-FET, the transistor is considered in saturation. Values of V_{gs} and V_{ds} are chosen and g_m and R_{ds} are then calculated. Figure 6.2 shows the variation of the cut-off frequency with g_m from Eq. (6.22) for a CNT-FET with chiral vector (11,3). Table 6.2 shows the dependence of cut-off frequencies of CNT-FETs on chiral vectors. The cut-off frequencies of CNT-FETs are obtained from SPICE using the small signal

Table 6.1. Small signal parameters for CNT-FETs

CNT-FET (n,m)	**g_m (μS)**	**R_{ds} (KΩ)**	**C_{gs} (aF)**
(3,1)	116	132	1.673
(3,2)	138	155	1.711
(4,2)	151	163	1.768
(4,3)	163	174	1.799
(5,1)	158	171	1.744
(5,3)	172	179	1.844
(6,1)	166	174	1.832
(7,3)	188	190	1.910
(9,2)	197	195	1.954
(11,3)	209	200	2.034

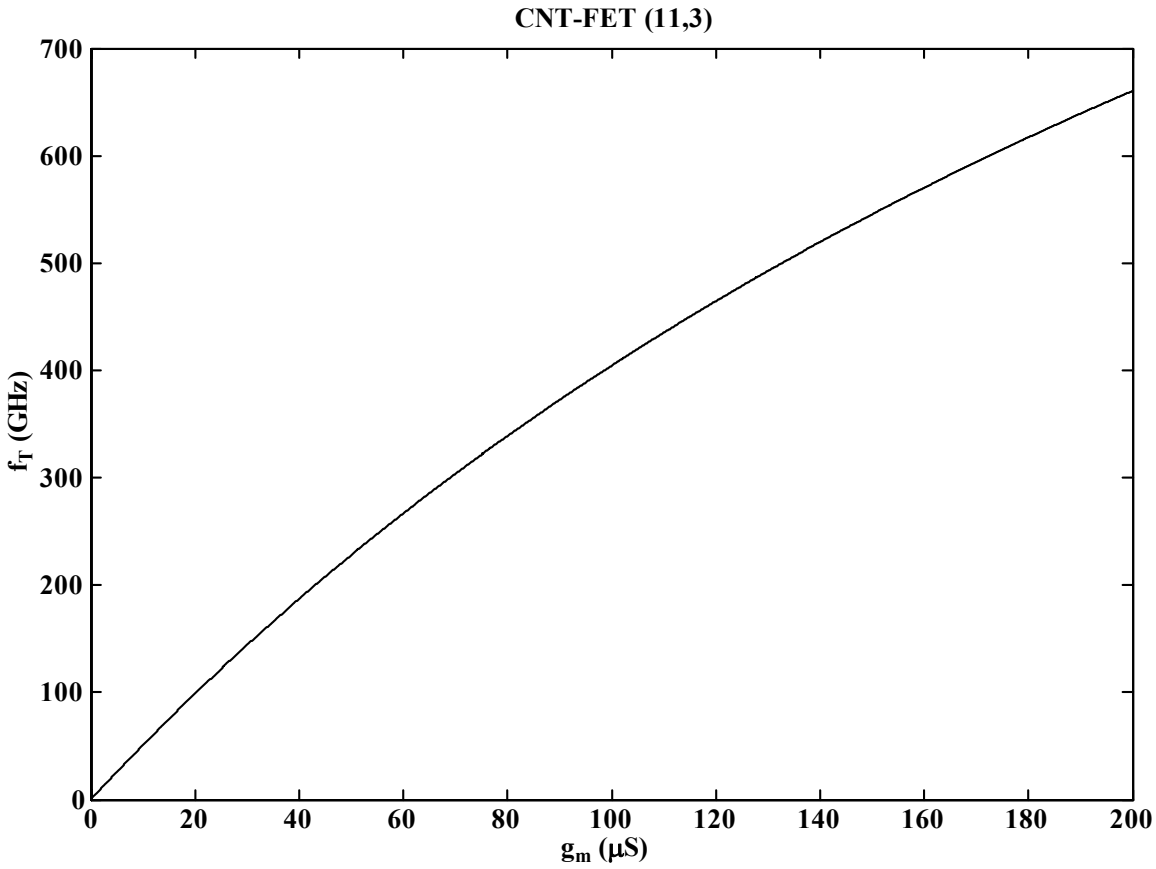

Figure 6.2: Dependence of cut-off frequency on g_m of a CNT-FET (11,3).

Table 6.2. Cut-off frequencies for CNT-FETs

CNT-FET (n,m)	**f_T (GHz)**
(3,1)	544
(3,2)	617
(4,2)	657
(4,3)	700
(5,1)	683
(5,3)	728
(6,1)	709
(7,3)	765
(9,2)	795
(11,3)	815

model parameters given in Table 6.1 for different chiral vectors.

6.3 Summary

We have developed a small signal equivalent circuit model for characterizing CNT-FETs at radio frequencies. The results of the cut-off frequencies show values in the upper GHz range, with a strong dependence on the chiral vectors and corresponding transconductance. The small-signal model can be easily used in SPICE for circuit design based on CNT-FETs.

6.4 References

[1] R. Martel, T. Schmidt, H. R. Shea, T. Hertel, and P. Avouris, "Single and multi wall carbon nanotube field effect transistors," *Applied Physics Letters,* vol. 73, pp. 2447-2449, October 1998.

[2] J. Wildoer, L. Venema, A. Rinzler, R. Smalley, and C. Dekker, "Electronic structure of atomically resolved carbon nanotubes," *Nature,* vol. 391, pp. 59-62, January 1998.

[3] K. Tanaka, T. Yamabe, and K. Fukui, *The Science and Technology of Carbon Nanotubes*. Amsterdam: Elsevier, 1999.

[4] H. S. P. Wong, "Field effect transistors - from silicon MOSFETs to carbon nanotube FETs," *Proc. 23th International Conference on Microelectronics, (MIEL)*, vol. 1, pp. 103-107, 2002.

[5] J. Guo, S. Datta, M. Lundstrom, M. Brink, P. McEuen, A. Javey, H. Dai, H. Kim, and P. McIntyre, "Assessment of silicon MOS carbon nanotube FET perfomance limits using a general theory of ballistic transistors," *IEDM Technical Digest,* pp. 711-714, December 2002.

[6] S. J. Wind, J. Appenzeller, R. Martel, V. Derycke, and P. Avouris, "Vertical scaling of carbon nanotube field-effect transistors using top gate electrodes," *Applied Physics Letters,* vol. 80, pp. 3817-3819, 2002.

[7] D. L. John, L. C. Castro, J. P. Clifford, and D. L. Pulfrey, "Electrostatic of coaxial Schottky barrier nanotube field effect transistors," *IEEE Transactions on Nanotechnology,* vol. 2, pp. 175-180, September 2003.

[8] C. Dwyer, M. Cheung, and D. J. Sorin, "Semi-empirical SPICE models for carbon nanotube FET logic," *Proc. 4th IEEE Conference on Nanotechnology*, pp. 386-388, 2004.

[9] A. Raychowdhury, S. Mukhopadhyay, and K. Roy, "A circuit-compatible model of ballistic carbon nanotube field effect transistors," *IEEE Transactions on Computer-Aided Design of Integrated Circuits and Systems,* vol. 23, pp. 1411-1420, October 2004.

[10] A. Raychowdhury and K. Roy, "Carbon nanotube based voltage-mode multiple-valued logic design," *IEEE Transactions on Nanotechnology,* vol. 4, pp. 168 - 179, March 2005.

[11] I. O'Connor, J. Liu, F. Gaffiot, F. Prégaldiny, C. Lallement, C. Maneux, J. Goguet, S. Frégonèse, T. Zimmer, L. Anghel, T.-T. Dang, and R. Leveugle, "CNTFET modeling and reconfigurable logic circuit design," *IEEE Transactions on Circuits and Systems, Part-1,* vol. 54, pp. 2365-2379, November 2007.

[12] A. Hazeghi, T. Krishnamohan, and H.-S. P. Wong, "Schottky-barrier carbon nanotube field effect transistor modeling," *IEEE Transactions on Electron Devices,* vol. 54, pp. 439-445, March 2007.

[13] P. J. Burke, "AC performance of nanoelectronics: towards a ballisitic THz nanotube transistor," *Solid State Electronics,* vol. 48, pp. 1981-1986, June 2004.

[14] P. J. Burke, "An RF circuit model for carbon nanotubes," *IEEE Transactions on Nanotechnology,* vol. 2, pp. 55-58, March 2003.

[15] L. C. Castro and D. L. Pulfrey, "Extrapolated fmax for Carbon Nanotube FETs," *Nanotechnology,* vol. 17, pp. 300-304, December 2006.

[16] L. C. Castro, D. L. Pulfrey, and D. L. John, "High-frequency capability of Schottky-barrier carbon nanotube FETs," *Solid-State Phenomena,* vol. 121-123, pp. 693-696, March 2007.

[17] J. Marulanda, A. Srivastava, and A. K. Sharma, "Current transport modeling in carbon nanotube field effect transistors (CNT-FETs) and bio-sensing applications," *Proc. SPIE Smart Structures and Materials & Nondestructive Evaluation and Health Monitoring: Nanosensors and Microsensors for Bio-System*, vol. 6931, pp. 693108-1-693108-12, San Diego, CA, 2008.

[18] J. Marulanda, A. Srivastava, and A. K. Sharma, "Transfer characteristics and high frequency modeling of logic gates using carbon nanotube field effect transistors (CNT-FETs)," *Proc. of The 20th Annual Conference on Integrated Circuits and Systems Design*, Rio de Janeiro, Brazil, pp. 202-206, 2007.

[19] W. B. Cheston, *Elementary Theory of Electric and Magnetic Fields*. United States: John Wiley Sons Inc., 1964.

[20] W. H. Hayt, *Engineering Electro-Magnetics*, 3th Ed. New York: McGraw-Hill, 1974.

[21] J. M. Marulanda, A. Srivastava, and R. K. Nahar, "Ultra-high frequency modeling of carbon nanotube field-effect transistors," *Proc. 13th International Workshop on the Physics of Semiconductor Devices (IWPSD)*, New Delhi, pp. G-11, 2005.

[22] A. Raychowdhury and K. Roy, "A Circuit Model for Carbon Nanotube Interconnects: Comparative Study with Cu Interconnects for Scaled Technologies," *Proc. ICCAD*, California, pp. 237-240, 2004.

[23] B. Lu and S. Torquato, "Chord-length and free-path distribution function for many body systems," *Journal of Chemical Physics,* vol. 98, p. 6474, April 1993.

[24] J. Y. Park, S. Rosenblatt, Y. Yaish, V. Sazonova, H. Üstünel, S. Braig, T. A. Arias, P. W. Brouwer, and P. L. McEuen, "Electron phonon scattering in metallic single walled carbon nanotubes," *Nano Letters,* vol. 4, pp. 517-520, 2004.

[25] J. M. Marulanda and A. Srivastava, "I-V characteristic modeling and parameter extraction for CNT-FETs," *Proc. International Semiconductor Device Research Symposium (ISDRS)*, Bethesda, MD, pp. 38-39, 2005.

[26] F. Pregaldiny, C. Lallement, and D. Mathiot, "Extrinsic capacitance model for advance MOSFET design," *ERM-Phase,* October 2002.

[27] R. Schrivastava and K. Fitzpatrick, "Simple model for the overlap capacitance of a VLSI MOS device," *IEEE Transactions on Electron Devices,* vol. 29, pp. 1870-1875, December 1982.

[28] W. Liu, *Fundamentals of III-V Devices: HBTs, MESFETs and HFETs/HEMTs*: John Wiley & Songs, Inc., 1999.

CHAPTER 7

BIO- AND CHEMICAL APPLICATIONS*

7.1 Introduction

Single-walled carbon nanotube (SWNT) graphite cylinders are composed of surface atoms. Because of their size, large surface area and hollow geometrical shape, carbon nanotubes are the best-suited materials for gas absorption, storage and molecular filtering [1]. Many carbon materials are known to possess excellent molecular adsorption properties. Carbon nanotube is among one of the materials, which has exhibited significant changes in its electronic properties when subjected to molecular adsorbates. The unique structure and sensitivity to molecular adsorbates have resulted in use of carbon nanotubes for bio- and chemical sensing applications. Both conductance and capacitance based CNT-sensors have been developed for detecting traces of a wide range of chemical vapors and gases including traces of nerve agents and explosives [2-6]. In this chapter, we have given a brief description of carbon nanotube field effect transistor (CNT-FET) based sensors for bio- and chemical sensing applications and we have shown how our presented model equations [7,8] in Chapter 3 can be used for interpreting the effect on the I-V characteristics when CNT-FETs are exposed to a bio-molecular environment.

7.2 Carbon Nanotube Sensing Mechanism

Snow, et al., [9] have provided an excellent review of chemical vapor detection using single-walled carbon nanotubes. Kong, et al., [10] and Collins, et al., [1] were the first ones to

* Part of the work is reported in the following publication:
J. M. Marulanda, A. Srivastava and A.K. Sharma, "Current transport modeling in carbon nanotube field effect transistors (CNT-FETs) and bio-sensing applications," *Proc. SPIE Smart Structures and Materials & Nondestructive Evaluation and Health Monitoring: Nanosensors and Microsensors for Bio-System*, vol. 6931, pp. 693108-1-693108-12, (San Diego, CA, March 9-13, 2008).

demonstrate change in conductance of p-type CNT to certain molecular adsorbates such as the NH_3, an electron donor and the NO_2, an electron acceptor, resulting in decrease and increase in conductance. NH_3 and NO_2 are known as hazardous gases.

Collins et al., [1] have shown that the electronic properties of SWNTs are extremely sensitive to oxygen or air and dramatically change the electrical resistance, thermoelectric power and local density of states, *N(E)*. Atashbar et al., [11] have fabricated a simple SWNT conductance based sensor for the detection of streptavidin and mouse monoclonal immunoglobulin G (IgG) antibody. Figure 7.1 shows the schematic representation of the bio-sensor for detecting G (IgG).

Carbon nanotubes have been used for the detection of DNA. The detection of DNA is important to the detection of infectious agents, drug delivery and warning against bio-warfare agents. Wang et al., [12] have demonstrated the use of CNTs for enzyme-based bioaffinity electrical sensing of proteins and DNA, which relies on hybridization or antigen-antibody (Ag-Ab) interactions. Tang et al., [13] have developed a fully electronic DNA sensor based on CNT-FETs. Figure 7.2(a) shows the optical image of the central region of a single sensor chip with four SWNT-FETs. Figure 7.2(b) shows the concept illustration of a single CNT-FET during electrical measurements.

After mercaptohexanol (MCH) attachment, I-V_g curves are taken by a sweeping silicon backgate. I-V_g characteristics exhibit the device conductivity due to change in alignment in the energy level before and after DNA hybridization as shown in Fig. 7.3.

Snow et al., [9] have experimented with a SWNT network type sensor, a cross-section of which is shown in Fig. 7.4. The SWNT sensor of the type shown in Fig. 7.4 can be used both as a conductance sensor and capacitive sensor [3].

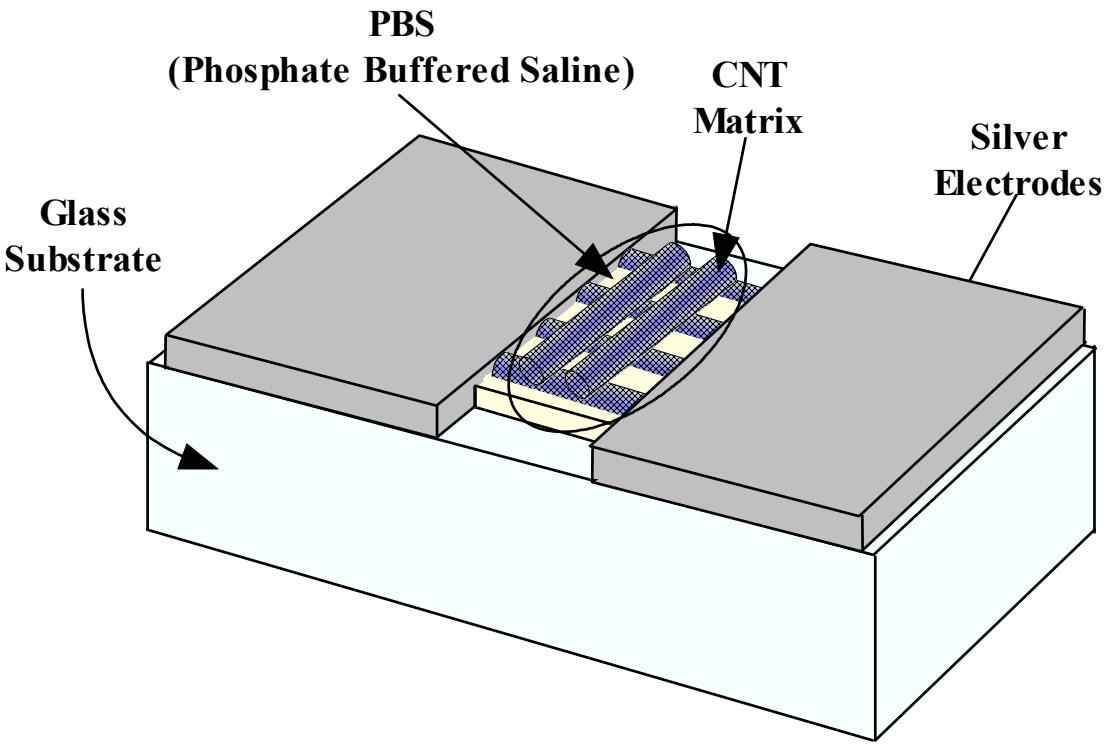

Figure 7.1: Simple SWNT conductance-based bio-sensor for detecting 10 µl IgG antibody [11].

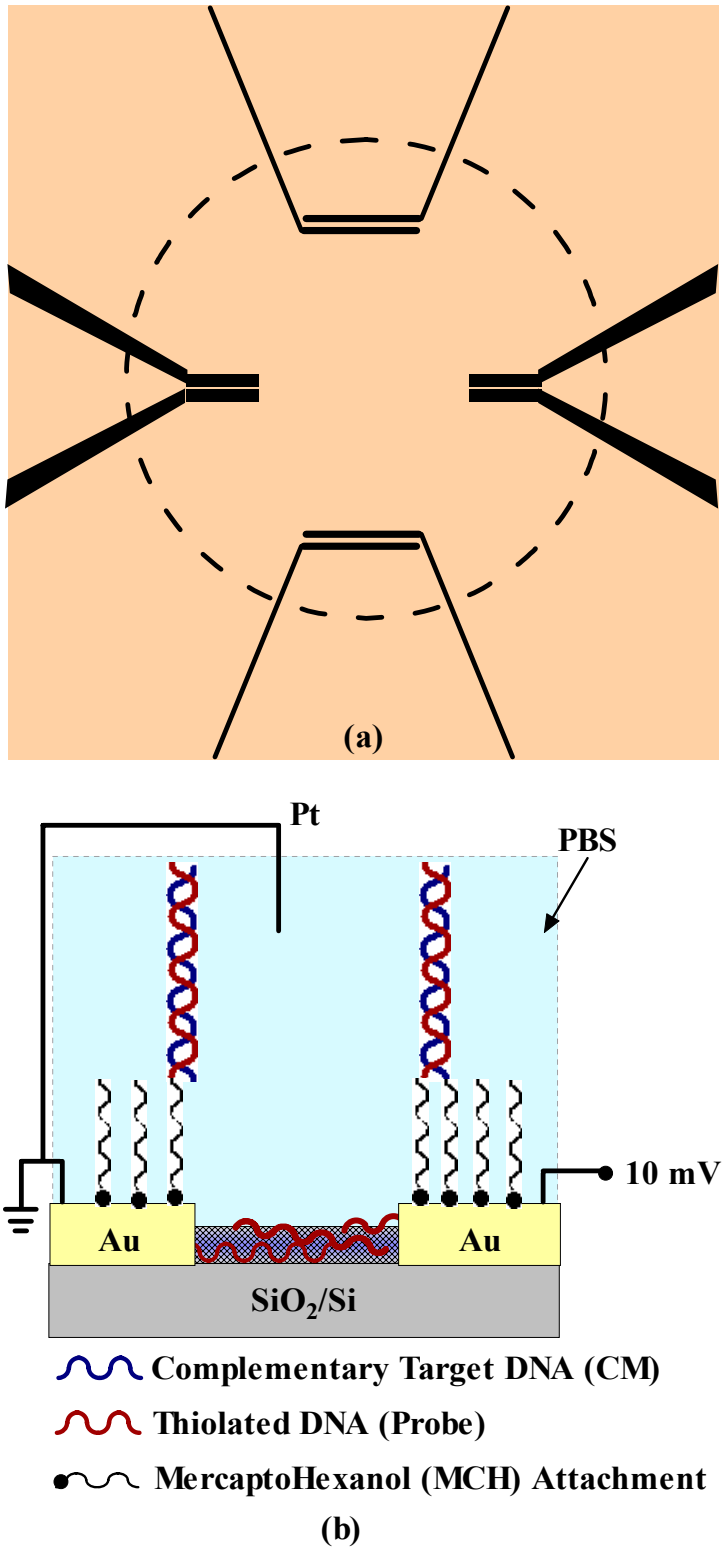

Figure 7.2: (a) Single sensor chip with four SWNT-FETs and (b) illustration of a single SWNT-FET during electrical measurements [13].

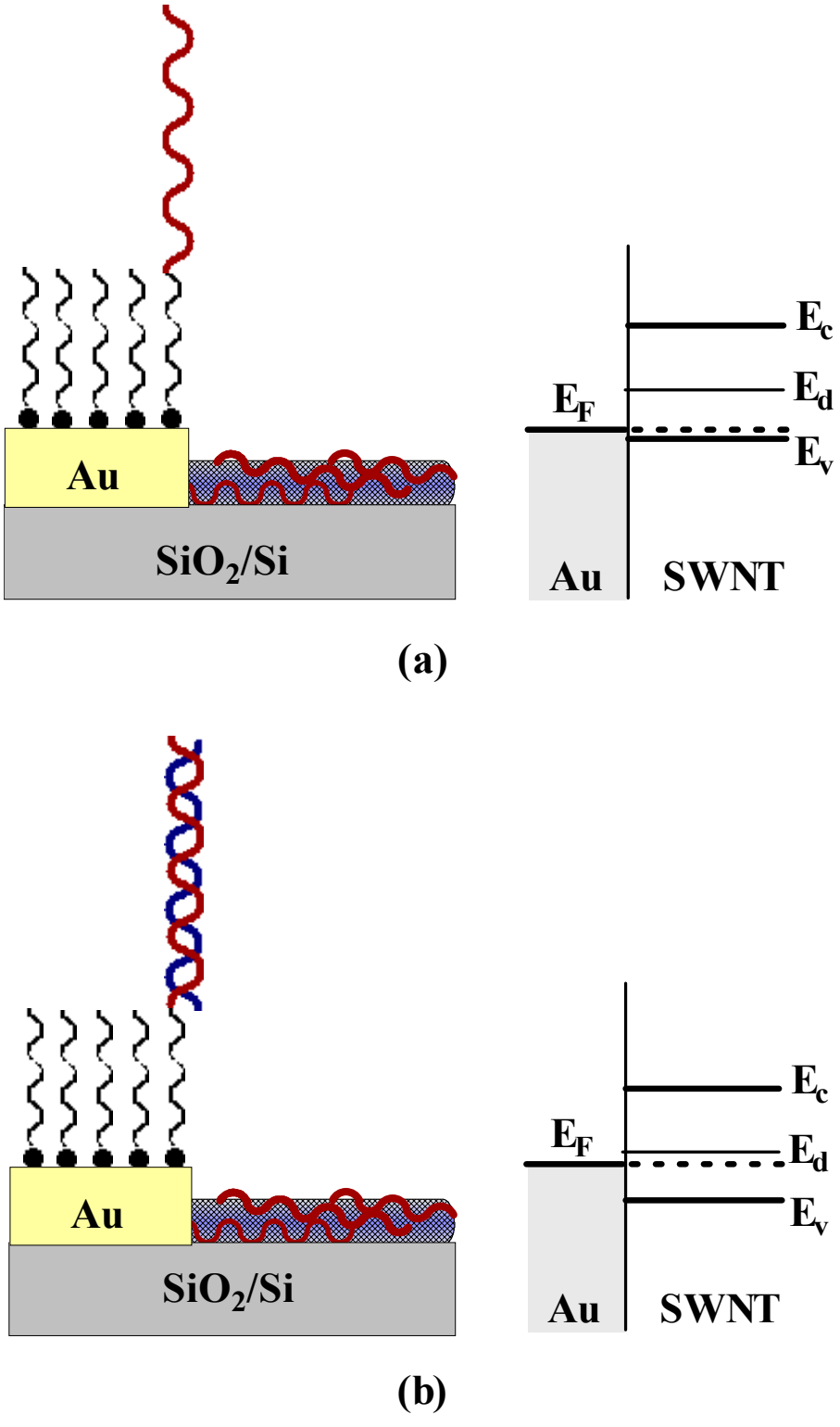

Figure 7.3: Energy level alignment between Au and SWNT (a) before and (b) after DNA hybridization [13].

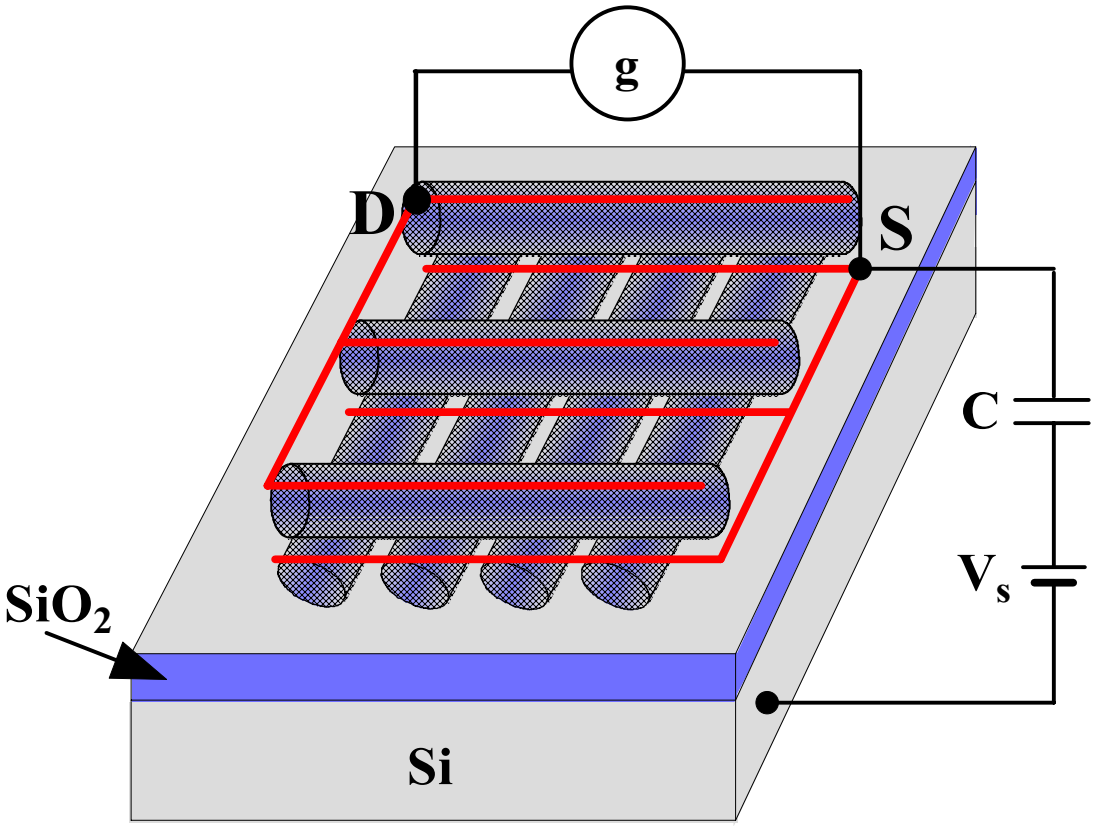

Figure 7.4: Cross-section of a SWNT network sensor [9].

7.3 Summary

Semiconducting SWNT molecular wires and SWNT-FET based sensors are promising compact ultra-sensitive and ultra low-power advanced miniaturized sensors in comparison to conventional sensors. Their ability to operate at room temperature and detect traces of bio-warfare agents and chemical agents (nerve agents, blister agents and explosives) show a great promise for defense and homeland security applications. The presented research on current transport modeling can be easily applied in providing explanations to reactions taking place in the CNT and CNT-FET sensors when exposed to traces of bio- and chemical agents at a molecular level. Carbon nanotubes field effect transistors are therefore very promising devices for use in bio-sensing applications.

7.4 References

[1] P. G. Collins, K. Bradley, M. Ishigami, and A. Zettl, "Extreme oxygen sensitivity of electronic properties of carbon nanotubes," *Science,* vol. 287, pp. 1801-1804, March 2000.

[2] J. P. Novak, E. S. Snow, E. J. Houser, D. Park, J. L. Stepnowski, and R. A. McGill, "Nerve agent detection using networks of single-walled carbon nanotubes," *Applied Physics Letters,* vol. 83, pp. 4026-4028, November 2003.

[3] E. S. Snow, F. K. Perkins, E. J. Houser, S. C. Badescu, and T. L. Reinecke, "Chemical detection with a single-walled carbon nanotube capacitor," *Science,* vol. 307, pp. 1942-1945, March 2005.

[4] P. Qi, O. Vermesh, M. Grecu, A. Javey, Q. Wang, H. Dai, S. Peng, and K. J. Cho, "Toward large arrays of multiplex functionalized carbon nanotube sensors for highly sensitive and selective molecular detection," *Nano Letters,* vol. 3, pp. 347-351, January 2003.

[5] C. Staii, Johnson, Jr., A. T., M. Chen, and A. Gelperin, "DNA-decorated carbon nanotubes for chemical sensing," *Nano Letters,* vol. 5, pp. 1774-1778, August 2005.

[6] A. Star, T. R. Han, V. Joshi, J. C. P. Gabriel, and G. Grüner, "Nanoelectronic carbon dioxide sensors," *Advanced Materials,* vol. 16, pp. 2049-2052, November 2004.

[7] J. Marulanda, A. Srivastava, and A. K. Sharma, "Transfer characteristics and high frequency modeling of logic gates using carbon nanotube field effect transistors (CNT-FETs)," *Proc. of The 20th Annual Conference on Integrated Circuits and Systems Design*, Rio de Janeiro, Brazil, pp. 202-206, 2007.

[8] J. M. Marulanda, A. Srivastava, and A. K. Sharma, "Current transport modeling in carbon nanotube field effect transistors (CNT-FETs) and bio-sensing applications," *Proc. SPIE Smart Structures and Materials & Nondestructive Evaluation and Health Monitoring: Nanosensors and Microsensors for Bio-System*, vol. 6931, pp. 693108-1-693108-12, San Diego, CA, 2008.

[9] E. S. Snow, F. K. Perkins, and J. A. Robinson, "Chemical vapor detection using single-walled carbon nanotubes " *Chemical Society Review,* vol. 35, pp. 790-798, May 2006.

[10] J. Kong, N. R. Franklin, C. Zhou, M. G. Chapline, S. Peng, K. Cho, and H. Dai, "Nanotube molecular wires as chemical sensors," *Science,* vol. 287, pp. 622-625, 28 January 2000.

[11] M. Z. Atashbar, B. Bejcek, S. Singamaneni, and S. Santucci, "Carbon nanotube based biosensors," *Proc. IEEE Sensor Conference*, Vienna, Austria, pp. 1048-1051, 2004.

[12] J. Wang, G. Liu, and M. R. Jan, "Ultrasensitive electrical biosensing of proteins and DNA: carbon-nanotube derived amplification of the recognition and transduction events," *Journal of American Chemical Society,* vol. 126, pp. 3010-3011, February 2004.

[13] X. Tang, S. Bansaruntip, N. Nakayama, E. Yenilmez, Y. l. Chang, and Q. Wang, "Carbon nanotube DNA sensor and sensing mechanism," *Nano Letters,* vol. 6, pp. 1632-1636, June 2006.

CHAPTER 8

CONCLUSION AND SCOPE OF FUTURE WORK

8.1 Conclusion

In this research, we have studied and analyzed the physical and electrical properties of carbon nanotubes. We have used the density of states function and energy band structure of carbon nanotubes to derive analytical solutions for calculating the intrinsic carrier concentration and effective mass in carbon nanotubes. The temperature dependence of the carrier concentration and energy band structure was also established.

Based on our reported carrier concentration model, we have related the carbon nanotube potential and the gate substrate voltage and developed analytical solutions relating these potentials. These solutions are then used to analytically model the current transport in a CNT-FET depending on the chiral vector and device geometry. Model equations for threshold and saturation voltages in CNT-FETs were each derived in the process and they are found to be dependent on the chiral vectors of carbon nanotubes.

The derived analytical current transport model has been used to generate CNT-FET I-V characteristics for two different chiral vectors and these I-V characteristics have been compared with recently reported experimental data for one of the chiral vectors, CNT (11,3). A close agreement is obtained between the analytical model and the experimental observations in linear and saturation regions. Theoretical results also show agreement with graphically extrapolated threshold and saturation voltages.

The derived analytical transport model equations have also been used to characterize voltage transfer characteristics of logic devices based on complementary CNT-FETs such as the inverter, NAND and NOR gates. The voltage transfer characteristics of the CNT-FET

inverter are similar to the voltage transfer characteristics of a typical CMOS inverter and show a sharp transition at the inverter logic threshold voltage. The gates, NAND and NOR also show a sharp transition in their transfer characteristics. In addition, a small signal equivalent circuit model for characterizing the CNT-FET at radio frequencies has also been developed, which can be easily implemented in SPICE for circuit design. The results of the cut-off frequencies show values in the upper GHz range with a strong dependence on the chiral vectors and corresponding g_m.

CNT-FET based sensors are promising compact ultra-sensitive and ultra-low power advanced miniaturized sensors in comparison to conventional sensors. Their ability to operate at room temperature and detect traces of bio-warfare agents and chemical agents show a great promise for defense and homeland security applications. The present work on current transport modeling can be easily applied in providing explanations to reactions taking place in CNT and CNT-FET sensors when exposed to traces of bio- and chemical agents at a molecular level.

The calculations obtained provide useful understanding of the conductivity in carbon nanotubes and electrical modeling, especially when dealing with impurities, doping concentrations and its effects on the electronic band structure of these hexagonal crystal lattice materials. The model equations also provide designers with useful mathematical expressions relating the properties of conductivity of carbon nanotubes and their response in circuit applications.

8.2 Scope of Future Work

Ballistic transport is not applicable to the current length of fabricated CNTs in CNT-FETs (~100 nm or more). However, with the advancements in technology of carbon nanotubes, channel lengths of few nanometers can be fabricated and I-V characteristics must then consider the ballistic transport. In our model, under subthreshold regime, a current equation has been

used based on a sub-band description of the electronic structure and ballistic transport. This equation can be further expanded to cover the normal operation of the transistor, which will incorporate the ballistic transport. The present work on current and charge transport model does not include velocity saturation for electrons in carbon nanotubes and the mobility is assumed constant. The present work can be further refined by inclusion of ballistic transport, velocity saturation effects and mobility considerations in carbon nanotubes.

Furthermore, the present research can be coupled with a carbon nanotube interconnect modeling for analysis and design of all CNT-FET based analog and digital integrated circuits. Similar to SPICE MOS models, SPICE CNT-FET models can also be developed and is suggested for future work.

It was shown in Chapter 7 that the present research on current transport modeling can be applied in providing an explanation to reactions taking place in the CNT and CNT-FET sensors when exposed to traces of bio- and chemical agents at a molecular level. Experimental CNT and CNT-FET bio- and chemical sensors can be designed and developed based on the current research.

APPENDIX A

CARRIER CONCENTRATION INTEGRAL

In Chapter 2, we came upon an indefinite integral for the carrier concentration given by,

$$I = \frac{1}{\sqrt{kT}} \int_0^{\frac{6E_c}{kT}} \frac{(kTx + E_c)}{x^{1/2}(kTx + 2E_c)^{1/2}} e^{-x} dx \,. \tag{A.1}$$

In Eq. (A.1), the integral, *I*, has no definite solution. However, an approximate solution can be found by representing the exponential function, e^{-x}, with a series of polynomial functions using the Taylor series expansion approximation [1,2] around a variable A.

We first represent the exponential function as:

$$e^{-x} \approx e^{-A}\left[1 - (x - A) + \frac{(x - A)^2}{2} - \frac{(x - A)^3}{6}\right], \quad \text{for} \quad A \le x \le A + 1 \tag{A.2}$$

Equation (A.2) is a very good approximation within the range of *A* to *A+1*. In order to extend the range of approximation from *A+1* to an arbitrary integer number *n*, we introduce a summation to cover all *x*. Equation (A.2) becomes

$$e^{-x} \approx \sum_{A=0}^{n} e^{-A}\left[1 - (x - A) + \frac{(x - A)^2}{2} - \frac{(x - A)^3}{6}\right], \quad \text{for} \quad A \le x \le A + 1 \tag{A.3}$$

Replacing the exponential term in the integral of Eq. (A.1) with the approximated polynomial expression for the exponential function (A.3) we obtain:

$$I = \frac{e^{-A}}{\sqrt{kT}} \sum_{A=0}^{A_{\max}} \int_A^{A+1} \frac{(kTx + E_c)}{x^{1/2}(kTx + 2E_c)^{1/2}} \left[1 - (x - A) + \frac{(x - A)^2}{2} - \frac{(x - A)^3}{6}\right] dx \,, \tag{A.4}$$

where A_{max} can be set at a maximum integer value of $\frac{6E_c}{KT}$ as discussed in Section 2.3.1. This integral can now be solved analytically. The procedure involved in solving the integral of Eq. (A.4) is a complicated mathematical process; however, the solution is only a polynomial

expression, which can be expressed as follows:

$$I = \sum_{A=0}^{\mathrm{int}\left(6\frac{E_c}{kT}\right)} \left\{ e^{-A}\sqrt{x\left(x+2\frac{E_c}{kT}\right)}\left[1-\tfrac{1}{2}x+A+\tfrac{1}{2}\tfrac{E_c}{kT}+\tfrac{1}{6}x^2-\tfrac{1}{6}\tfrac{E_c}{kT}x-\tfrac{1}{2}Ax+\tfrac{1}{2}\left(\tfrac{E_c}{kT}\right)^2+\tfrac{1}{2}A\tfrac{E_c}{kT}\right.\right.$$
$$+\tfrac{1}{2}A^2-\tfrac{1}{4}A^2x+\tfrac{5}{16}\left(\tfrac{E_c}{kT}\right)^3+\tfrac{1}{6}A^3-\tfrac{1}{24}x^3+\tfrac{1}{24}\tfrac{Ec}{kT}x^2$$
$$\left.-\tfrac{5}{48}\left(\tfrac{Ec}{kT}\right)^2x+\tfrac{1}{2}A\left(\tfrac{Ec}{kT}\right)^2+\tfrac{1}{2}A^2\tfrac{E_c}{kT}+\tfrac{1}{6}Ax^2-\tfrac{1}{6}A\tfrac{E_c}{kT}x\right]$$
$$\left.+\tfrac{1}{2}\left(\tfrac{E_c}{kT}\right)^2\left[1+A+\tfrac{E_c}{kT}+\tfrac{1}{2}A^2-A\tfrac{Ec}{kT}-\tfrac{5}{8}\left(\tfrac{Ec}{kT}\right)^2\right]\ln\left[\tfrac{E_c}{\sqrt{kT}}+\sqrt{kT}x+\sqrt{kTx^2+2xE_c}\right]\right\}_{x=A}^{x=A+1} \quad . \quad \text{(A.5)}$$

It should be noted that this integral is independent of the Fermi energy and characteristic of the chiral vector (n,m) of any particular carbon nanotube. Thus, it will remain constant at any bias voltage but dependent only on the temperature.

References

[1] D. E. Johnson and J. R. Johnson, *Mathematical Methods in Engineering and Physics*. New York: The Ronald Press Company, 1965.

[2] J. Stewart, *Calculus Early Transcendentals*, 3th Ed. United States: Brooks/Cole Publishing Company, 1995.

APPENDIX B

ANALYTICAL DERIVATION FOR THE CARBON NANOTUBE SURFACE POTENTIAL

In Chapter 3, we found an equation for the gate to substrate voltage of the form:

$$V_{gb} = \psi_{cnt,s} + \delta f\left(\psi_{cnt,s}, V_{cb}\right) + V_{fb}, \tag{B.1}$$

where

$$f\left(\psi_{cnt,s}, V_{cb}\right) = \begin{cases} Ie^{\frac{\Delta E_F + q\left(\psi_{cnt,s} - V_{cb} - \phi_0\right) - E_c}{kT}}; & for\ \psi_{cnt,s} \le V_{cb} + \phi_0 - \frac{\Delta E_F}{q} + \frac{E_c}{q} - \frac{kT}{q} \\ \frac{\sqrt{\left(\Delta E_F + q\psi_{cnt,s} - qV_{cb} - q\phi_0\right)^2 - E_c^2}}{kT}; & for\ \psi_{cnt,s} \ge V_{cb} + \phi_0 - \frac{\Delta E_F}{q} + \frac{E_c}{q} + \frac{kT}{q} \end{cases}, \tag{B.2}$$

and

$$\delta = \frac{qLN_c}{C_{ox1}}. \tag{B.3}$$

As it was discussed in Chapter 3 the gate voltage can be defined using three regions of operation. However, Eq. (B.1) is only defined for two regions due to the boundary condition of $\psi_{cnt,s}$: Region 1 for $\psi_{cnt,s} \le V_{cb} + \phi_0 - \frac{\Delta E_F}{q} + \frac{Ec}{q} - \frac{kT}{q}$ and Region 3 for $\psi_{cnt,s} \ge V_{cb} + \phi_0 - \frac{\Delta E_F}{q} + \frac{Ec}{q} + \frac{kT}{q}$. Region 2 is obviously undefined by Eq. (B.1) and the limits of this region can be expressed as:

$$V_{cb} + \phi_0 - \frac{\Delta E_F}{q} + \frac{Ec}{q} - \frac{kT}{q} < \psi_{cnt,s} < V_{cb} + \phi_0 - \frac{\Delta E_F}{q} + \frac{Ec}{q} + \frac{kT}{q}. \tag{B.4}$$

Furthermore, Eq. (B.1) cannot be solved explicitly for $\psi_{cnt,s}$ in terms of the terminal voltages. In this appendix, we will show a derivation for a gate voltage equation in Region 2, which covers the gap predicted by Eq. (B.1). We will also describe how the gate voltage equation can be solved analytically for the carbon nanotube surface potential and using only two regions of operation. As a result, a carbon nanotube surface potential equation is found

under two regions of operation and explicitly dependent in the terminal voltages.

The discontinuity in the gate voltage equation comes from the term $f(\psi_{cnt,s}, V_{cb})$. We can extrapolate a linear equation for the Region 2 by first picking two points: Point 1 for the higher limit of Region 1 at $\psi_{cnt,s_1} = V_{cb} + \phi_0 - \frac{\Delta E_F}{q} + \frac{Ec}{q} - \frac{kT}{q}$ and Point 2 for the lower limit of Region 2 at $\psi_{cnt,s_2} = V_{cb} + \phi_0 - \frac{\Delta E_F}{q} + \frac{Ec}{q} + \frac{kT}{q}$, we can then write:

$$f_1\left(\psi_{cnt,s_1}, V_{cb}\right) = Ie^{-1}, \tag{B.5}$$

$$f_2\left(\psi_{cnt,s_2}, V_{cb}\right) = \sqrt{\frac{2E_c}{kT} + 1}. \tag{B.6}$$

From Eqs. (B.5) and (B.6) we obtain a slope, 'm' given by,

$$m = \frac{f_2 - f_1}{\psi_{cnt,s_2} - \psi_{cnt,s_1}} = \frac{\sqrt{\frac{2E_c}{kT} + 1} - Ie^{-1}}{\frac{2kT}{q}}. \tag{B.7}$$

From basic mathematics we can write a linear equation for $f(\psi_{cnt,s}, V_{cb})$ as:

$$f\left(\psi_{cnt,s}, V_{cb}\right) - f_1\left(\psi_{cnt,s_1}, V_{cb}\right) = m\left(\psi_{cnt,s} - \psi_{cnt,s_1}\right). \tag{B.8}$$

By substituting Eqs. (B.5) and (B.7) in Eq. (B.8) we arrive at a final expression for the $f(\psi_{cnt,s}, V_{cb})$ in Region 2 expressed as:

$$f\left(\psi_{cnt,s}, V_{cb}\right) = m\left(\psi_{cnt,s} - \phi_0 - \frac{E_c}{q} - V_{cb} + \frac{kT}{q}\right) + Ie^{-1}. \tag{B.9}$$

By substituting Eq. (B.9) in Eq. (B.1) we can write a gate voltage equation for Region 2,

$$V_{gb} = \psi_{cnt,s} - V_{fb} + \delta m\left(\psi_{cnt,s} - \phi_0 + \frac{\Delta E_F}{q} - \frac{E_c}{q} - V_{cb} + \frac{kT}{q}\right) + Ie^{-1}. \tag{B.10}$$

Equation (B.10) can be used to solve for $\psi_{cnt,s}$ as follows:

$$\psi_{cnt,s} = \frac{V_{gb} - \delta Ie^{-1} - V_{fb} + \delta m\left(V_{cb} + \phi_0 - \frac{\Delta E_F}{q} + \frac{E_c}{q} - \frac{kT}{q}\right)}{1 + \delta m}, \tag{B.11}$$

for $V_{cb} + \phi_0 - \frac{\Delta E_F}{q} + \frac{Ec}{q} - \frac{kT}{q} < \psi_{cnt,s} < V_{cb} + \phi_0 - \frac{\Delta E_F}{q} + \frac{Ec}{q} + \frac{kT}{q}$.

The rapidly decreasing exponential behavior of $f(\psi_{cnt,s},V_{cb})$ in Eq. (B.1) for $\psi_{cnt,s} \le V_{cb} + \phi_0 - \frac{\Delta E_F}{q} + \frac{Ec}{q} - \frac{kT}{q}$ allows us to assume that the dependence of the gate voltage on the carbon nanotube surface potential in this Region 1 is linear. Therefore, the term $\delta f(\psi_{cnt,s},V_{cb})$ becomes negligible in Region 1. In addition, as it was discussed in Chapter 3, for low power conditions Region 2 can be further extended to cover Region 3. Under these assumptions we can define the carbon nanotube surface potential to be given by two regions of operation as:

Region 1, for $0 \le V_{gb} \le V_{cb} + V_{fb} + \phi_0 - \frac{\Delta E_F}{q} + \frac{E_c}{q} - \frac{kT}{q} - \frac{Ie^{-1}}{m}$:

$$\psi_{cnt,s} = V_{gb} - V_{fb}, \tag{B.12}$$

Region 2, for $V_{gb} \ge V_{cb} + V_{fb} + \phi_0 - \frac{\Delta E_F}{q} + \frac{E_c}{q} - \frac{kT}{q} - \frac{Ie^{-1}}{m}$:

$$\psi_{cnt,s} = \frac{V_{gb} - \delta Ie^{-1} - V_{fb} + \delta m\left(V_{cb} + \phi_0 - \frac{\Delta E_F}{q} + \frac{E_c}{q} - \frac{kT}{q}\right)}{1 + \delta m}, \tag{B.13}$$

where the inequalities in Eqs. (B.12) and (B.13) for Region 1 and Region 2, respectively, can be recognized as the threshold voltage. The threshold voltage is addressed and derived in more detailed in Chapter 4.

APPENDIX C

MODEL PARAMETERS

Symbol	Units	Description
n	-	Number of hexagons along the a_1 direction
m	-	Number of hexagons along the a_2 direction
L	nm	Length of the carbon nanotube
$\|R\|$	nm	Circumference of the carbon nanotube
$V_{pp\pi}$	eV	Energy transfer integral for carbon nanotubes
E_c	eV	Conduction band energy
$\pm \Delta E_F$	eV	Amount by which the Fermi level shifts from intrinsic energy level. It is negative for p-type and positive for n-type carbon nanotubes
V_{gb}	Volt	Gate to substrate (back gate) voltage
ψ_{cnt}	Volt	Carbon nanotube potential
$\psi_{cnt,s}$	Volt	Carbon nanotube surface to substrate potential
ψ_{ox1}	Volt	Gate oxide potential
ψ_{ox2}	Volt	Substrate oxide potential
ϕ_{ms}	Volt	Gate to substrate (back gate) work function difference
ϕ_{mc}	Volt	Gate to carbon nanotube work function difference
ϕ_{cs}	Volt	Gate to substrate work function difference
ϕ_0	Volt	Value of the potential of $\psi_{cnt,s}$ when $V_{gb} = V_{fb}$ and $\psi_{cnt} = 0$
V_{fb}	Volt	Flat band voltage
Q_g	Coulomb	Charge in the gate
Q_{01}	Coulomb	Charge in the gate oxide
Q_{02}	Coulomb	Charge in the substrate oxide
Q_{cnt}	Coulomb	Charge inside the carbon nanotube
Q_{subs}	Coulomb	Charge in the substrate
T_{ox1}	Angstrom	Thickness of the gate oxide
T_{ox2}	Angstrom	Thickness of the substrate oxide
C_{ox1}	Faraday	Gate oxide capacitance
C_{ox2}	Faraday	Substrate oxide capacitance
ε_{ox1}	Faraday/cm	Permittivity constant of the gate oxide
ε_{ox2}	Faraday/cm	Permittivity constant of the substrate oxide
V_{gs}	Volt	Gate to source voltage
V_{sb}	Volt	Source to substrate voltage
V_{ds}	Volt	Drain to source voltage
T	Kelvin	Temperature
N_c	cm^{-1}	Effective density of states
$n_{cnt,i}$	cm^{-1}	Intrinsic carrier concentration

Symbol	Units	Description
N	cm^{-1}	Ionized impurity concentration of donor atoms (N_D) or acceptor atoms (N_A)
I	-	Integral factor for the density of states
μ	$cm^2/Vsec$	Mobility of graphite
γ	-	Conversion factor from the mobility of graphite to carbon nanotubes
β	$Ampere/V^2$	Current gain
I_{ds}	Ampere	Current between drain and source
R_c	Ω	Contact resistance of the carbon nanotube
R_s	Ω	Contact resistance at the source
R_d	Ω	Contact resistance at the drain
R_{ds}	Ω	Resistance between drain and source
g_{ds}	Siemens	Conductance between drain and source
g_m	Siemens	Transconductance
T_{poly}	Angstroms	Thickness of the gate material
C_{par}	Faraday	Overlap capacitance between the gate and the source/drain
C_{gs}	Faraday	Capacitance between the gate and source
L_0	nm	Mean free path of electrons
$\hbar\Omega_n$	eV	The energy of the n_{th} scattering event

APPENDIX D

COPYRIGHT PERMISSION

Copyright permission for Fig. 1.2.

From: C.Dekker@tudelft.nl
Subject: Re: Copyright permission
Date: April 16, 2008 4:02:35 AM CDT
To: jmarul1@lsu.edu

Sure, you have my permission.
kind regards
Cees Dekker

On 16 apr 2008, at 00:33, Jose Marulanda wrote:

Dear Dr. Dekker

My name is Jose Marulanda, I just defended my dissertation at Louisiana State University, Baton Rouge, LA. USA. I want to use in my final dissertation a figure in one of your publications: Figure 1(a) in "Electronic structure of atomically resolved carbon nanotubes, *Nature* 391, pp. 59, 1998."

I appreciate your time,

Best Regards
Jose Marulanda

Cees Dekker
Distinguished University Professor (Universiteitshoogleraar)
Delft University of Technology
Kavli Institute of NanoScience
Lorentzweg 1, 2628 CJ Delft, The Netherlands
phone: +31 15 2786094
fax: +31 15 2781202
e-mail: c.dekker@tudelft.nl
website: http://ceesdekker.net

APPENDIX E

LIST OF PUBLICATIONS

1. J. M. Marulanda and A. Srivastava, "I-V characteristics modeling and parameter extraction for CNT-FETs," *Proc. 2005 International Semiconductor Device Research Symposium*, (Bethesda, Maryland, December 7-9, 2005).

2. J. M. Marulanda, A. Srivastava and R. K. Nahar, "Ultra-high frequency modeling of carbon nanotube field-effect transistors (CNT-FETs), *Proc. 13th International Workshop on the Physics of Semiconductor Devices (IWPSD)*, pp. G-11, (Delhi, India, December 13-17, 2005).

3. J. M. Marulanda and A. Srivastava, "Carrier density and effective mass calculations for carbon nanotubes," *Proc. International Conference on Integrated Circuit Design and Technology*, pp. 234-237, (Austin, Texas, May 30th – June 1st, 2007).

4. J. M. Marulanda, A. Srivastava and A. K. Sharma, "Transfer characteristics and high frequency modeling of logic gates using carbon nanotube field effect transistors (CNT-FETs)," *Proc. of The 20th Annual Conference on Integrated Circuits and Systems Design (SBCCI 2007)*, pp. 202-206, (Rio de Janeiro, Brazil, September 3-6, 2007).

5. J. M. Marulanda, A. Srivastava and A. K. Sharma, "Current transport modeling in carbon nanotube field effect transistors (CNT-FETs) and bio-sensing applications," *Proc. SPIE Smart Structures and Materials & Nondestructive Evaluation and Health Monitoring: Nanosensors and Microsensors for Bio-System*, vol. 6931, pp. 693108-1-693108-12, (San Diego, California, March 9-13, 2008).

6. J. M. Marulanda, A. Srivastava and S. Yellampalli, "Numerical modeling of the I-V characteristics of the carbon nanotube field effect transistors," *Proc. IEEE 40th Southeastern Symposium on System Theory (SSST 2008)*, pp. 235-238, (New Orleans, Louisiana, March 16-18, 2008).

7. Y. Xu, A. Srivastava, and J. M. Marulanda, "Emerging carbon nanotube electronic circuits, modeling and performance," *Proc. 51st IEEE International Midwest Symposium on Circuits and Systems (MWSCAS 2008)*, (August 10-13, Knoxville, Tennessee).

8. J. M. Marulanda, A. Srivastava, "Carrier density and effective mass calculations in carbon nanotubes," *physica status solidi (a)*, 2008 (in press).

9. J. M. Marulanda, A. Srivastava and A. K. Sharma, “Threshold and saturation voltages modeling of carbon nanotube field effect transistors (CNT-FETs),” *NANO*, 2008, under revision.

10. J. M. Marulanda, A. Srivastava and A. K. Sharma, “Current transport modeling of carbon nanotube field effect transistors,” *physica status solidi (a)*, 2008, communicated.

11. A. Srivastava and J. M. Marulanda, “Carbon electronics, bio- and chemical sensing applications,” US Army RATADEC, Warren, MI, March 5, 2008, (invited lecture by Dr. Srivastava).

VITA

Jose Mauricio Marulanda Prado was born in February 1981, in San Salvador, El Salvador. His parents are Armando Marulanda Blanco and Ana Lucia Prado de Marulanda, both from Cali, Colombia. He graduated from High School in El Salvador in 1997. He came to The United States in 1998 where he enrolled in Louisiana State University. He obtained his Bachelor of Science in Electrical Engineering in 2001. He entered the graduate program in 2001 and obtained his Master of Science in Electrical Engineering in 2002. He continued in the graduate program for his doctoral studies and obtained his doctoral degree in August 2008. He speaks four languages fluently. His research interests include carbon nanotube field effect transistor (CNT-FET) modeling/simulation and integration, low power VLSI design, computer-aided modeling and nanotechnology.